Cooling and Crystallization of Tholeiitic Basalt, 1965 Makaopuhi Lava Lake, Hawaii

GEOLOGICAL SURVEY PROFESSIONAL PAPER 1004

Cooling and Crystallization of Tholeiitic Basalt, 1965 Makaopuhi Lava Lake, Hawaii

By THOMAS L. WRIGHT *and* REGINALD T. OKAMURA

GEOLOGICAL SURVEY PROFESSIONAL PAPER 1004

An account of the 4-year history of cooling, crystallization, and differentiation of tholeiitic basalt from one of Kilauea's lava lakes

UNITED STATES GOVERNMENT PRINTING OFFICE, WASHINGTON : 1977

UNITED STATES DEPARTMENT OF THE INTERIOR

CECIL D. ANDRUS, *Secretary*

GEOLOGICAL SURVEY

V. E. McKelvey, *Director*

Library of Congress Cataloging in Publication Data

Wright, Thomas Loewelyn.
Cooling and crystallization of tholeiitic basalt, 1965 Makaopuhi Lava Lake, Hawaii.

(Geological Survey Professional Paper 1004)
Includes bibliographical references.
Supt. of Docs. No.: I 19.16:1004
1. Basalt–Hawaii–Kilauea. I. Okamura, Reginald T., joint author. II. Title.
III. Title: Makaopuhi Lava Lake, Hawaii. IV. Series: United States. (Geological Survey. Professional Paper 1004)

QE462.B3W73 552'.2 76-608264

For sale by the Superintendent of Documents, U.S. Government Printing Office
Washington, D.C. 20402
Stock number 024-001-02990-1

CONTENTS

ILLUSTRATIONS

TABLES

COOLING AND CRYSTALLIZATION OF THOLEIITIC BASALT, 1965 MAKAOPUHI LAVA LAKE, HAWAII

By Thomas L. Wright and Reginald T. Okamura

ABSTRACT

A pond of lava 84 m deep and 800 m wide formed in Makaopuhi crater during an eruption of Kilauea volcano March 5–15, 1965. The tholeiitic lava (MgO about 8 percent, SiO_2 about 50 percent) was erupted at about 1,190°C. Foundering of the lake-surface crust following the eruption reduced the temperature of the upper 10 m of the lake by as much as 40°C. The following studies were conducted between March 1965 and February 1969, when the lake was covered by lava from a subsequent eruption of Kilauea.

1. Twenty four small-diameter (1.5 cm) and three large-diameter (6 cm) holes were drilled to trace the growth of the upper crust of the lake. The 1,070°C isothermal surface separates rigid, partly molten crust (solidus=980°C) from melt into which probes may be pushed by hand.

2. Open holes and holes cased with stainless steel were used subsequently for measurement of temperature, oxygen fugacity, a single measurement of melt viscosity, and collection of samples of melt and gases exsolving from the melt.

3. Elevations of a grid of nails set in the lake surface crust were periodically determined.

4. The specific gravity of drill core was measured, and the core was used in a variety of petrographic and petrochemical studies.

This report summarizes all of the quantitative studies relevant to the cooling and crystallization of ponded basaltic lava. Principal results and interpretations of these aspects are as follows:

1. Thermal history: Isotherms in the upper crust migrated downward in the lake, first, as a linear function of square root of elapsed time ($\sqrt{t}$); then, they were irregularly depressed to greater depths than predicted by this function, the initial change in slope being triggered by a period of heavy rainfall. Isotherms in the melt (1,070–1,130°C) were likewise initially linear with $\sqrt{t}$, but their slopes flattened and began to vary erratically in the period March-December 1966. This behavior is interpreted as being caused by the initiation of convection in the ponded basaltic melt. By late 1968 all isothermal surfaces were at greater depths than predicted from the $\sqrt{t}$ function.

2. Oxygen fugacity (fO_2): Drill holes showed buffered fO_2-T profiles over much of the period, with fO_2 values slightly higher than the quartz-fayalite-magnetite buffer. Superimposed on normal profiles were transient high values of fO_2 as much as 10_{-2} atmospheres (atm) between 400–800°C. Core became oxidized soon after exposure to high fO_2, evidenced by hematitic alteration of mafic minerals and increased Fe_2O_3/FeO ratios in analyzed core. The high oxygen fugacities are tentatively ascribed to deep circulation of oxygen-saturated rain water.

3. Chemistry and petrography: Samples collected during the eruption and to a depth of 7.9 m have MgO contents of 7.5–8.5 percent and show olivine-controlled chemical variation. Large olivine crystals are inferred to have settled toward the bottom of the lake. Below 7.9 m, MgO decreases to 6.1 percent at 16.5 m, and samples are differentiated by removal of olivine, augite, and plagioclase. This process is interpreted as flow differentiation promoted by convection of the melt. Segregation veins have compositions explainable by low-temperature (1,030°–1,070°C) filtration of liquid from partially molten crust into open-gash fractures. Grain size increases markedly to a maximum at a depth of 14 m, where median-grain values exceed 0.001 mm^3 (diam=0.2 mm). Residual glass composition is that of a calc-alkaline rhyolite, and the content of residual glass increases slightly with depth as an apparent function of the amount of differentiation.

4. Core density: Core density reaches a maximum at 6.1 m depth (sp gr=2.7 g/cc) and then decreases to 2.5 at 15.2 m. Melt density is low (<2.5 g/cc) at a depth of 4.6–7.6 m (numerous vesicles) but high (2.8 g/cc) at a depth of 16.5–18.3 m. Evidently the temperature of vesiculation decreases with increasing pressure, and the resultant difference in the amount of an exsolved gas phase in the melt causes density differences that are considered to be the driving force for convection.

5. Surface altitude changes: The surface of the central part of the lake subsided at a decreasing rate (relative to $\sqrt{t}$) until the middle of 1967 and was subsequently uplifted through the last measurement date in 1968. This variation in altitude is the resultant of thermal contraction and density change on solidification, the latter critically controlled by the temperature at which vesiculation takes place.

INTRODUCTION

Many eruptions of Kilauea volcano have left thick ponds of liquid lava, called lava lakes, in pit craters (fig. 1). Three historic lakes were accessible and sufficiently long lived to warrant study; these were formed in 1959 (Kilauea Iki), 1963 (Alae), and 1965 (Makaopuhi). Of these only Kilauea Iki lava lake is still exposed, the others having been covered by flows erupted in 1969 and later. In addition to the historic lava lakes, one prehistoric lava lake, exposed in the east wall of the west pit of Makaopuhi crater, was studied by Moore and Evans (1967) and Evans and Moore (1968). Data for this lake are important because they represent a complete section through a solidified lava lake whose size and chemical composition are comparable with the 1965 Makaopuhi lava lake.

The Kilauea lava lakes have been natural laboratories in which to study the cooling and crystallization of tholeiitic basalt magma. The solidification of Makaopuhi lava lake was followed from the time of its formation in March 1965 up to a few weeks before the surface was covered by new lava in February 1969. Methods of study included core drilling of the upper crust, repeated altitude surveys of the lake surface,

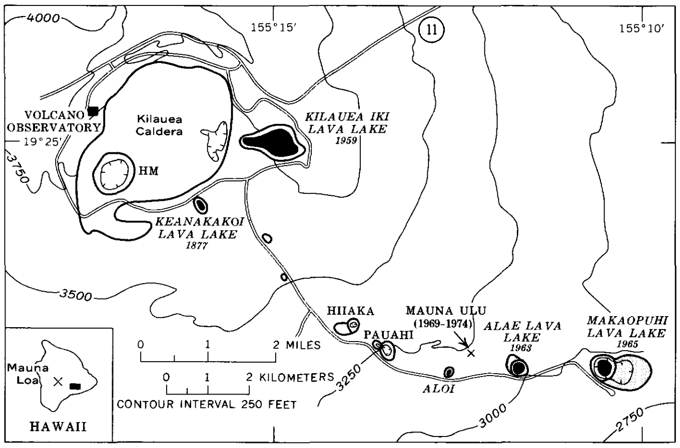

FIGURE 1.—Index map of Kilauea lava lakes (modified from Peck and others, 1966). Craters, lava lakes, and roads are shown as they existed prior to 1968. Eruptions beginning in February, 1969 crossed the Chain of Craters Road in several places. The long Mauna Ulu eruption, centered between Aloi and Alae craters, erupted lava that by the summer of 1974 had completely filled Aloi crater, Alae crater, and the west pit of Makaopuhi crater. HM=Halemaumau crater. Black rectangle in inset indicates area covered by index map.

and direct measurement of temperature and oxygen fugacity in holes drilled into the upper crust. Additional field studies of the molten basalt underlying the upper crust included temperature profiles in holes cased with stainless steel, sampling of melt in ceramic and stainless steel tubes emplaced through open drill holes, and a single set of measurements of melt viscosity. Laboratory work included studies of bulk chemical analyses of petrography of drill core and melt samples, and of bulk densities determined on drill core. Currently we are modeling the thermal history of Makaopuhi lava using thermal conductivities measured by Robertson and Peck (1974) and a computer-based finite element analysis. The purpose of this paper is to describe the methods of study, to summarize the data gathered, and to interpret these data in terms of the changing chemical and physical properties of the basalt during solidification.

This paper was originally conceived as a progress report, as we had plans for further drilling into the lake at intervals of 2 to 5 years. However, lava erupted in February 1969 crossed the Chain of Craters Road (fig. 1), cutting off access to Makaopuhi crater and spilling into the crater to form a 3 m-deep sheet of aa over the surface of the 1965 lava lake. In May 1969, Kilauea began essentially continuous activity centered at Mauna Ulu (fig. 1), further blocking the crater from access. In early 1972, lava from Mauna Ulu began cascading into the west pit of Makaopuhi, which was filled by spring 1973. Thus, the present paper presents the results of an aborted, though nonetheless rather successful, study of the 1965 Makaopuhi lava lake.

ACKNOWLEDGMENTS

The Kilauea lava lake studies represent a combined effort of the entire staff of the Hawaiian Volcano Observatory. H.A. Powers was scientist-in-charge during the study of Makaopuhi lava lake and his consistent encouragement is gratefully acknowledged. Personnel who were essential to this study were: Dallas Peck, Richard S. Fiske, Donald A. Swanson, Elliot Endo, George Kojima, Bill Francis, John Forbes, Burton Loucks, Ken Yamashita, and Jeffrey Judd.

H. R. Shaw helped in the early drilling of the lake and designed experiments to measure the viscosity of the Makaopuhi melt. P. R. Brett constructed the standards for calibration of temperatures in the drill holes. Continuing collaboration with Shaw and with Rosalind Tuthill Helz have materially improved the "Discussion" section of the paper, although the conclusions reached are the responsibility of the authors.

PREVIOUS WORK

Published studies on Makaopuhi lava lake include an account of the eruption (Wright and others, 1968), preliminary mineralogic data (Wright and Weiblen, 1967; Häkli and Wright, 1967; Evans and Wright, 1972), determination of viscosity of the Makaopuhi melt (Shaw and others, 1968), determination of oxygen fugacity of gas in the drill holes (Sato and Wright, 1966), composition of gases emitted from the drill holes (Finlaysen and others, 1968), and a study of oxidation during cooling of the lava lake (Grommé and others, 1969). Related studies of other recent Kilauea lava lakes are summarized by Wright, Peck, and Shaw (1976; see especially the annotated bibliography).

THE ERUPTION OF MARCH 5–15, 1965

CHRONOLOGY

The following account of the March 1965 eruption and the formation of the lava lake is condensed from Wright, Kinoshita, and Peck (1968).

The eruption in Makaopuhi Crater occurred in two stages: an initial period of fountaining on March 5 lasted 8 hours and filled the crater to a depth of 50 m[1]; eruption resumed on March 6 after an 18-hour pause and continued until the end of the eruption on March 15. Crust formed during stage 1 and the early days of

[1]All measurements were originally recorded in feet. In particular the core barrels used in drilling and the thermocouples used to measure temperature were marked in feet. In this report we observe the following conventions:

1. In the text, all values are given in meters or in feet and meters if the original measurement was in feet.
2. In the tables, values are reported in feet.
3. In the figures, scales are given in both English and metric units.

stage 2 piled up in a circumferential pressure ridge, and parts of this ridge persisted as "islands" of crust barely emergent from the surface during the rest of the eruption. During the last 5 days of eruption, the rate of extrusion increased, and the surface of the lake consequently remained hot and plastic, so that no permanent crust formed during this time. Following the end of eruption, the surface dropped 20 m as lava drained back down the vent, and remnants of the pressure ridge were left standing 5–10 m above the general lava surface. Following drainback, much of the solid crust on the lake was renewed repeatedly by episodes of crustal foundering, the last of which was on March 19. The process of crustal foundering is illustrated and briefly described by Wright, Kinoshita, and Peck (1968, fig. 10d, and p. 3191 ff), and by Shaw, Kistler, and Evernden (1971).

The lake surface as it appeared following the eruption is shown in figure 2. Surface features are labeled in figure 3. Figure 4 shows the relation of lake levels during the eruption to the thickness of the upper crust at the time the lake was last drilled in 1968–69.

INITIAL CONDITIONS FOLLOWING FORMATION OF A PERMANENT CRUST

The mode of eruption affects the chemical composition, initial temperature distribution, volatile content, and distribution of previously formed crust in the lake. These factors cannot all be quantitatively evaluated but are important in interpreting the subsequent cooling and solidification history.

Chemical composition.—Samples of pumice and lava collected during the eruption are uniform in chemical composition and in phenocryst content (Wright and

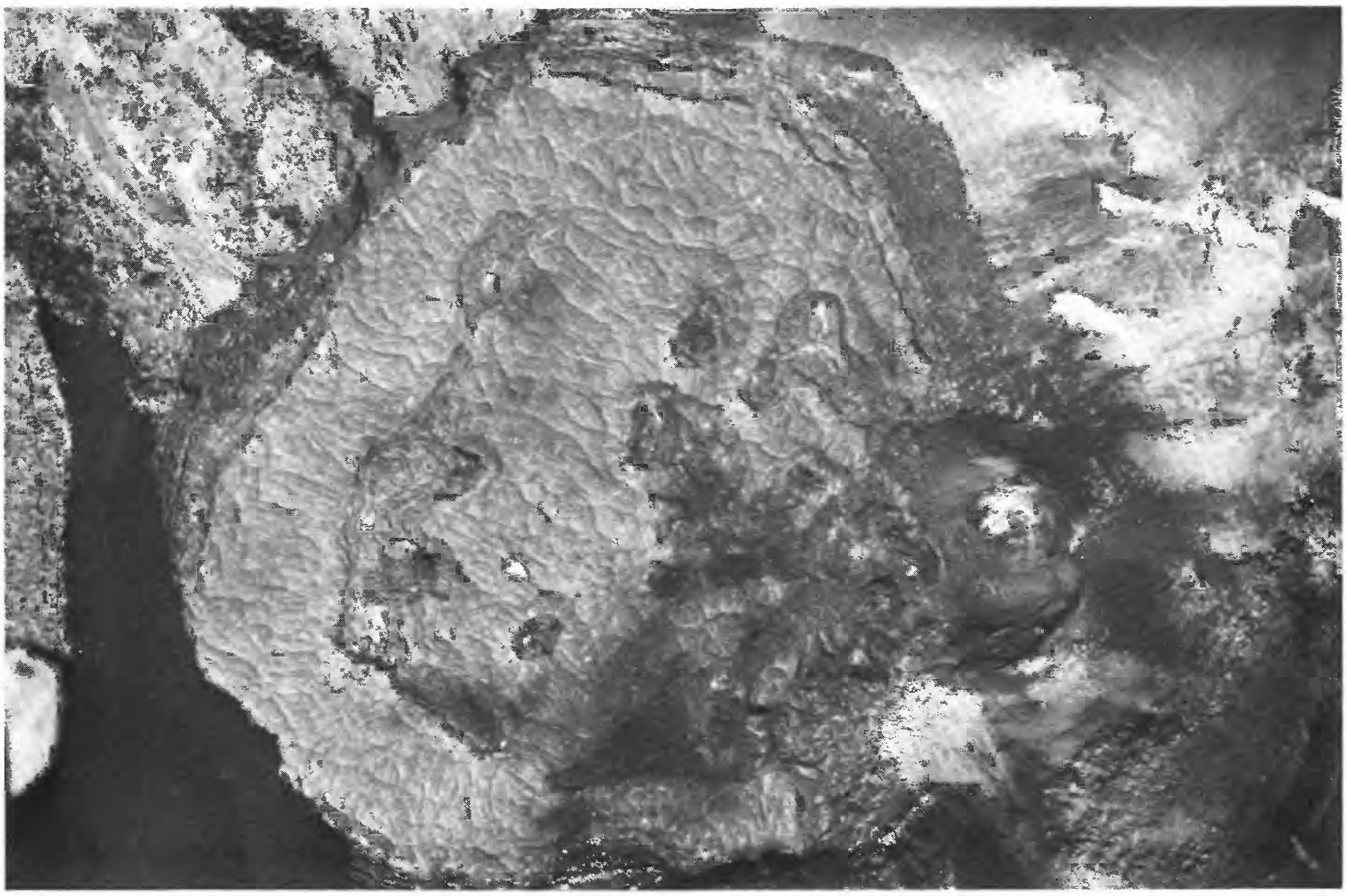

FIGURE 2.—Posteruption surface, Makaopuhi lava lake. Vertical photograph. The vent is to the left and the diameter of the lake surface is about 365 m. Drainback rim surrounds the lake. The east wall of the craters is in shadow. Part of the shallower east pit is shown at the far right. Surface features are labeled in figure 3. The relatively smooth surface, marked by polygonal cracks and flow lines, formed following the last crustal foundering episode on March 19, 1965. The elongate area in the right center and some smaller areas near the vent are lower in altitude than the overturn crust surface and were the locus of the latest ooze-outs on March 20. Darker areas are islands of crust; those associated with the low area to the right are remnants of a pressure ridge that was formed during the first eruptive phase on March 5. Those at the left are pieces of the vent rafted out on the lake surface.

FIGURE 3.—Index map showing surface features of Makaopuhi lava lake drawn from figure 2. Level stations are numbered and shown as small solid dots (•). Drill holes, labeled in larger type, are shown as open circles (○). Cross section shown in figure 4 is drawn approximately along the line connecting level stations 1 and 52.

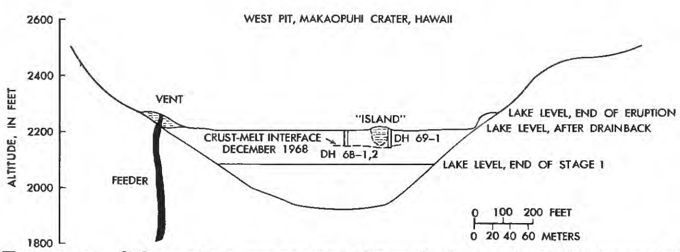

FIGURE 4.—Schematic cross section through the west pit, Makaopuhi crater. Horizontal = vertical scale. Line of section goes through the vent and level station 1 (fig. 3.). The island near station 4 is projected onto the section; its base is conjectured.

others, 1968, table 6; this report, table 10). An average composition is given in table 12. Thus we assume that any chemical heterogeneity is imposed by processes taking place after lava ponded in the crater.

Temperature distribution.—The best estimate of eruption temperature is 1,190°C, if we use the crystallinity of pumice and apply it to the plot of glass versus temperature (fig. 17; see also discussion in Wright and others, 1968, p. 3198 ff). Cooling of the lava-lake surface by radiation augmented by foundering of solidified crust during the eruption reduced temperatures in the upper part of the lake as evidenced by the greater crystallinity of samples collected from the rising lake compared with the erupted pumice (Wright and others, 1968, table 4). Crustal foundering following the eruption further reduced temperatures in the upper part of the lake. Crystallinity of the upper surface of the permanent crust (sample M–1–1G) yields a temperature of 1,140°C. H. R. Shaw (written commun., 1975) calculated the total heat loss during crustal foundering and found that it corresponded to a cooling of 50° over the upper 40 feet (12.2 m) of the lake. A temperature profile obtained 1 month after the eruption (table 3, fig. 10) showed temperatures of 1,128°–1,136°C between 9 and 21 feet (2.7–6.4 m). Finite-element modeling shows that these temperatures can be matched if the lake is layered with a cooler upper 40–45 feet (12.2–13.7 m) at 1,140°C and a lower part where the maximum temperature is 1,190°C. Thus the crystallinity of the surface crust, measured-temperature distribution, and two kinds of theoretical analysis all suggest that, when final solidification began, the upper 40 feet (12.2 m) of the lake was 1,140°C, and the lower part was 1,190°C with a transition zone of unkown but probably small thickness between the two layers.

Volatile content.—We have no way of quantitatively specifying the volatile content of the magma. In addition to volatiles released during fountaining, significant degassing accompanied crustal foundering. Thus it is possible that Makaopuhi lava lake was relatively degassed prior to solidification.

Distribution of foundered crust.—The "islands" of crust left after the eruption have an unknown vertical extent. They were sufficiently rigid to resist movement during crustal foundering, yet did subside isostatically following drainback. No evidence of foundered crust was found in drilling holes 68–1 to depths of 54 feet (16.5 m). However, there is the possibility that unremelted foundered crust was present elsewhere in the lake. Some of the irregularities in temperature distribution and core density may reflect inhomogeneities traceable to foundered crust, but we have no way of treating these effects quantitatively.

DEFINITION OF "CRUST" AND "MELT"

The investigations of the lava lake provide a rigorous, if empirically derived, definition of the terms "crust" and "melt," terms that are used throughout this report and in reports on other Kilauea lava lakes. The interface separating crust from melt is a zone across which the rigidity of the basalt changes drastically. A finite hydraulic pressure must be maintained when drilling through crust, but the drill will fall under its own weight with no additional hydraulic pressure once melt is penetrated. The crust-melt interface is found to be an essentially isothermal surface, 1,065°C in Kilauea Iki and Alae lava lakes (Richter and Moore, 1966; Peck and others, 1964, 1966); 1,070°C in Makaopuhi lava lake. The temperature of the crust-melt interface represents the "softening" temperature of the basalt, above which a steel or ceramic probe may be pushed by hand into the melt. This property makes it possible to take samples and measure temperatures in the melt below the depth to which core-drilling is possible.

When drilling within the crust, coolant water is dissipated as steam through fractures in the basalt in the vicinity of the drill hole and does not reappear at the top of the drill hole. In contrast, coolant water introduced into melt already saturated in H_2O collects as a giant "bubble," and when the drill string is disconnected the water is expelled as a blast of superheated steam. When the upper crust is less than about 9.1 m thick, the steam returns to the top of the drill hole. At deeper levels, steam generated at the crust-melt interface condenses and is lost through fractures before reaching the surface.

METHODS OF STUDY

During and after the eruption, the surface of the lake was reached by a pig-hunter's trail that originated about 160 m east of the Makaopuhi crater overlook (Wright and others, 1968, fig. 9). Within 1 month after the end of the eruption, an aerial tramway was set up about 62 m east of the overlook and was affixed at its lower end to an island of crust near the center of the lake (fig. 5). The tramway was used to carry supplies for drilling and scientific studies. In 1968 it was replaced by a larger tramway at the same location (fig. 6).

MEASUREMENT OF SURFACE ALTITUDE CHANGES

Within 72 hours after the permanent crust was formed, a grid of nails was installed to detect altitude changes of the lake surface during solidification. Later, more stations were added. The final net is shown in figure 3, and the dates when stations were added are given in table 28. Altitude changes were measured using a Zeiss self-leveling pendulum level and 12-foot (3.658 m) Invar rods (fig. 9*A*). The reference point assumed to remain unchanged in altitude was originally a nail driven into a talus block near the trail on the east end of the lake (station 44 in table 28, not shown in fig. 3). Later, station 45, at the base of the drainback was used as the reference, and eventually station 1, on the lake surface, was used. Readings were made to 0.001 foot (0.3 mm) and are precise to about 0.005 foot (1.5 mm). Most observed altitude changes exceed the precision of measurement by a factor of 10 or greater.

CORE DRILLING

Twenty four holes were drilled between April 19, 1965, and July 22, 1966, using 2.9 cm (SP size)[2]

[2]Hole #17 (fig. 3) was drilled with Ex bits (1½ in. (3.8 cm) diam).

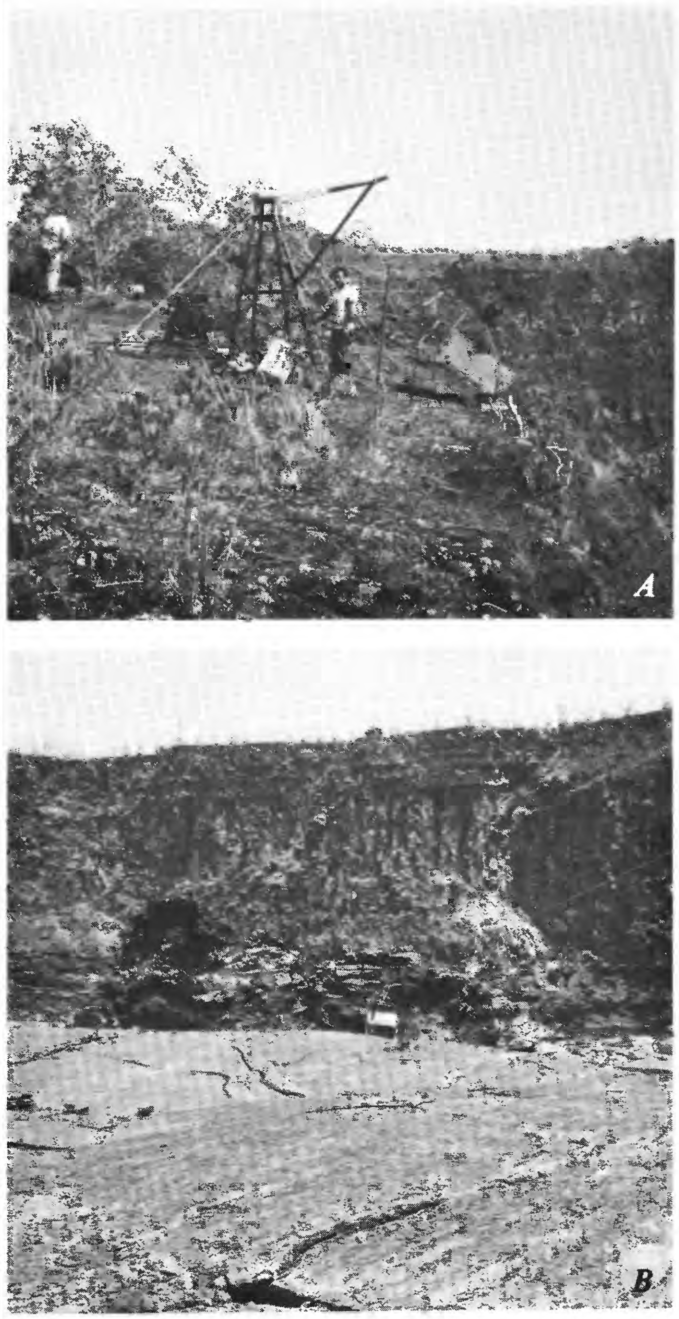

FIGURE 5.—Photographs of the tramway used to transport equipment from the rim to the crater floor in 1965–67. *A*, Scale is given by the wooden box which is about 1 m long. A ⅜ in. steel cable is fastened at the upper end to an A-frame set in concrete and at the lower end to a chain wrapped around the island. Equipment is lowered in a wooden box attached to a pulley running on the steel cable. A rope attached to the box is reeled on a winch (left of A-frame) which in turn is connected by rope to a pulley attached to the axle of a jeep, jacked up and blocked in position (not shown). *B*, The foreground shows the relatively smooth surface of the lake near level station 5. The surface of the east pit of Makaopuhi crater (top of photo) is underlain by four lava flows which in turn overlie the prehistoric Makaopuhi lava lake, distinguished by prominent columnar jointing.

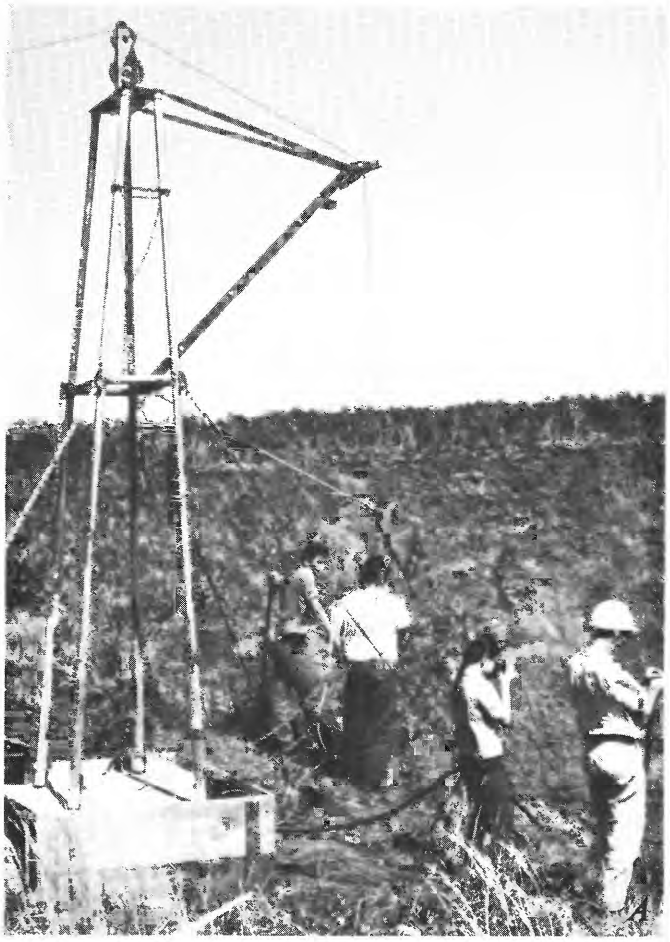

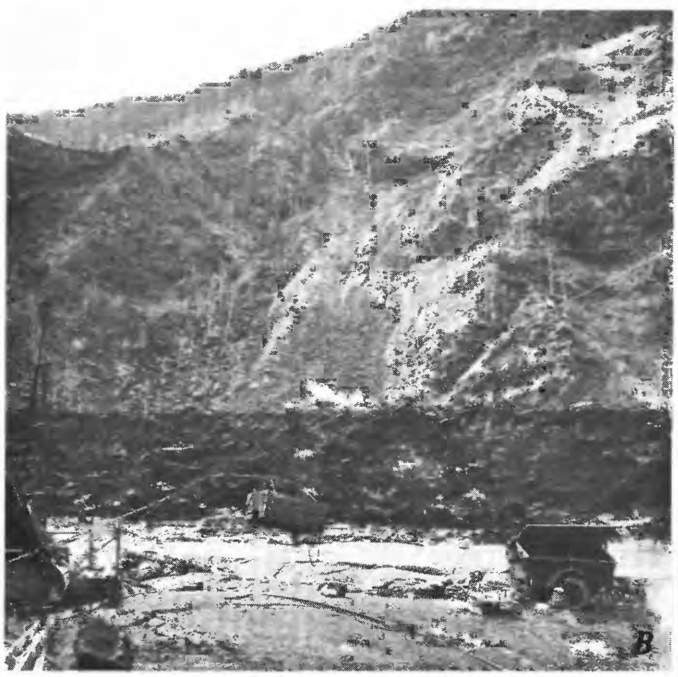

FIGURE 6.—Photographs of the tramway used to transport equipment from the rim to the floor in 1968–69. *A*, The arrangement is similar to that shown in figure 5 but a higher A-frame and heavier cable were used. *B*, Foreground shows equipment trailer, litter used to take equipment from tram to drill site, core box (lower left) and sheathed thermocouple (center). Trail to get in and out of crater goes up the left side of the talus in the background, thence up the ridge between the east and west pits, to the top.

tungsten carbide bits in a portable mast-mounted drill powered by a 9-hp gasoline engine (fig. 7). Drilling pressure was maintained by a separate hydraulic feed mounted on the drill mast. Coolant water was pumped by a 3¼-hp gasoline-powered water pump to the drill string from a 50-gallon steel drum at the drilling site. The steel drum was filled by gravity feed through ¾-in. plastic hose from a 400-gallon tank trailer parked on the rim of the crater. Water consumption averaged about 20–25 gallons per linear foot of drilling. A 1-foot long starting barrel and a 5-foot long core barrel were used in all of the holes. The drill stem was pulled from the hole at intervals of 1 or 2 feet, and core was removed from the core barrel. Core recovery was poorest in the highly vesicular crust from 0.3–1.2 m below the surface and in the interval where the temperature of the crust was between 700°C and 950°C before drilling. The reason for poor recovery in the deeper zone is not known. Recovery was very good between 950°C and the crust-melt interface at 1,070°C. No true core was recovered from the melt at temperatures above 1,070°C, but melt samples were obtained by other means. A core log for the first 24 holes is given in table 24.

The drilling operation was suspended after July 22, 1966, pending acquisition of a new heavy-duty drilling rig (fig. 8), which was moved by helicopter into Makaopuhi crater in October 1968. The rig was mounted on a trailer and powered by a gasoline engine rated at 14 hp at 2,200 rpm. Drilling pressure was maintained by an internal hydraulic system, and coolant water was supplied by a 7-hp gasoline-powered water pump. The drill stem, consisting of an NX (3 in. diam) core barrel fitted with tungsten carbide bit and reaming shell, and AX rods (1½ in. diam), was assembled and raised or lowered into the hole with the aid of a cable winch attached to the top of the drill. The design and construction of the superstructure on the trailer was by the shop staff of the Hawaiian Volcano Observatory. Coolant water was provided by a sled-mounted pump powered by a 9-hp gasoline engine. Water consumption was considerably higher than in

FIGURE 7.—Photograph of portable drilling rig used in 1965–66. Drill (left) is powered by a connected chain saw motor (left hand) and drill is lowered and raised by a hydraulic feed (right hand). Coolant water is pumped (right center) from two 50-gallon drums. Steam rises from the March 1965 vent area; main vent is out of picture toward right background. Highest level of lava lake before drainback is recorded by the "bathtub ring" in background.

the earlier drilling, averaging over 100 gallons per linear foot.

Three holes were drilled between November 6, 1968, and January 31, 1969, two at the same site near the center of the lake, one adjacent to the island of crust to which the lower end of the tramway was attached (locations are shown in figs. 3 and 4, numbers 68–1, 68–2, 69–1). The drill stem was pulled and core removed every 1 foot for the first 3 feet and every 5 feet below that. Core recovery was excellent, averaging about 80 percent overall, and 100 percent recovery was common for many 5-foot intervals. Core samples for drill holes 68–1, 68–2, and 69–1 are shown in figures 24–26, and core logs are given in table 25.

Two unexpected incidents accompanied the drilling of holes 68–1, 68–2, and 69–1 near the crust-melt interface. In 68–1 and 68–2, drilling somewhat past the crust-melt interface resulted in eruption of gushers of glassy black sand onto the surface. This sand was evidently produced by the quenching of melt to a glass (sideromelane) by the contact with drilling water; the glass then shattered because of thermal stresses. In

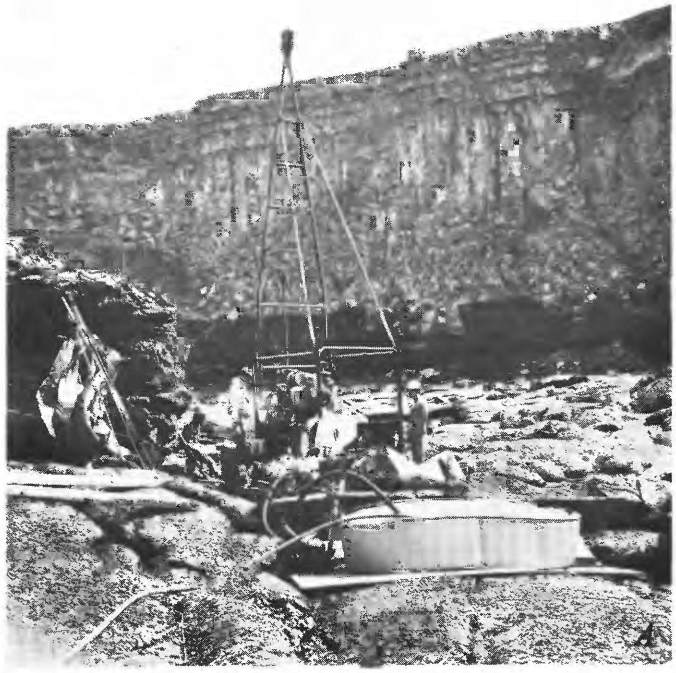

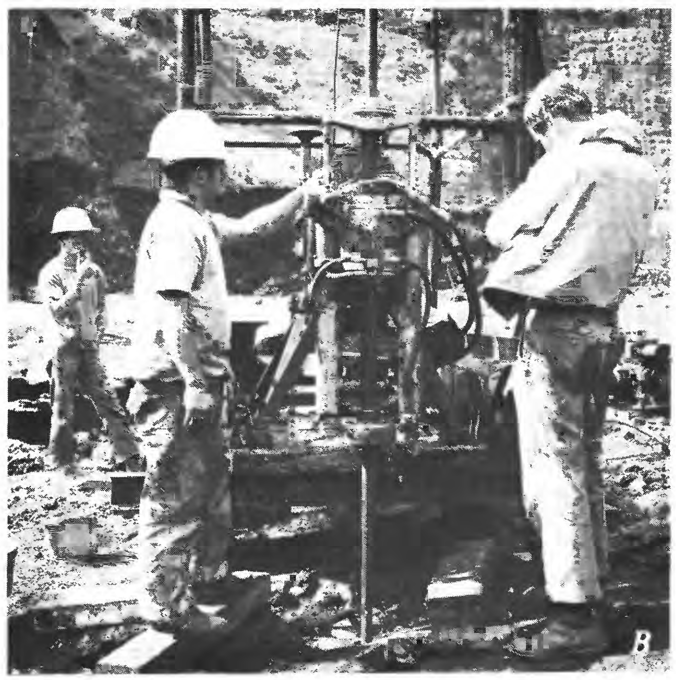

FIGURE 8.—Photographs of trailer-mounted drill rig used during 1968–69. *A*, A distant view showing the A-frame. Water is brought from the rim by hose and stored in a child's swimming pool (foreground) from which it is pumped to cool the drill string. *B*, A closer view of the drilling head. The water pump is shown in the right background. Drilling was done using an NX core barrel and bits attached to an AX drill string.

drill hole 69–1 we were able to continue drilling for 2 feet into the melt, but no core was removed when the drill stem was pulled. The glassy core probably shattered but the greater depth of the hole prevented the products from reaching the surface. We reentered the hole successfully, but while drilling another 5 feet the cooling water was insufficient to quench the melt and molten basalt poured into the core barrel. The drill stem was pulled with difficulty, and the core barrel contained a 5-foot-long sample of almost pure glass, presumably a reasonable sample of the melt (probably minus some crystals) near the maximum depth of penetration.

SAMPLING OF MELT AND CASING DRILL HOLES BELOW THE CRUST-MELT INTERFACE

Several different techniques were devised over the years for penetrating melt in order to obtain samples or emplace steel casings for temperature measurements. The first successful technique was to drill 1 to 2 feet into the melt, remove the drill stem,[3] and wait for the bottom of the hole to heat to 1,070°C. In the most successful attempts this took less than 1 hour, after which a stainless-steel casing having a loose-fitting cap packed with asbestos was pushed into the melt. Then a 2-foot long, open ceramic tube fastened to a ⅜ in. (1 cm) solid stainless-steel rod was lowered in the casing and used to push out the cap. Melt was collected directly in the ceramic tube and, after retrieval of the tube, by flow into the stainless-steel casing. Samples M20–11 to 13, M21–24, 26, and 27, and M22–18 (table 24) were collected in this way. This method was not entirely satisfactory, because the ceramic tube broke in all of the sampling attempts, so that a relatively small amount of sample was collected directly. The stainless steel casings, however, contained up to 5 feet of quenched liquid. The samples in the casing were not suitable for all studies as they were found to be modified in three ways: reduction of some ferric to ferrous iron; gain of total iron and gain or loss of minor elements through reaction with the steel; and differential removal of crystals from liquid during flow.

During these early sampling attempts, the crust was about 4.6 m thick. Later, when the crust was 7–8.8 m thick, this sampling technique no longer worked. Drilling 1 or 2 feet into melt either resulted in an immediate blast of superheated steam, or, if the water supply was shut down, the hole heated up too much even before the drill string was uncoupled and melt flowed into the drill bit. Samples of melt adhering to the bit are very glassy and at the time of collection were believed to have had crystals removed during flow into the bit, an observation verified when chemical data were obtained.

[3]Generally there was no return of superheated steam. Where steam did return, controlled sampling was impossible because the bottom of the hole heated up during the steam blast and melt flowed into the bit.

The problem of emplacing a solid end[4] casing in melt was solved by a drilling technique devised by R. S. Fiske and R. T. Okamura. A stainless-steel casing was prepared prior to drilling by affixing a doubly threaded solid plug between the threaded casing and drill bit. By use of normal drilling techniques, the melt was penetrated to a depth of several inches (not 1–2 ft as in earlier attempts), and the drill string was withdrawn and immediately replaced by the stainless-steel casing and attached bit. Drilling was resumed without coolant water, which enabled us to penetrate several additional inches into the melt without any danger of a blast of superheated steam. Penetration during "dry" drilling ceased because either the entry of the cold steel casing chilled the melt or a temperature inversion formed below the crust-melt interface. In any case, within an hour after drilling, the hole had warmed sufficiently to enable the casing to be pushed by hand to any desired depth in the melt. Temperature profiles in the melt were obtained within casing emplaced in this manner for drill holes 23 and 24.

MEASUREMENT OF TEMPERATURE

During the eruption, temperatures were measured at the edge of the lava lake using a glowing-filament optical pyrometer and a Cr-Al thermocouple. These temperatures were all found to be too low to correspond to the true temperature of samples collected at the time the temperature measurements were made. The reasons for this are discussed elsewhere (Wright and others, 1968, table 4 and discussion, p. 3198 ff).

Temperature profiles in open and cased drill holes were obtained using 14, 18, and 20 gage Cr-Al and 20 gage Pt-Pt Rh_{10} thermocouple elements threaded into 2-, 4-, or 6-hole ceramic beads and protected by a ½ in. or ⅜ in. outer diameter stainless-steel sheathing. Electromotive force (emf) values were measured using a portable millivolt potentiometer and an ice-water mixture as a reference. Absolute temperatures are accurate to more than 1 percent of the measured value (±10° at 1,000°C); relative temperatures are good to less than ±5°C judging from single temperature-depth profiles. A complete record of temperature measurements is contained in table 26 and figure 27. Thermal equilibrium was reestablished within 1 week after drilling as judged by the regular variation of isotherm

[4]This type of casing was used solely for temperature measurements.

depth with time (fig. 10). Most temperature profiles were obtained in drill holes left open in the upper crust of the lake. Several profiles in 1966 were obtained in holes cased with stainless steel to a maximum depth of 15 feet (4.6 m) below the crust-melt interface. Thermocouples were calibrated in the drill holes by use of melting-point standards enclosed in evacuated silica glass capsules: Ag (melting point = 961°C.); Au (melting point = 1,063°C); hexagonal GeO_2 (melting point = 1,115° ± 4°C).

The thermocouple elements were used repeatedly up to temperatures as much as 1,070°C with reproducible accuracy. When the thermocouples were first exposed to temperatures of more than 1,100°C in holes cased with stainless steel, serious contamination of the elements resulted in reduced emf's and erroneous temperature determinations. The contamination effects could not be reproduced by heating to similar temperatures in laboratory furnaces; consequently, the mechanism of contamination is not known. Our best guess is that the stainless-steel casing and the thermocouple sheathing in contact with molten basalt were permeable to gas exsolved from the melt, which catalyzed reaction between the stainless steel and the thermocouple elements. The Pt-$PtRh_{10}$ elements became contaminated within 15 minutes after exposure to temperatures of more than 1,100°C. Temperatures obtained subsequent to contamination were as much as 100°C low at true temperatures of 900°–1,100°C. Cr-Al elements remained uncontaminated for a longer period (up to several hours after exposure to temperatures of more than 1,100°C), and the effect of contamination was less severe, producing nearly constant drop in apparent temperature over the whole range of temperatures measured (fig. 28).

The problem of contamination was, in part, traceable to use of ungraded stainless steel for sheathing. Later, use of 14-gage Cr-Al elements protected by Type 304 stainless sheathing extended the time before detectable contamination to about 10 hours.

Table 1 shows semiquantitative spectrographic analyses of the stainless-steel casing before contact with melt and fresh and contaminated thermocouple elements. Appreciable exchange of Fe and Cr evidently took place between the casing and the thermocouple elements. Other mobile elements were Pd, Mn, Mg, and Cu. Ni was notably unreactive, at least as far as the platinum thermocouple elements are concerned.

Differential thermal expansion of the stainless-steel sheathing relative to the enclosed thermocouple elements, particularly Pt-$PtRh_{10}$ elements, resulted in the junction being separated from the bottom of the sheathing. Sometimes the junction itself was broken by tension put on the thermocouple during expansion. These problems were solved in various ways, but they constitute another reason for favoring the use of Cr-Al over Pt-$PtRh_{10}$ thermocouple elements.

ADDITIONAL FIELD STUDIES

In August 1965, when the crust was 4.6 m thick, we successfully emplaced a rotational viscometer in the melt. Results of this viscosity study are reported by

TABLE 1.—*Contamination effects of thermocouple elements used in Makaopuhi lava lake*

[Semiquantitative spectrographic analysis; M=major constituent, n.d.=looked for, but not detected; other numbers are reported in percent to the nearest number in the series 1, 0.7, 0.3, 0.2, 0.15, and 0.1, etc. which represent approximate midpoints of interval data on a geometric scale. The assigned interval will include the quantitative value about 30 percent of the time. Data for each wire are given as fresh (as purchased, before exposure to the lava lake, or used (after about 3 hours exposure at temperatures about 1,100–1,140°C in drill hole 23). Analysts: Nancy Conklin (type 304), Joseph L. Harris (all others)]

	Type 304 Stainless	Cromel wire (Leeds and Northrop)		Alumel wire (Leeds and Northrop)		Pt wire (Englehard Industries)		$Pt_{90}Rh_{10}$ wire (Englehard Industries)	
	Fresh	Fresh	Used	Fresh	Used	Fresh	Used	Fresh	Used
Si	n.d.	0.7	0.7	3.0	3.0	n.d.	n.d.	n.d.	n.d.
Al	0.1	.001	.001	2.0	1.5	n.d.	n.d.	n.d.	n.d.
Fe	M	.2	.7	n.d.	2.0	n.d.	0.3	n.d.	0.2
Mg	.005	.001	.001	.007	.001	n.d.	n.d.	n.d.	n.d.
Ba	.005	n.d.	n.d.	n.d.	.0007	n.d.	n.d.	n.d.	n.d.
Cd	n.d.	.0015	.001	.1	.1	n.d.	n.d.	n.d.	n.d.
Co	.07	.1	.1	1.0	.7	n.d.	n.d.	n.d.	n.d.
Cr	M	M	M	.007	.7	n.d.	.1	n.d.	.03
Cu	.2	.01	.015	.015	.05	n.d.	.007	0.0007	.002
Mn	1.5	.002	.03	.7	.7	n.d.	.01	.0007	.05
Mo	.15	n.d.	n.d.	n.d.	n.d.	n.d.	n.d.	n.d.	n.d.
Ni	M	M	M	M	M	n.d.	n.d.	n.d.	n.d.
Pd	n.d.	n.d.	n.d.	n.d.	n.d.	n.d.	.002	.005	n.d.
Pt	n.d.	n.d.	n.d.	n.d.	n.d.	M	M	M	M
Sn	n.d.	n.d.	.002	n.d.	.003	n.d.	n.d.	n.d.	n.d.
V	.015	n.d.	n.d.	n.d.	n.d.	n.d.	n.d.	n.d.	n.d.

Shaw, Wright, Peck, and Okamura (1968). In June 1965, we began a program of direct measurement of oxygen fugacity in the drill holes, using a probe devised by M. Sato (fig. 9*B*). Preliminary results of these studies are reported by Sato and Wright (1966); later results are summarized by Grommé, Wright, and Peck (1969) and in this paper. During and following the eruption, members of the chemistry department of the University of Hawaii in cooperation with the Hawaii Institute of Geophysics made gas collections from the drill holes; their results were published by Finlaysen, Barnes, and Naughton (1968).

FIGURE 9.—Photographs of field studies. *A*, Leveling on the surface of Alae lava lake. Zeiss level is shown at left, 12 foot Invar rod at right. This equipment was also used throughout the study of Makaopuhi lava lake. *B*, Measurement of oxygen fugacity. The oxygen probe sheathed in ceramic is attached to a hollow stainless steel rod through which platinum leads are threaded. The leads are connected to an electrometer (lower right) from which the emf is read.

Temperature measurements are made in analagous fashion using thermocouple wire threaded through ceramic leads and sheathed in stainless steel; leads are connected through a cold junction (ice-filled thermos jug at lower right) to a millivolt potentiometer (not shown).

OBSERVATIONS

THERMAL HISTORY

Figure 10 summarizes our best estimate of the position of isothermal surfaces as a function of time and depth in the lake. Temperature-depth profiles (figs. 27, 28) were drawn for each set of measurements from raw data given in table 26. The interpolated depths to selected isotherms (tables 2, 3) are taken from profiles measured at least 1 week after drilling, so that the cooling effect of drill water is minimized. Data for the 500°, 961°, and 1,070°C isotherms taken from *all* drill holes are shown as an inset in figure 10 to give some idea of the control on drawing the isothermal surfaces. The depth of the crust-melt interface determined from drilling is summarized in table 4. Table 5 gives the results of melting experiments on Ag, Au, and GeO_2 that were used to calibrate the temperature profiles in the melt. The data of tables 2–5 form the basis for the construction of figure 10.

The isotherms of figure 10 are drawn from data collected from below the central part of the lava lake and thus reflect loss of heat to the surface of the lake. Two drill holes, 11 and 12 (figs. 3, 27), close to the edge of the lake cooled faster than predicted from the gradients shown in figure 10, because of heat loss through the wall as well as at the surface of the lake. Hole 12 was drilled through the thin crust at the edge of the lake. At the time of the first temperature measurement the maximum temperature was 750°C at a depth of 5.3 m, the base of the lake being about 6.4 m.

At any one time the depth measured to an isotherm in different drill holes differed by as much as 0.5 feet, although generally less than 0.3 feet (table 2). This probably reflects in a qualitative way differing physical properties of the wallrock from hole to hole and the uncertainty (0.1 ft) in placement of thermocouple junc-

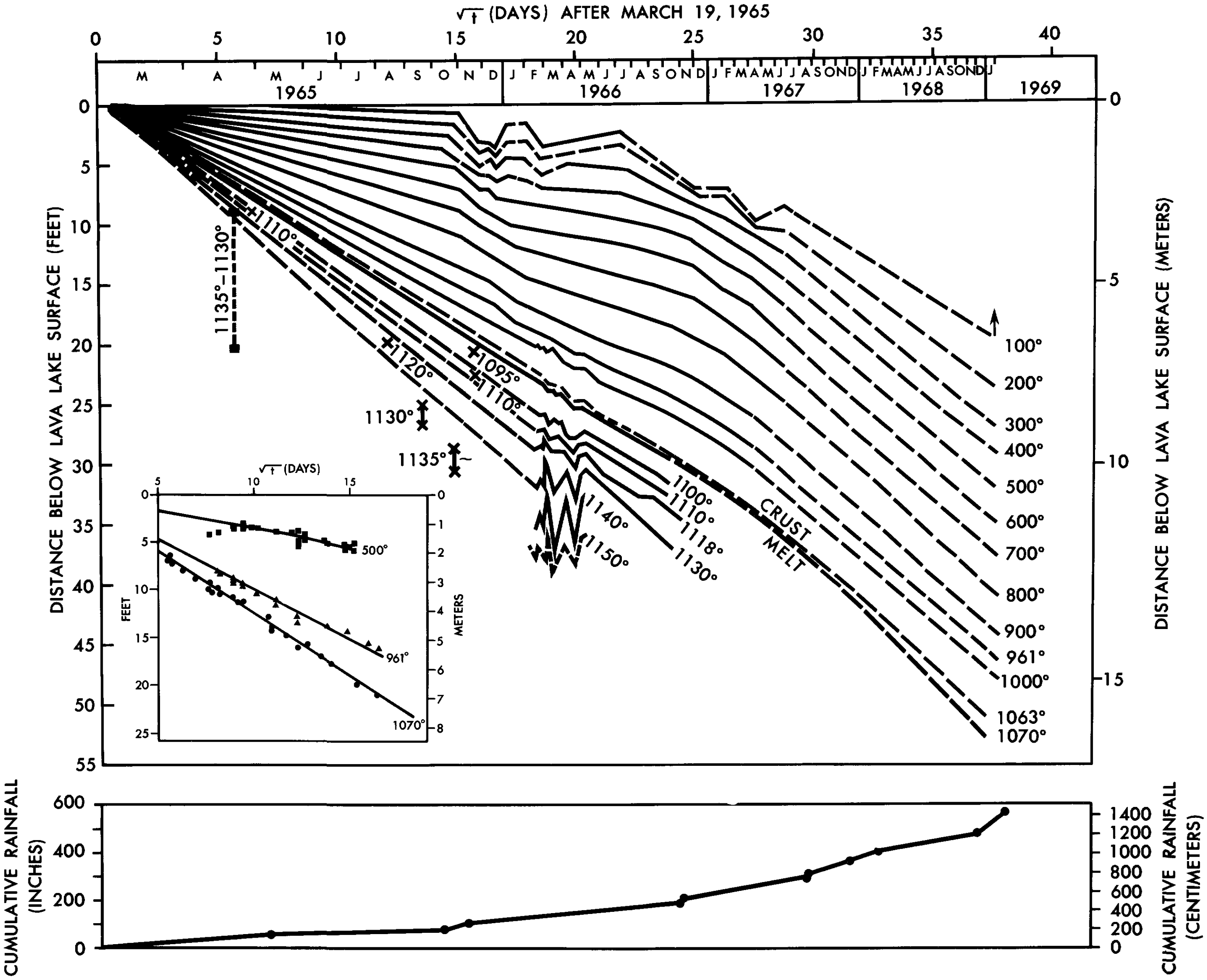

FIGURE 10.—Isotherms plotted as a function of square root of time $\sqrt{t}$ (days) and depth below lava-lake surface. Isotherms are dashed where interpolated. Data used to construct the figure are given in tables 2–5. Plotted below, at the same square root of time scale, is the cumulative rainfall that fell on the lake surface. The inset (lower left) shows all measurements made at least 2 weeks after drilling for three different isotherms. Single temperature profiles are reproducible within 5°C; most of the scatter represents real temperature differences between drill holes.

A single temperature profile in melt on April 19, 1965, is shown by a vertical dashed line. Solid squares (■) represent temperatures of melt samples estimated from their crystallinity (fig. 17); these are consistent with the isotherm extrapolations. Temperature fluctuations in the 1,070–1,140°C isotherms in early 1966 are real. All isotherms lower than 1,130°C can be extrapolated linearly back to a common origin at depth=0, $\sqrt{\text{time}}$=0.5 day, but each isotherm begins to deviate from linearity at different times between October 1965 and January 1966. Depression of low temperature isotherms reflects the effect of heavy rainfall; fluctuations of high-temperature isotherms are attributed to melt convection. Isotherms have been dashed to fit the last temperature profile obtained in January 1969 but the temperatures in the crust measured at this time may be depressed because of the effects of drilling water.

See text for further explanation and interpretation of the figure.

tions. For example, a hole that intersected few fractures might be hotter than a hole in which heat was dissipated laterally through fractures. Insofar as possible, the isotherms drawn in figure 10 were constructed from data in a single drill hole over the period of time that the maximum temperature in the drill hole exceeded the isotherm in question.

During early cooling, the isothermal surfaces moved downward as a linear function of the square root of time ($\sqrt{t}$ (days)), behavior expected of lava cooling mainly by conduction. The isotherms extrapolate to an intersection at $\sqrt{t}$ (days)=0.5 days, about 17 hours

TABLE 2.—*Depth to isothermal surfaces in the upper crust of Makaopuhi lava lake*

[Left hand column gives the date, followed, in parentheses, by the square root of time in days after March 19, 1965; the second column gives the drill hole number, followed, in parentheses, by the number of days separating drilling of the hole from measurement of the reported temperatures; the remaining columns give the depth (in feet) to the isotherm listed in the reading. Depths enclosed by parentheses are extrapolated; others are read directly from the temperature profiles (see table 26, figures 27, 28)]

Date	Drill hole No.	Temperature (°C)											
		100	200	300	400	500	600	700	800	900	961	1,000	1,063
4/21/65 (5.72)	1(2)			1.9	2.3	2.8	3.3	3.8	4.4	5.1		5.9	6.7
4/28/65 (6.31)	3(1)			1.9	2.3	2.8	3.3	3.9	4.6	5.5		6.6	7.4
5/5/65 (6.83)	3(7)			2.9	3.3	3.7	4.2	4.8	5.5	6.4		7.5	
5/17/65 (7.67)	3(19)			2.9	3.6	4.2	4.9	5.7	6.5				
5/24/65 (8.11)	3(26)	1.7	2.3	2.7	3.3	4.1	4.9	5.6	6.6				
	4(7)		1.3	2.1	2.9	3.7	4.5	5.3	6.3	7.4	8.2	8.9	
5/26/65 (8.23)	6(9)	1.0	1.7	2.4	3.1	3.8	4.6	5.5	6.5	7.7	8.5	9.2	
6/7/65 (8.93)	4(21)		0.9	1.7	2.6	3.5	4.4	5.4	6.6	8.0	8.9		
	5(19)		.9	1.7	2.5	3.5	4.5	5.6	6.8	8.3	9.3	10.0	
	6(21)		1.1	1.8	2.6	3.5	4.5	5.6	6.8	8.3			
	8(14)		1.1	1.8	2.6	3.4	4.4	5.4	6.6	8.0	8.9	9.6	
	9(12)		1.1	1.8	2.6	3.5	4.5	5.6	6.8	8.1	9.0	9.7	
	10(12)		1.3	2.1	2.9	3.8	4.8	5.8	6.9	8.2	9.1	9.8	
6/16/65 (9.42)	4(30)		0.8	1.6	2.4	3.3	4.4	5.5	6.8	8.4			
	5(28)		.8	1.5	2.4	3.4	4.5	5.7	7.0	8.5	9.5		
	6(30)	0.6	1.0	1.6	2.4	3.4	4.5	5.7	7.0	8.5			
	8(23)		.9	1.7	2.5	3.4	4.4	5.6	6.9	8.4	9.5		
	9(21)		.9	1.6	2.5	3.4	4.5	5.7	6.9	8.4	9.4		
	10(21)		.9	1.7	2.6	3.5	4.6	5.8	7.1	8.5	9.6	10.3	
6/26/65 (9.93)	6(32)				2.5	3.5	4.6	5.9	7.4				
6/30/65 (10.14)	4(44)		1.0	1.8	2.7	3.6	4.7	6.0					
	8(37)		1.0	1.7	2.5	3.5	4.5	5.7	7.2	8.8			
	9(35)		.9	1.7	2.6	3.6	4.7	6.2	7.6	9.4			
	10(35)			1.6	2.5	3.6	4.7	6.0	7.4	9.0	10.3		
7/21/65 (11.13)	10(56)			2.0	2.8	3.9	5.2	6.6	8.2	10.0			
	13(40)		1.1	2.0	2.9	4.0	5.2	6.6	8.2	10.0			
	14(35)			2.0	2.9	4.0	5.2	6.5	8.0	9.8	11.1		
	17(5)		1.8	2.6	3.4	4.4	5.5	6.8	8.4	10.2	11.5	12.4	14.2
8/10/65 (11.99)	10(76)		1.3	2.1	2.9	4.1	5.5	7.0	8.7				
8/17/65 (12.28)	8(85)		0.9	1.8	2.8	4.0	5.5	7.2	9.1				
	16(33)		1.3	2.2	3.3	4.7	6.2	7.9	9.7	11.9	13.6		
	20(15)		1.5	2.5	3.7	5.0	6.3	7.8	9.5	11.4	12.8	13.9	

TABLE 2.—*Depth to isothermal surfaces in the upper crust of Makaopuhi lava lake*—Continued

Date	Drill hole No.	Temperature (°C)											
		100	200	300	400	500	600	700	800	900	961	1,000	1,063
8/25/65	6(100)				2.0	3.0	4.3	5.9	7.6				
(12.60)	17(40)		0.8	1.4	2.4	3.5	4.7	6.1	7.8	9.6			
9/23/65	6(129)			--			4.9	6.5	8.2				
(13.70)	10(120)			1.5	2.5	3.7	5.0	6.5	8.1	9.9			
9/27/65	16(74)				2.5	3.7	5.1	6.6	8.4	10.4	12.8		
(13.85)	20(56)				2.7	3.9	5.1	6.6	8.3	10.2	12.4	14.0	
10/24/65	17(101)			2.0	3.0	4.1	5.4	7.0	8.8	11.0			
(14.82)	21(24)				3.2	4.3	5.6	7.1	8.9	10.8	13.0	14.6	16.0
10/27/65	8(156)		1.0	1.9	2.9	4.1	5.4	7.0	8.8				
(14.92)	16(104)		0.6 ±	1.8	2.9	4.1	5.5	7.1	9.0	11.1	13.6		
11/4/65	10(162)			--	2.6	3.8	5.2	6.9	8.8				
(15.16)	20(95)		0.9	1.8	3.0	4.3	5.8	7.3	9.0	11.1	13.5		
11/27/65	21(57)		3.2	4.1	5.1	6.1	7.3	8.6	10.1	11.9	14.1	15.8	
(15.90)													
12/13/65	20(134)		3.4	3.6	4.7	6.1	7.5	9.1	10.8	12.7			
(16.38)	22(34)			--	4.0	5.5	7.0	8.7	10.5	12.5	14.8	16.3	
12/20/65	21(80)		4.0	4.6	5.5	6.5	7.8	9.3	10.8	12.7	15.2		
(16.61)													
1/5/66	22(57)		1.8	2.7	4.1	5.7	7.3	9.1	11.0	13.1	15.6		
(17.08)	23(23)				4.8	6.5	8.2	9.9	11.6	13.6	15.9	17.5	18.7
1/19/66	23(37)								11.9	14.0	16.5	18.2	19.5
(17.48)													
2/1/66	21(123)		4.0	5.5	6.9	8.5	10.3	12.3	14.5				
(17.85)	22(84)		2.4	4.0	5.7	7.6	9.6	11.7	14.0				
2/3/66	20(186)	1.6	3.2	4.7	6.4	8.1	10.0	12.1					
(17.91)													
2/18/66	23(15)									17.3	19.0	(20.2)	(22.8)
(18.33)													
2/25/66	14(254)	3.6	4.5	5.9	7.3	8.9	10.6						
(18.51)	16(225)		4.7	6.0	7.4	9.0	10.9	12.9					
	20(208)			5.3	6.8	8.5	10.5	12.6					
	21(147)				7.3	8.8	10.6	12.5	14.8				
	22(108)				6.8	8.5	10.3	12.4	14.8				
	23(22)											(20.6)	(23.2)
3/3/66	23(34)						10.9	12.8	15.0	17.7	(19.5)	(20.8)	(23.6)
(18.31)													

TABLE 2.—*Depth to isothermal surfaces in the upper crust of Makaopuhi lava lake*—Continued

Date	Drill hole No.	Temperature (°C)											
		100	200	300	400	500	600	700	800	900	961	1,000	1,063
3/15/66 (18.99)	23(41)									18.0	19.6	20.8	23.6
3/28/66 (19.34)	21(178)					9.1	11.0	13.1	15.7				
4/4/66 (19.52)	23(61)						11.1	13.1	15.6	18.4	20.3	21.7	24.2
4/11/66 (19.70)	20(253)			5.1	7.0	8.9	11.0	13.4					
	21(192)				7.1	8.9	11.0	13.4					
	22(153)					8.4	10.5	12.9	15.6				
	23(68)										20.5	21.9	24.7
4/19/66 (19.90)	23(76)										20.9	22.2	25.1
4/25/66 (20.05)	23(82)										(20.7)	(22.0)	(24.9)
5/6/66 (20.32)	23(93)										20.9	(22.2)	(25.0)
6/1/66 (20.95)	22(204)				7.1	9.0	11.2	13.7					
6/2/66 (20.97)	20(304)			5.3	7.3	9.3	11.5	14.0					
	24(9)			5.7	7.8	10.0	12.4	14.7	17.1	19.8	21.9	23.3	
7/8/66 (21.81)	21(280)						11.8	14.4	17.2				
	22(241)				7.3	9.2	11.5	14.1					
	24(45)	2.4	3.6	5.5	7.5	9.5	11.9	14.3	17.2	20.4	22.4		
8/15/66 (22.67)	21(318)					10.1	12.1	14.8	17.7				
9/13/66 (23.30)	21(347)					10.3	12.5	15.3	18.3				
	24(112)					10.1	12.5	15.2	18.2	21.4	23.3	25.4	
10/13/66 (23.93)	24(142)								18.4	22.0	24.4	26.0	29.2
11/29/66 (24.89)	24(189)	7.2	7.6	8.4	9.7	11.5	13.7	16.3	19.5	23.0	25.5	27.2	30.4
2/2/67 (26.17)	24(254)	7.2	7.9	9.5	11.3	13.3	15.7	18.1	21.0	24.5	27.1	28.8	
4/7/67 (27.36)	24(319)	10.0	10.3		12.7	14.7	17.0	19.8	22.8	26.3	28.8		
6/22/67 (28.72)	24(395)	8.8	10.8	12.7	14.8	17.0	19.5	22.2	25.0				
12/11/68 (36.90)	68-1 (21)	20.8	23.9	27.0	30.1	33.2	36.3	39.4	42.4	45.0	47.0	48.2	51.8
1/22/69 (37.47)	68-1 (35)	20.6	24.5	27.4	29.8	32.5	35.4	38.2	41.5	45.0	47.3	48.6	52.1

TABLE 3.—*Temperature profiles used to construct isotherms in the melt of Makaopuhi lava lake*

[A complete record of measured temperature is included in figures 27,28. See text for discussion of thermocouple contamination and the corrections applied as a result of contamination. Numbers in parentheses have been corrected from measured values.]

Date	$\sqrt{t}$ (days) after 3/19/65	Drill hole No.	Depth (ft)	Temperature (°C)	Thermocouple notes[1]
4/21/65	5.72	2	9.1	1,131	5 junction Cr-Al (18 gauge wire).
			12.1	1,134	
		(cased with	15.1	1,128	
		drill steel)	18.1	1,134	
			21.1	1,136	
4/28/65	6.31	3	9.0	1,110	
7/20/65	11.08	17	12.0	995	Single junction Pt-PtRh10 (20 gauge wire).
		(cased with	13.0	1,032	
		ceramic)	14.0	1,064	
			14.6	1,076	
11/9/65	15.35	22	21.0	1,085	Single junction Pt-PtRh10 (temperature still rising when ooze came into sampler).
		(open stainless steel sampling tube)	21.6	1,092+	
12/13/65	16.39	23	20.9	1,072	Single junction Pt-PtRh10 (20.9 ft just above crust-melt interface. Temperature rose to 1072°, and levelled off in 6 hours).
2/9/66	18.08	23 (cased with stainless steel)	36.7	1,150	Single junction Pt-PtRh10. Reading obtained in first 10 minutes prior to contamination.
2/18/66	18.33	23	23.1	(1,070)	Single junction Pt-PtRh10.
			23.6	(1,080)	
			24.6	(1,090)	Reproduced profile corrected by +17°C from measured values.
			25.9	(1,100)	
			27.3	(1,110)	
			28.8	(1,118)	
			32.7	(1,130)	
			36.0	(1,140)	
2/23/66		23			Single junction Pt-PtRh10. Erratic profiles with apparently high temperature corrections. Not used.
2/28/66					
3/1/66					
3/3/66					
3/8/66	18.81	23	24.2	(1,070)	Single junction Pt-PtRh10. Reproduced profile corrected by +27°C from measured values.
			24.9	(1,080)	
			25.9	(1,090)	
			26.8	(1,100)	
			28.0	(1,110)	
			29.0	(1,118)	
			31.0	(1,130)	
			33.7	(1,140)	
			37.0	(1,150)	
3/15/66	18.99	23	24.0	1,070	New, single junction Cr-Al, 14 gauge wire. Uncorrected profile.
			24.7	1,080	
			25.5	1,090	
			26.5	1,100	
			28.0	1,110	
			29.4	1,118	
			32.5	1,130	
			37.5	1,140	
3/22/66		23			Erratic profile. Not used.
3/28/66	19.33	23	24.4	(1,070)	Single junction Cr-Al, 14 gauge wire. Reproduced profile corrected by +20°C from measured values.
			25.0	(1,080)	
			25.7	(1,090)	
			26.6	(1,100)	
			27.7	(1,110)	
			29.0	(1,118)	
			31.0	(1,130)	
			34.2	(1,140)	
4/4/66	19.52	23	24.7	1,070	New, single junction Cr-Al, 14 gauge, wire. Some erratic readings. Uncorrected profile.
			25.3	1,080	
			26.5	1,090	
			27.5	1,100	
			28.5	1,110	
			29.3	1,118	
			30.7	1,130	
			33.0	1,140	
4/11/66	19.70	23	25.1	1,070	Single junction, Cr-Al, 14 gauge wire. Uncorrected profile.
			25.9	1,080	
			26.8	1,090	
			27.8	1,100	
			29.0	1,110	
			30.1	1,118	
			32.5	1,130	
			35.6	1,140	

TABLE 3.—*Temperature profiles used to construct isotherms in the melt of Makaopuhi lava lake*—Continued

Date	$\sqrt{t}$ (days) after 3/19/65	Drill hole No.	Depth (ft)	Temperature (°C)		Thermocouple notes[1]
4/19/66	19.90	23	25.5	1,070		New, single junction Cr-Al, 14 gauge wire. Uncorrected profile.
			26.2	1,080		
			27.1	1,090		
			28.0	1,100		
			29.0	1,110		
			30.3	1,118		
			32.6	1,130		
			37	1,140	(extrapolated)	
4/25/66	20.05	23	25.2	(1,070)		Single junction Cr-Al, 14 gauge wire. Reproduced profile corrected by +17°C from measured values.
			25.9	(1,080)		
			26.5	(1,090)		
			27.3	(1,100)		
			28.3	(1,110)		
			29.2	(1,118)		
			30.6	(1,130)		
			32.3	(1,140)		
5/6/66	20.32	23	25.5	(1,070)		Single junction Cr-Al, 14 gauge wire. Reproduced profile corrected by +13°C from measured values.
			26.1	(1,080)		
			26.8	(1,090)		
			27.8	(1,100)		
			28.8	(1,110)		
			29.7	(1,118)		
			30.7	(1,130)		
			32.5	(1,140)		
9/13/66	23.28	24 (cased with stainless steel)	28.6	1,070		New, two-junction Cr-Al, 14 gauge wire. Uncorrected profile.
			29.4	1,080		
			30.0	1,090		
			31.0	1,100		
			32.0	1,110		
			33.2	1,118		
			36.0	1,130		
			39.0	1,135		
10/13/66	23.92	24	29.6	1,070		Two-junction Cr-Al, 14 gauge wire. Uncorrected profile.
			30.3	1,080		
			31.0	1,090		
			32.0	1,100		
			33.1	1,110		
			34.6	1,118		
			37.5	1,130		
			40.5	1,135		

[1]Several types of thermocouples were used in the melt, single junction Pt-$PtRh_{10}$, single junction Cr-Al, and multijunction Cr-Al. All thermocouples were protected by stainless steel casings and all, with repeated use, showed effects on contamination of thermocouple elements above 1,100 C, as described in the text. The data plotted in fig. 10 is taken from profiles made with uncontaminated thermocouples and from profiles with contaminated thermocouple elements to which a constant independent temperature measurement correction based on melting of Ag, Au, and GeO_2 (table 5), has been applied. The melting experiments indicate that the contamination corrections are essentially linear to at least 1,120 C.

after a permanent crust formed on the lake. This 17-hour displacement reflects the fact that the lake surface was hotter than ambient air temperature during the early cooling. Later deviations from linearity of the isotherms (apart from brief effects of coolant water noted immediately after drilling) are ascribed to two factors:

1. Depression of isotherms in the crust following periods of heavy rainfall;
2. Variable nonlinear behavior of isotherms because of nonconductive cooling.

These factors are discussed below in connection with the crust-melt cooling regime.

TEMPERATURE OF THE CRUST-MELT INTERFACE

The depth to the crust-melt interface was determined during drilling (table 4). The temperature of the interface was estimated from measurements made immediately after drilling and by extrapolation backwards from later temperature profiles obtained in cased drill holes in the melt. (table 3, fig. 10). The best estimate of the temperature of the crust-melt interface is 1,070°±5°C. The 1,063° isotherm (fig. 10), calibrated by melting of gold wire, is clearly at depths shallower than the crust-melt interface, and thus established a lower limit to the temperature of the interface. The actual points determined from drilling fall within the envelope approximately defined by the 1,063°–1,090° isotherms (fig. 10 inset). We do not interpret these as reflecting real temperature differences at the interface but rather reflecting the uncertainty in estimating the depth at which the interface was penetrated. These uncertainties become greater at greater depths, and in the 1968 drilling the depth is only known to within 0.6 m.

COOLING OF THE CRUST (T<1070°C)

The position of isotherms in the crust is a function of both conductive cooling and of the amount of rainfall on the surface. During the first 7 months following the

TABLE 4.—*Depth to crust-melt interface determined from drilling, and temperatures measured following drilling in Makaopuhi lava lake.*

Date	$\sqrt{t}$ (days) after 3/19/65	Drill hole No.	Depth to crust-melt interface (ft)	Temperature measured following drilling[1] depth (ft)	temperature (°C)
4/19/65	5.57	1	6.8		
Do	5.57	2	6.5		
4/21	5.72	2	7.2		
Do	5.72	1		6.7	1,064
4/22	5.80	1	7.0		
Do	5.80	2		7.0	1,055
4/28	6.31	3	8.0		
Do	6.31	3		8.25	1,064*
				8.0	1,056*
5/6	6.91	7	8.8		
Do	6.91	7		9.0	1,017
5/7	6.98	7		9.5	1,064
5/17	7.67	6	10.0		
Do	7.67	4	9.3		
5/19	7.79	5	10.3		
5/24	8.11	8	9.9		
5/26	8.23	9	10.2		
Do	8.23	10	10.4		
6/7	8.93	13	10.85		
6/11	9.16	13	11.3		
Do	9.16	13		11.0	1,051*
Do	9.16	13		11.75	1,068*
6/16	9.42	14	11.25		
Do	9.42	14		11.9	1,060
7/12	10.72	16	12.9		
7/16	10.91	16	13.9		
Do	10.91	17	14.2		
8/2	11.65	20	14.65		
8/17	12.28	21	16.0		
Do	12.28	21		18.0	1,069*
8/30	12.81	21	15.7		
9/16	13.42	21	16.9		
Do	13.42	21		19.0	1,076*
10/1	14.00	21	17.7		
Do	14.00	21		20.0	1,075*
11/9	15.33	22	19.7		
12/13/65	16.39	23	20.9		
Do	16.39	23		20.9	1,072*
1/19/66	17.48	23	22–22.5		
Do	17.48	23		20.9	1,072*
2/3/66	17.91	23	23±0.5		
5/23/66	20.74	24	26±		
7/28/66	22.26	24	29.0–29.3		
9/13/66	23.30	24		29.0	1,075*
11/18/68	36.59	MP68–1	52±2		
12/11/68	36.90	MP68–1		51.0	1,063*
12/18/68	37.00	MP68–2	53±2		

[1]Represents a minimum value for the equilibrium temperature at the stated depth. Starred * values are believed to be within 10° of equilibrium.

eruption, the isotherms moved downward as a linear function of the square root of time. This behavior is apparently independent of rainfall (table 6, fig. 10) which was great for 2 months following the eruption and much less for several months thereafter. We have no explanation for the absence of a rainfall effect, although it may be related to the position of the 100°C isotherm at the surface of the lake.

From mid-October to early November 1965, the isothermal surfaces began to be depressed to greater depths, the lower temperatures showing the effect earlier. This change is correlated with heavy rains beginning in October and especially evident in November (table 6; base of fig. 10). Then the isotherms showed recovery toward the linear extrapolation of their initial slope between March and September 1966, a dry period. Isotherms at 961°C and higher returned to their original projected slopes. After September 1966, the isotherms plunged abruptly, probably in part due again to increased rainfall and continued to be depressed through the last measurement date in June 1967.

Two temperature profiles (table 26) were obtained in drill hole MP68–1 in December 1968 and January 1969. Temperatures from the later profile are plotted in figure 10 and represent maximum depths for the labeled isotherms. An independent estimate of the depth to the 1,000° isotherm is made from microscopic

TABLE 5.—*Melting point data for* Ag *(961°C),* Au *(1,063°C), and* GeO_2 *(1,115°±4°C)*[1]

[Runs in Drill hole No. 23 are 10–15 minutes. Runs for GeO_2 in Drill hole No. 24 are ½ hour]

Date	$\sqrt{t}$ (days) after 3/19/65	Drill hole No.	Sample	Results
5/6/66	20.32	23	Ag	Melt precisely at 20.9 ft.
5/13/66	20.49	23	Au	25.5 (melt); 25.0 ft (no melt).
5/17/66	20.59	23	Au	25.6 ft (melt); 25.5 ft (no melt).
			GeO_2	30.8 ft (completely melted).
5/23/66	20.74	23	GeO_2	30.8 ft 30.3 ft (melt).
6/1/66	20.95	23	Ag	21.85 ft (melt); 21.70 ft (no melt).
			Au	26.2 ft (melt); 26.0 ft (no melt).
			GeO_2	30.8 ft (melt with few crystals); 30.2 ft (crystalline).
8/15/66	22.67	24	Au	27.9–29.0 ft (melt).
			GeO_2	33.0 ft (melt); 32.8–32.2 ft (melt+ progressively more crystals).
8/22/66	22.80	24	Au	28.03 ft (melt); 27.89 ft (no melt).
			GeO_2	32.6–31.85 ft (melt+crystals).
9/6/66	23.13	24	Ag	23.8 ft (melt); 23.6 ft (partly melted); 23.4 ft (no melt).
			Au	28.45 ft (melt); 28.35 ft (no melt).
			GeO_2	33.0 ft (melt); 32.2–32.8 ft (melt+crystals)
9/13/66	23.28	24	GeO_2	31.0–30.25 ft (some melt, mostly crystalline).
10/13/66	23.92	24	Ag	24.5 ft (melt); 24.3 ft (no melt).
			Au	29.5 ft (melt); 29.3 ft (no melt).
			GeO_2	34.5 ft (melt).
10/31/66	24.29	24	GeO_2	33.6–34.6 ft (mostly crystalline).
12/11/68	36.90	MP68–1	Ag	47.5 ft (melt).
			Au	51.5 ft (melt); 50.5 ft (no melt).

[1]When GeO_2 was melted concurrently with thermocouple measurements, the best melting temperature was 1,118°C.

TABLE 6.—*Rainfall record at Makaopuhi crater*

[Rain gage installed 3/19/65; destroyed 2/22/69]

Month	Year	Rainfall (in.)	Cumulative rainfall (in.)
March	1965	4.56	4.56
April		28.70	33.26
May		27.40	60.66
June		3.99	64.65
July		3.85	68.50
August		2.84	71.34
September		5.27	76.61
October		7.63	84.24
November		27.74	111.98
December		10.73	122.71
January	1966	6.82	129.53
February		9.53	139.06
March		5.18	144.24
April		3.02	147.26
May		8.27	155.53
June		5.62	161.15
July		8.67	169.82
August		4.37	174.19
September		8.78	182.97
October		11.36	194.33
November		27.00	221.33
December		5.95	227.28
January	1967	14.22	241.50
February		9.80	251.30
March		15.25	266.55
April		12.65	279.20
May		12.14	291.34
June		5.42	296.76
July		9.02	305.78
August		16.06	321.84
September		2.65	324.49
October		4.65	329.14
November		27.63	356.77
December		24.39	381.16
January	1968	29.49	410.65
February		10.58	421.23
March		8.77	430.00
April		20.16	450.16
May		6.89	457.05
June		8.79	465.84
July		6.40	472.24
August		4.86	477.10
September		3.53	480.63
October		8.07	488.70
November		10.05	498.75
December		34.09	532.84
January	1969	34.27	567.11
February		9.21	576.32

study of samples cored from MP68–1 assuming the solidus is the same temperature (980°C) as found higher in the hole (Wright and Weiblen, 1967). This depth is about 1 m shallower than that indicated by the temperature profile. We can conclude that either (1) the temperatures are not at equilibrium because of large amounts of water introduced during drilling or (2) that the assumption regarding solidus temperature is wrong, the solidus at these depths being closer to 900° than 980°C.

COOLING OF THE MELT (T>1,070°C)

Limited parts of isothermal surfaces in the Makaopuhi melt are shown in figure 10 for the following isotherms: 1,100°C, 1,110°C, 1,118°C (estimated melting point of GeO_2), 1,130°C, 1,140°C, and 1,150°C (extrapolated). Most of the data were obtained from profiles in cased holes 23 and 24 (fig. 10, table 3) obtained from February to October 1966. Data from a single profile obtained on April 21, 1965 (table 3), is also shown, as are single temperature readings obtained during sampling of melt, and also temperatures of melt samples estimated from their crystallinity (Table 14). Corrections were made for thermocouple contamination as discussed in connection with figure 28. The lines in figure 10 are our best estimate of isothermal surfaces consistent with all of the data.

Isothermal surfaces up to about 1,130°C are drawn between the origin for crustal isotherms ($\sqrt{t}$=0.5 day at depth 0.0 ft) and the time of the first complete profile obtained in February 1966. These are consistent with single temperatures, either measured or inferred, at times in between. Subsequently the isothermal surfaces are perturbed, and slopes are generally flatter in the period March to October 1966, when the last complete profile was measured. The slope of the 1,070° isotherm also flattened in the period January to October 1966. Much later, when hole 68–1 was drilled, the 1070° isotherm was depressed relative to the position predicted from its initial slope.

From February to May 1966, the melt isotherms fluctuated erratically in depth. These fluctuations cannot be attributed to errors of measurement and correction for the following reasons:

1. The points defined by melting GeO_2 are not colinear, nor are isotherms defined by uncorrected profiles alone.
2. The shape of successive temperature profiles changes, and crossovers are not uncommon (figs. 27, 28).

The temperature variation in the melt is interpreted in a later section. We emphasize that the depths to isotherms show distinct departures from a linear relation to $\sqrt{t}$ expected from a conductive cooling model, and over part of the time the change in slope of the melt isotherms is opposite in sign to the change in slope of the crust isotherms.

OXYGEN FUGACITY MEASUREMENTS

Sato and Wright (1966) reported preliminary results of measurement of oxygen fugacity in drill holes. The data upon which their work was based, as well as those obtained subsequently, are summarized in table 27 and figure 11.

Two kinds of measuring devices, called oxygen probes, were used. The first, described by Sato and Wright (1966) and Sato (1971), used a mixture of nickel and nickel oxide (Ni–NiO) packed in a zirconia tube. A temperature profile was determined in each drill hole on the same day that the oxygen probe was used. Emf was measured on a high-impedance electrometer and converted to $\log f O_2$ using the following formula.

$$\log f O_2 \text{ (unknown)} = \log f O_2 \text{ (Ni-NiO)} - \frac{\text{emf (volts)}}{RT/4F} \quad (1)$$

where

R is the gas constant, F is the Faraday constant, and T is in Kelvins.

The reference oxygen fugacity for Ni-NiO is given by the formula (Huebner and Sato, 1970):

$$\log f O_2 \text{ (Ni–NiO)} = \frac{-24930}{T} + 9.36 \quad (2)$$

The Ni–NiO oxygen probe was used with good reproducibility through September 1965. Subsequently, problems were encountered that were not fully diagnosed and never resolved. The emf fluctuated erratically during the later measurements, apparently because of an electrical short in the casing of the probe. The fluctuations of emf, although annoying at the time, correspond to $f O_2$ variation of no more than one order of magnitude and do not seriously affect the interpretation of the results.

In December 1966, we began to use a gas reference oxygen probe which had a design similar to that described by Sato and Moore (1973, fig. 2). Oxygen was

FIGURE 11.—Log $f O_2$ plotted against the reciprocal of absolute temperature for profiles obtained in 11 drill holes. *A*, DH6. *B*, DH8. *C*, DH9. *D*, DH10. *E*, DH11. *F*, DH14, 16, 17. *G*, DH20. *H*, DH21, 24. Measurements were made using an oxygen probe like that pictured in figure 9. The date of measurement is given beside each profile. Each profile is represented by a different set of symbols.

Most holes show at least one buffered profile with values lying close to and parallel with the experimental buffers quartz-fayalite-magnetite (QFM) and nickel-nickel oxide (Ni-NiO). Most drill holes also show some time period when $f O_2$ values approached or exceeded that of the hematite-magnetite (H-M) buffer at temperatures from 450 to 800°C. See text for further explanation and interpretation.

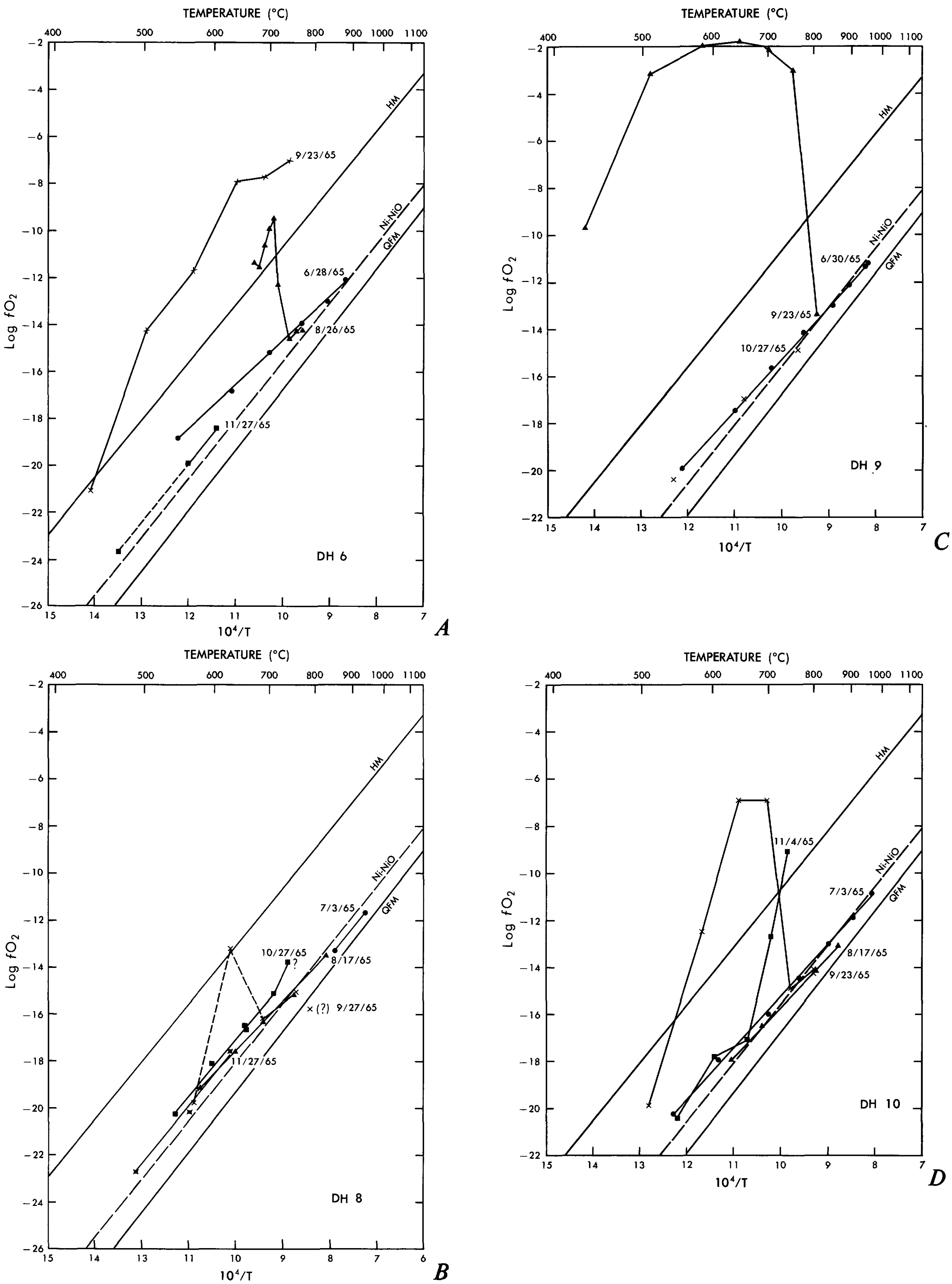
TEMPERATURE (°C)
400 500 600 700 800 900 1000 1100
Log fO_2
$10^4/T$
HM
Ni-NiO
QFM
9/23/65
6/28/65
8/26/65
11/27/65
DH 6
A
7/3/65
10/27/65
8/17/65
?
×(?) 9/27/65
11/27/65
DH 8
B
6/30/65
9/23/65
10/27/65
DH 9
C
11/4/65
7/3/65
8/17/65
9/23/65
DH 10
D

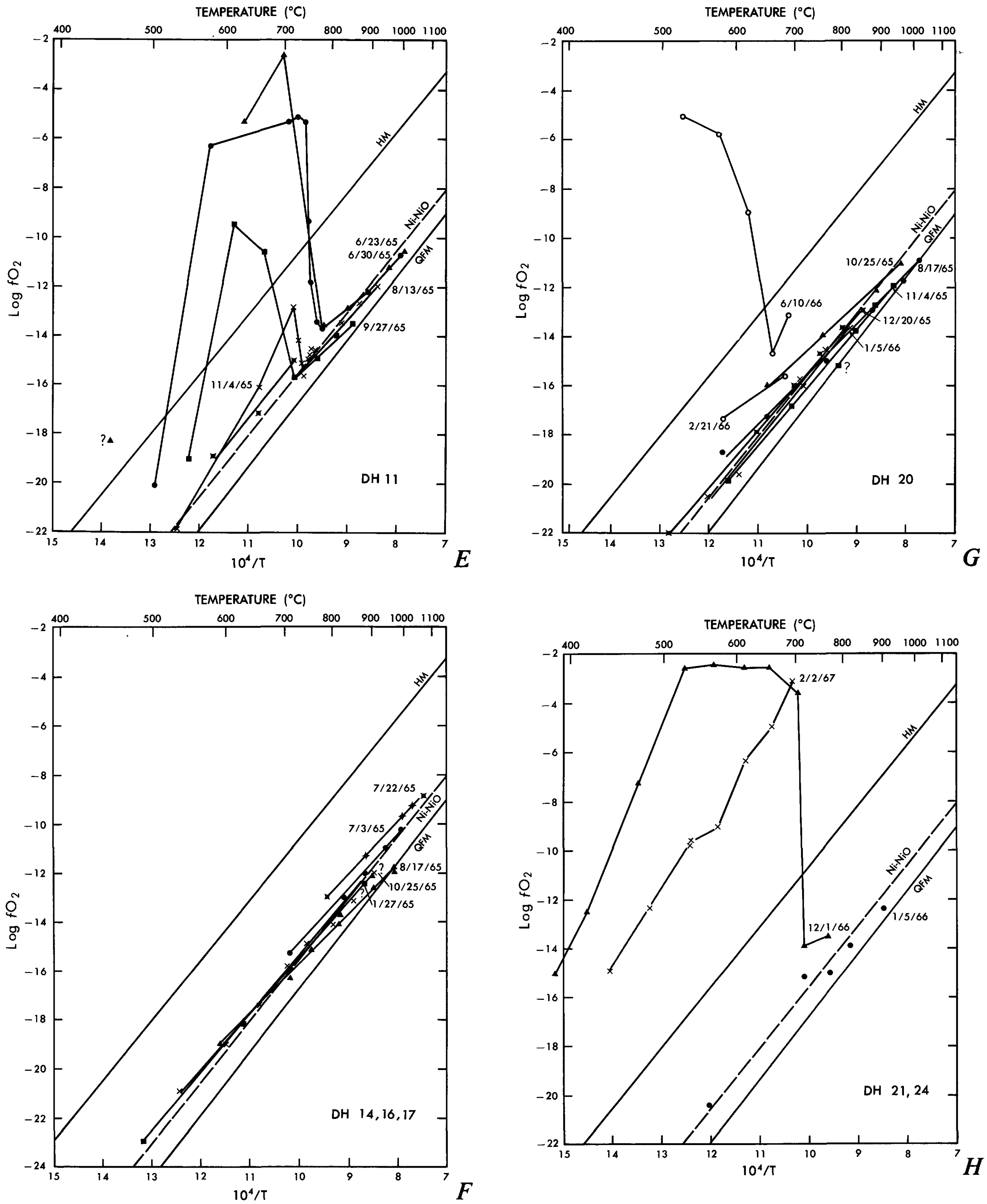

FIGURE 11.—Continued.

used as the reference gas, and reproducible measurements were obtained at the low temperatures then prevailing in the open drill holes. The last set of measurements was obtained in February 1967.

The following observations can be summarized from the oxygen fugacity studies (see also Sato and Wright, 1966).

1. Most drill holes showed, at some interval of time, a fO_2-T profile in which log fO_2 varies linearly with the reciprocal of absolute temperature. The position of such normal profiles indicates that the equilibrated basalt-gas system had oxygen fugacities greater than that of the QFM (quartz-fayalite-magnetite) buffer and within one log unit of the Ni-NiO reference buffer. The slopes of such profiles are commonly shallower than those of the buffers; that is, the conditions in the drill hole became relatively more oxidizing as temperature decreased. The position of the profiles changed with time, varying within one order of magnitude of fO_2 at the same temperature. The variations are not regular, and although they probably represent real changes in the drill hole conditions, some variation could have been caused by differing probe construction, aging of the Ni-NiO, or other factors related to the techniques of measurement.

2. All drill holes showed at some time a zone of very high fO_2 between extreme temperatures of 800° and 400°C. Generally, the highest fO_2 exceeds that of the hematite-magnetite (HM) buffer at the same temperature, but the values of the bracketing temperatures and maximum fO_2 vary among drill holes and among different times in the same drill hole. Drill hole 11, near the edge of the lake, showed the zone of high fO_2 on the first measurement date (June 23, 1965). Drill holes 20 and 21, near the center of the lake, did not show high fO_2 until 1966. Drill hole 8 showed a small fO_2 anomaly in September 1965 bracketed by normal profiles in August and October. Drill hole 16, within 15 m of drill hole 8, was not measured in September 1965, but showed normal profiles in August, October, and November.

3. The zone of high fO_2 moved down in the hole with the isothermal surfaces for a limited period of time, but in many holes a normal profile was reestablished. The duration of the high fO_2 anomalies in each hole is summarized in table 7.

TABLE 7.—*Summary of observations on oxygen fugacity (fO_2) profiles.*

Drill hole No.	Distance from edge of lake	Dates of observation		Zone of high fO_2		
		Beginning	End	First observed	Last observed	T (°C)
11	60 ft	6/23/65	11/4/65	?	9/27/65	760–550
10	120 ft	7/3/65	11/4/65	9/27/65	--	730–550
9	230 ft	6/30/65	10/27/65	9/23/65	9/23/65	790–<450
8	440 ft	7/3/65	11/27/65	9/27/65	9/27/65	680–570
16	440 ft	8/7/65	11/27/65	10/25/65?	10/25/65?	~750
14	500 ft	7/3/65	(only date measured - no high fO_2)			
6	640 ft	6/28/65	11/27/65	8/25/65	9/23/65	>740–<450
20	740 ft	8/17/65	6/10/66	6/10/66	?	650–<500
21	740 ft	1/5/66	2/2/67	12/1/66	?	700–<400
17	780 ft	7/23/65	(only date measured - no high fO_2)			

4. The zone of high fO_2 is definitely correlated with oxidation of the adjacent basalt. Core from drill hole 11 shows hematitic alteration of olivine in the same depth range that showed high fO_2. Fe_2O_3 shows values up to 3.89 weight percent (M11–11, table 10), and (Fe_2O_3/$FeO+Fe_2O_3$) to 0.34, in the oxidized zone compared with normal values of 1.3 and 0.11 respectively in unoxidized core (table 10, 11). Core obtained from drill hole 6 is unoxidized, in agreement with a normal oxygen fugacity profile obtained during the first set of measurements (fig. 11). Subsequently, however, drill hole 6 showed a zone of high fO_2. Drill hole 23 was drilled next to hole 6 to see if the basalt was altered, and hematitic alteration of olivine was found at a depth corresponding to the measured high fO_2 in hole 6.

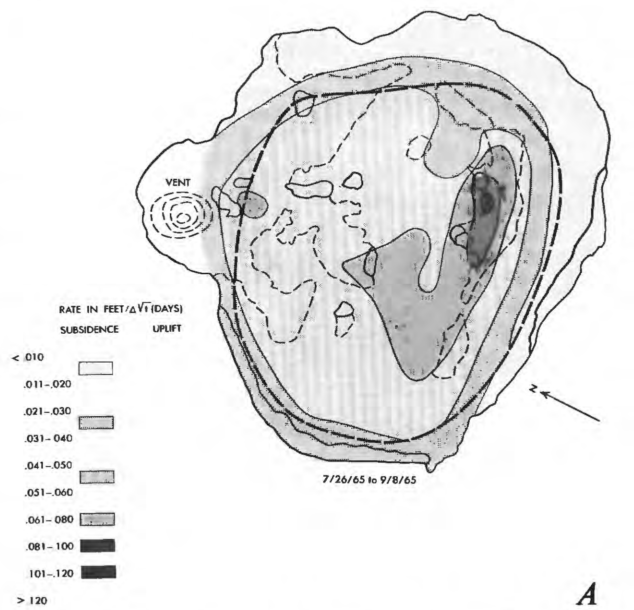

FIGURE 12.—Contoured elevation changes on the surface of Makaopuhi lava lake. *A*, 7/26 to 9/8/65. *B*, 9/8 to 10/20/65. *C*, 10/20 to 12/22/65. *D*, 12/22/65 to 3/7/66. *E*, 3/7 to 5/18/66. *F*, 5/18 to 8/9/66. *G*, 8/9 to 10/31/66. *H*, 10/31/66 to 1/31/67. *I*, 1/31 to 5/31/67. *J*, 5/31 to 10/2/67. *K*, 10/2/67 to 1/29/68. *L*, 1/29 to 7/10/68. *M*, 7/10 to 12/11/68. Base map is taken from figure 3 and shows only the outlines of physical features on the lake. Surface contouring was done after converting the altitude differences for each station (table 28 and 29) to a rate by dividing each difference by the difference in square root of time (days) for each leveling period. This is done to reduce the effect of the changing crustal growth rate and instead emphasize changes between level maps that result from density contrast between melt and the crust forming from it.

The heavy solid line separates uplift from subsidence. The heavy dashed line enclosing the area within which the volume of subsidence (uplift) is calculated (table 8, fig. 14). The contoured data are corrected for tilts associated with East rift eruptions in the periods 12/22/65–3/7/66 and 7/10/68–12/11/68 (see fig. 13). The perturbed pattern shown for the period 12/22/65–3/7/66 is probably induced by the tilting; the effects are seen to die out by 8/9/66.

The interpretation of the level maps is complicated and is discussed in the text.

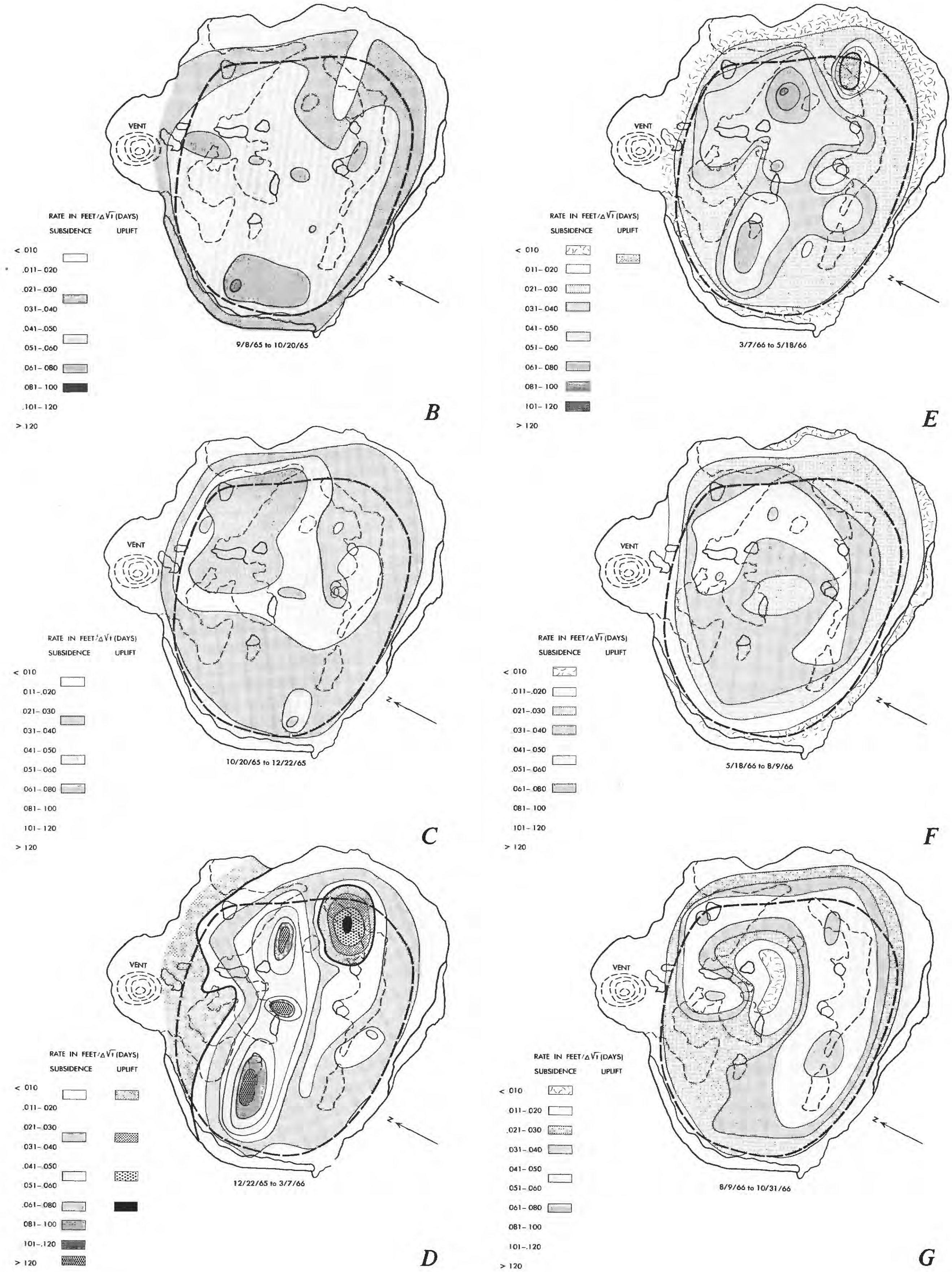

FIGURE 12.—Continued.

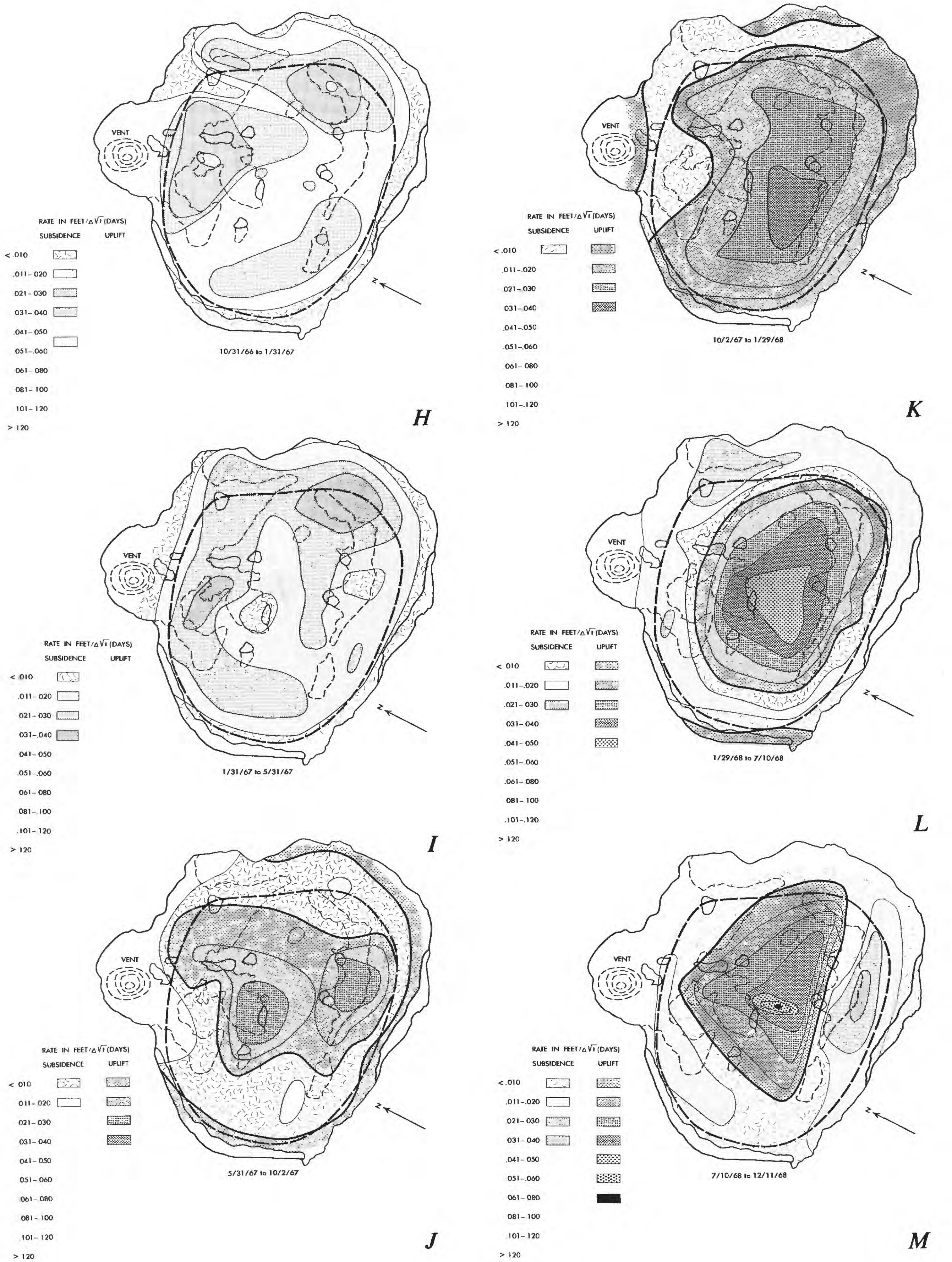

FIGURE 12.—Continued.

CHANGES IN SURFACE ALTITUDE

Altitudes of each leveling station are given in table 28 along with altitude differences for each survey interval. Altitude differences are assumed to reflect changing lake conditions, not external causes, such as uplift or subsidence of crater floor, although tilting of the crater floor was detected twice (see below). The altitude data have been converted to rate by dividing the difference in altitude by the difference in $\sqrt{t}$ in days between each leveling period.[5] The reduced data are contoured for each leveling interval in figure 12, beginning July 26, 1965, when the full level net was first occupied. Before then, changes (all in a subsidence sense) were larger and more erratic than later, presumably because of early, continued degassing of the molten lava. For example, some stations subsided several feet in the first survey period (March 24 to April 7, 1965).

Leveling data for two periods (December 22, 1965–March 7, 1966 and July 10–December 12, 1968) have been corrected for apparent tilt of the lake surface that took place during eruptions elsewhere on the upper east rift zone. Figure 13 shows the observed elevation changes for inactive stations near the edge of the lake and the best fit tilt vector estimated from these data. Tilt corrections were calculated for each station, and the corrected elevations and differences are shown in table 29. The tilting is assumed to represent a permanent deformation of the lake surface, and elevation differences subsequent to tilting are compared with those of the tilted surface.

Tilting associated with the eruption of December 25, 1965, induced a very complicated pattern (fig. 12), perhaps reflecting the "sloshing" of liquid lava beneath a thin crust, which died out over several months. No anomaly was associated with tilting during the October 1968 eruption, perhaps because the crust had grown much thicker.

In order to present more clearly the overall pattern of uplift and subsidence with time, an integrated volume rate of subsidence was calculated using a computer program based on Simpson's rule (USGS computer

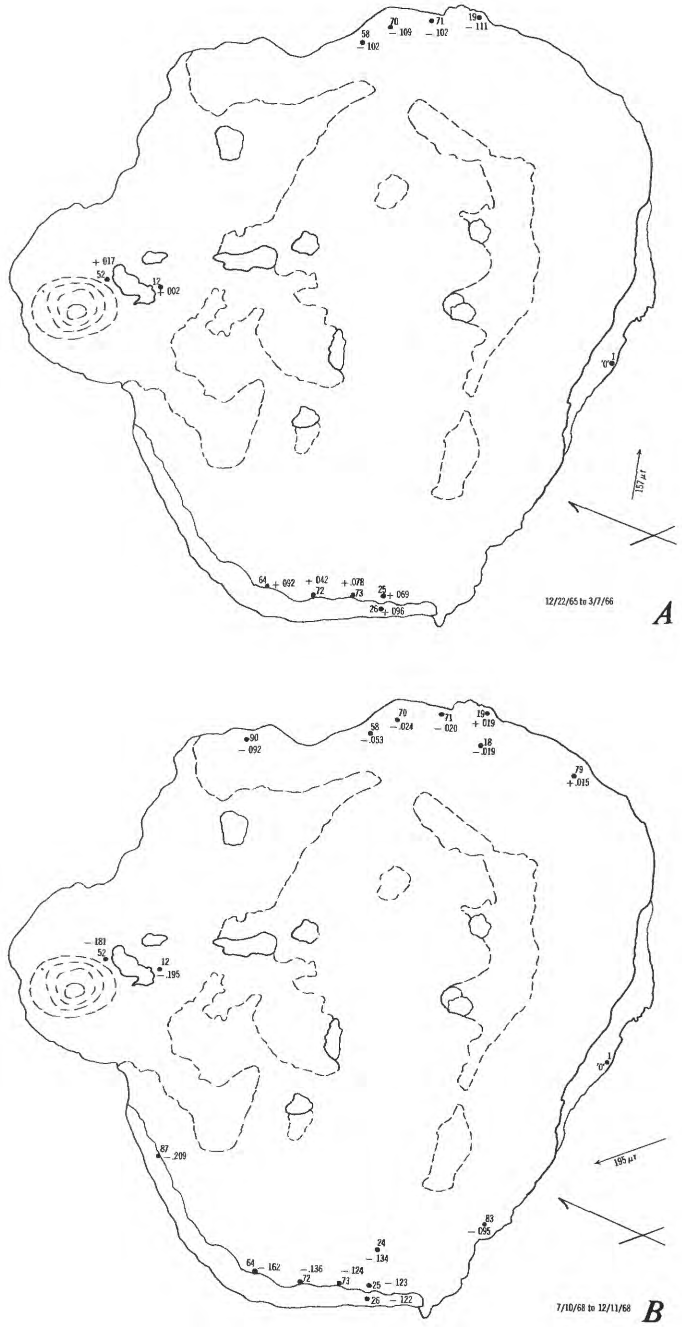

FIGURE 13.—Tilting of the Makaopuhi lava lake surface. *A*, 12/25/65 to 3/7/66. *B*, 7/10/68 to 12/11/68. Altitude changes (ft) are plotted for edge stations that should have showed no change over the period. Orientation and magnitude (in microradians (μr)) of the tilt vector are determined at right angles to the approximate azimuth of "O" change. Map base is the same as figure 12. Larger dots represent station locations whose numbers are adjacent.

[5]The theoretical basis for contouring the leveling data in terms of differences in rate instead of elevation is as follows: The general formula for altitude changes as a function of a phase change (density change) on solidification:

$$\frac{\rho c}{\rho m} = 1 - \frac{dV/d\sqrt{t}}{dh'/d\sqrt{t}} \tag{3}$$

where

ρc=bulk density of crust (including densities of upper and lower crust) at the crust melt interface.

ρm = bulk density of melt at the crust-melt interface.

$\frac{dV}{d\sqrt{t}}$ = change in volume of a fixed mass of melt becoming crust per unit time (positive sign if the volume of crust is greater than the volume of melt).

$\frac{dh'}{d\sqrt{t}}$ = rate of thickening of crust (upper plus lower) per unit time.

We make the following simplifying assumptions: (1) the rate of growth of crust ($dh'/d\sqrt{t}$) is constant and (2) the altitude change (dh) is ⅓ of the volume change (dV), and then divide dh by the difference in $\sqrt{t}$ taken over each leveling period ($d\sqrt{t}$ calculated from the second line from the top of table 28). The crust/melt density ratio should be proportional to 1 minus the rate of altitude change or $\frac{\rho c}{\rho m} = 1 - \frac{dh}{d\sqrt{t}} \times (\text{constant})$.

On these assumptions a constant ratio of crust to melt density would be reflected by a constant set of $dh/d\sqrt{t}$ values, at least for stations near the center of the lake.

program C628="Volume of ground swelling" by Patrick C. Doherty). A rectangular grid of 500 points, outlined by a short dashed line in figure 12, was superimposed on the contour maps, and the interpolated rate data at each grid intersection were used as input to the program. Data obtained from the program are summarized in table 8 and figure 14. The calculated volumes are meant as a qualitative means of interpreting average changes of the lake surface through time whereas the contour maps show the pattern of changes related to position on the lake surface in a single time interval.

The size of the grid is arbitrary and not altogether satisfactory, because in the later leveling periods the effects of cooling from the crater wall were more pronounced at the edges of the grid. Relative volumes are consistent for all leveling periods—the absolute values of volume depend on the grid area chosen and may be compared with the total lake volume (after drainback) of about 5.12×10^8 m^3 (Wright and others, 1968, fig. 11).

The overall pattern of altitude and volume changes after July 26, 1965, is as follows: net subsidence from August 1965 through October 1966, becoming less in magnitude over the next 7 months, and finally changing to uplift in the center of the lake, though subsidence continued around the margin after May 1967. This pattern, unpredicted by any simple model of constant density change on solidification combined with thermal contraction, is discussed later in the paper.

TABLE 8.—*Volume of subsidence/uplift determined from surface altitude changes, Makaopuhi lava lake*

Dates of observation	$\Delta\sqrt{t}$(days) after 3/24/65	$\Delta V(m^3)$	$\frac{\Delta V(m^3)}{\Delta\sqrt{t}(days)}$	Cumulative $\Delta V(m^3)$ from July 26, 1965
7/26/65 to 9/8/65	11.14 12.96	−1853	−1018	−1853
9/8/65 to 10/20/65	12.96 14.49	−1654	−1081	−3507
10/20/65 to 12/22/65	14.49 16.52	−2057	−1013	−5564
12/22/65 to 3/7/66	16.52 18.65	−1720	−808	−7284
3/7/66 to 5/18/66	18.65 20.49	−1533	−833	−8817
5/18/66 to 8/9/66	20.49 22.43	−1617	−833	−10434
8/9/66 to 10/31/66	22.43 24.31	−1437	−807	−11871
10/31/66 to 1/31/67	24.31 26.04	−934	−511	−12805
1/31/67 to 5/31/67	26.04 28.25	−1021	−462	−13826
5/31/67 to 10/2/67	28.25 30.36	+203	+96	−13623
10/2/67 to 1/29/68	30.36 32.26	+642	+338	−12981
1/29/68 to 7/10/68	32.26 34.70	+609	+250	−12371
7/10/68/ to 12/11/68	34.70 36.85	+148	+69	−12224

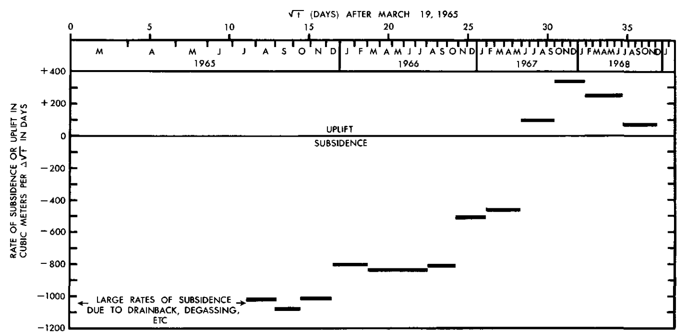

FIGURE 14.—Volume rate of subsidence or uplift of the lava surface plotted against square root of time. Volumes are calculated by computer for the area enclosed by a dashed line in figure 12. Differences in the values, for different time periods, are caused by variable crustal growth rate (fig. 10), changes in vesicularity (fig. 21) as a reflection of changes in crust/melt density ratios, and possible irregular behavior of different parts of the lava lake. Further discussion and interpretation are given in the text.

CHEMICAL AND PETROGRAPHIC STUDIES

All samples collected during the eruption were studied in thin section, and many were analyzed chemically to define the variation in the erupted magma. Core and melt samples from drill holes 1–24 were studied in thin section, and modes were made of all partially molten samples and selected holocrystalline samples in order to determine the mineral paragenesis as a function of temperature. Selected samples were analyzed chemically. Later, a systematic chemical and petrographic study was made of core from holes 68–1 and 68–2.[6] Samples were analyzed at 4-foot intervals to a depth of 22 feet and 2-foot intervals to the crust-melt interface at 54 feet. Modes were made of all samples collected at temperatures of more than 950°C, in order to define the mineral paragenesis at greater depth than could be obtained from drill holes 1–24. Melt samples and segregations were analyzed to detect differences in composition due to differentiation of the initial magma. After chemical and petrographic studies were completed, the drill core was again inspected to describe megascopic changes in mineralogy and texture with depth in the lake. The results of all these studies are summarized in the next few sections.

MAJOR ELEMENT CHEMISTRY

Chemically analyzed samples (tables 9, 10, 11) may

[6]Drill hole 69–1 was placed next to an island of layered crust (fig. 3) in order to study the interaction of the molten lake with layered crust. The anomalous textures and chemistry of core from this hole are the subject of a separate study, not reported here. Melt from the bottom of the drill hole is, however, considered to be part of a continuous molten zone beneath the center of the lake and this is described along with melt obtained from drill holes 68–1 and 68–2.

TABLE 9.—*Sample data for chemical analyses shown in tables 10 and 11*

[All samples were analyzed in the U.S. Geological Survey rock-analysis laboratory, Denver, Colorado, under the direction of L. C. Peck. Column 1 gives the sample number keyed as follows: M–etc. Sample collected during the eruption; M13–etc. Sample collected during 1965–66 from drill hole number 13 (1–cm diameter core); MP68–1–etc. Sample collected during 1968–69 from drill hole 68–1 (6–cm diameter core). Column 2 describes the type of material. Columns 3–5 give date, depth, and temperature of collection. Columns 6–8 give the laboratory identification. Column 9 gives additional information on the chemistry. Samples are classified as 'olivine-controlled," "contaminated," or, "differentiated," according to their chemistry compared with that of the erupted pumice (see text for further explanation)]

Sample No.	Type of material	Date of collection	Depth of collection (ft)	Temperature of collection (°C)	Analyst	Laboratory data Lab. No.	Laboratory data Report No.	Comment
M–1	Pumice	March 5, 1965		Ambient	G.O. Riddle	D100969	65DC–33	Olivine-controlled
M–1A	Do	do		do	E. L. Munson	D101324	66DC–32	Do.
M–20	Do	March 14, 1965		do	G. O. Riddle	D100972	65DC–33	Do.
M–26	Do	March 15, 1965		do	do	D101012	65DC–60	Do.
M1–1G	Glassy skin on lava lake surface	April 19, 1965	Surface	do	E. L. Munson	D101352	66DC–32	Do.
M–3	Melt dipped from rising lava lake	March 7, 1965	Surface	Approx. 1,160–1,180	G. O. Riddle	D100970	65DC–33	Do.
M–8	Do	March 11, 1965	do	do	do	D101010	65DC–60	Do.
M–12	Do	March 12, 1965	do	do	E. L. Munson	D101325	66DC–32	Do.
M–18	Do	March 14, 1965	do	do	G. O. Riddle	D100971	65DC–33	Do.
M–22	Do	March 15, 1965	do	do	E. L. Munson	D101326	66DC–32	Do.
M1–7	Do	April 23, 1965	10.8–11.4	Approx. 1,130	do	D101351	66DC–32	Fe contamination and reduction of Fe_2O_3 by reaction with steel.
M21–24 bottom	Melt collected in drill steel	August 30, 1965	22	do	do	D101332	66DC–32	Do.
M21–24 top	Do	August 30, 1965	19 (flowed in from 22)	do	do	D101331	66DC–32	Do.
M21–25	Ooze left in drill hole after collection of M21–24	September 16, 1965	15.4–16.05	1,060–1,080	do	D101333	66DC–32	Pyroxene-enriched
M21–26 sampler	Melt collected in ceramic	September 16, 1965	25–26.75	Approx. 1,130	do	D101327	66DC–32	Slight Fe contamination
M21–26 top	Melt collected in stainless steel	do	25–26.75	do	do	D101329	66DC–32	Do.
M21–27 sampler	Melt collected in ceramic	September 27, 1965	29–30.5	Approx. 1,135	do	D101328	66DC–32	Slight Fe contamination
M21–27 top	Melt collected in stainless steel	do	29–30.5	do	do	D101330	66DC–32	Do.
M23–21	Melt in bit	January 19, 1966	24.0	Approx. 1,095	G. O. Riddle	D101741	67DC–21	Differentiated by loss of augite and plagioclase during collection.
M24–3	Melt in core barrel	July 28, 1966	29.0–30.0	1,090–1,100	do	D101740	67DC–21	Do.
M1–6	Drill core	April 19, 1965	6.1–7.1	1,040–1,100	E. L. Munson	D101334	66DC–32	Olivine-controlled
M2–4	Do	April 19, 1965	6.1–7.1	1,040–1,100	do	D101335	66DC–32	Do.
M13-13	Do	June 7, 1965	9.1–10.1	980–1,025	do	D101337	66DC–32	Do.
M13–14	Do	do	10.1–11.1	1,025–1,080	do	D101336	66DC–32	Do.
M3–2	Do	April 22, 1965	0–0.45	Ambient	do	D101345	66DC–32	Do.
M4–1	Do	do	0.0–0.45	Ambient	do	D101346	66DC–32	Do.
M5–9	Do	May 19, 1965	6.1–7.1	850–930	do	D101347	66DC–32	Do.
M10–10	Do	May 26, 1965	6.0–7.0	805–885	do	D101348	66DC–32	Do.
M11–9	Do	do	5.0–6.0	560–645	do	D101340	66DC–32	Do.
M11–10	Do	do	6.0–7.0	645–725	do	D101341	66DC–32	Do.
M11–11	Do	do	7.0–8.0	725–795	do	D101342	66DC–32	Do.
M11–12	Do	do	8.0–9.0	795–865	do	D101343	66DC–32	Do.
M11–14	Do	do	10.0–11.0	920–980	do	D101344	66DC–32	Do.
M13–11	Do	June 7, 1965	7.1–8.1	845–915	do	D101339	66DC–32	Do.
M13–12	Do	do	8.1–9.1	915–980	do	D101338	66DC–32	Do.
M21–12	Do	August 17, 1965	10.95–11.95	890–935	do	D101349	66DC–32	Do.
M22–10	Do	November 1, 1965	11.0–12.0	780–820	do	D101350	66DC–32	Do.
M23–19A	Drill Core	January 19, 1966	19.4–21.0	1,000–1,060	G. O. Riddle	D101739	67DC–21	Differentiated; liquid segregated after drilling.
68–2–10.0	Do Segregation vein	December 12, 1968	10.0	<100	do	D103502	75 LA CR 0007	Differentiated
68–2–17.7	Drill core containing a small vesicle sheet	December 16, 1968	17.7	<100	do	D103503	75 LA CR 0007	Do.
68–1–28	Drill core: segregation vein	November 15, 1968	28.0	320–350	E. L. Munson	D102404	69 DC–29	Do.
68–1–44.5	Drill core: segregation vein	November 18, 1968	44.5	>900	G. O. Riddle	D103504	75 LA CR 0007	Do.
69–1–55.5	Drill core: segregation vein	January 31, 1969	55.5	Not known	do	D103506	75 LA CR 0007	Do.
68–1	Drill Core	November 6, 1968	3.7	Not accurately[1] known	E. Engleman	D103069	72 DC–10	Olivine-controlled
68–1–2	Do	November 12, 1968	8.0	do[1]	do	D103070	72 DC–10	Do.
68–1–3	Do	do	12.0	do[1]	do	D103071	72 DC–10	Do.
68–1–4	Do	do	17.5	do[1]	do	D103072	72 DC–10	Do.
68–1–5	Do	November 15, 1968	22.1	do[1]	do	D103073	72 DC–10	Do.
68–1–6	Do	do	24.0	do[1]	do	D103074	72 DC–10	Do.
68–1–7	Do	do	26.0	do[1]	do	D103075	72 DC–10	Do.
68–1–8	Do	do	27.9	do[1]	do	D103076	72 DC–10	Do.
68–1–9	Do	do	30.0	do[1]	do	D103077	72 DC–10	Differentiated
68–2–10	Do	December 16, 1968	32.0	do[1]	do	D103078	72 DC–10	Do.
68–1–11	Do	November 15, 1968	33.8	do[1]	do	D103079	72 DC–10	Do.
68–1–12	Do	November 18, 1968	36.0	do[1]	do	D103080	72 DC–10	Do.
68–2–13	Do	December 16, 1968	38.0	do[1]	do	D103081	72 DC–10	Do.
68–1–14	Do	November 18, 1968	39.8	do[1]	do	D103082	72 DC–10	Do.
68–2–15	Do	December 16, 1968	42.0	do[1]	do	D103083	72 DC–10	Do.
68–1–16	Do	December 18, 1968	44.2	(1,011)[1]	do	D103084	72 DC–10	Do.
68–1–17	Do	do	46.1	(1,029)	do	D103085	72 DC–10	Do.
68–1–47–6	Do	do	47.6	(1,040)[1]	E. L. Munson	D102405	69 DC–29	Do.
68–1–18	Do	do	48.0	(1,043)[1]	do	D103086	69 DC–29	Do.
68–1–19	Do	do	49.5	(1,055)[1]	do	D103087	69 DC–29	Do.
68–2–20	Do	December 18, 1968	51.5	(1,060)[1]	do	D103088	69 DC–29	Do.
68–1–21	Melt in bit	November 18, 1968	54.0	(1,082)[1]	do	D103089	69 DC–29	Do.
68–1–57	"Black sand"	November 20, 1968	57.0	(1,090)[1]	G.O. Riddle	D103505	75 LA CR 0007	Do.
68–2–59	Melt in bit	December 18, 1968	59.0	(1,100)[1]	E. L. Munson	D102406	69 DC–29	Do.
69–1–24–7	Drill core vesicular	January 28, 1969	24.7	Not known	G. O. Riddle	D103507	75 LA CR 0007	Olivine-controlled
69–1–25–6	Drill core massive	do	25.6	do	do	D103508	75 LA CR 0007	Differentiated
69–1–41–0	Drill core vesicular	January 31, 1969	41.0	do	do	D103509	75 LA CR 0007	Olivine-controlled
69–1–42–0	Drill core massive	do	42.0	do	do	D103510	75 LA CR0007	Differentiated
69–1–22	Melt in core barrel	do	60–66	1,080–1,100?	E. Engleman	D103090	72 DC–10	Differentiated

[1]Minimum temperatures are given in table 25. Temperatures estimated from glass content are shown in parenthesis.

TABLE 10.—*Major element chemical analyses, Makaopuhi lava lake samples collected in 1965–66*

A. Samples collected during the eruption

Sample	M–1	M–1A	M–20	M–26	M1–1G	M–3	M–8	M–12	M–18	M–22
SiO_2	50.19	50.24	50.11	50.02	50.06	50.27	50.29	50.45	50.33	50.09
Al_2O_3	13.46	13.52	13.42	13.35	13.31	13.50	13.57	13.63	13.59	13.34
Fe_2O_3	1.39	1.42	1.38	1.47	1.49	1.41	1.34	1.24	1.23	1.32
FeO	9.88	9.85	9.88	9.81	9.81	9.90	9.91	9.97	10.01	9.98
MgO	8.34	7.94	8.33	8.49	8.52	8.14	7.95	7.59	7.97	8.56
CaO	10.81	10.90	10.83	10.73	10.72	10.84	10.90	11.04	10.95	10.75
Na_2O	2.34	2.36	2.30	2.28	2.23	2.36	2.29	2.38	2.34	2.29
K_2O	0.55	0.53	0.54	0.53	0.49	0.55	0.54	0.52	0.55	0.53
H_2O	0.11	0.12	0.11	0.17	0.42	0.05	0.07	0.04	0.06	0.05
TiO_2	2.59	2.69	2.64	2.62	2.60	2.65	2.70	2.74	2.68	2.65
P_2O_5	0.27	0.28	0.27	0.27	0.27	0.27	0.27	0.28	0.26	0.27
MnO	0.17	0.17	0.17	0.17	0.17	0.17	0.17	0.17	0.17	0.17
CO_2	0.01	0.0	0.01	0.01	0.01	0.01	0.01	0.01	0.01	0.02
Cl	0.02	0.0	0.03	0.02	0.0	0.01	0.02	0.0	0.01	0.0
F	0.04	0.0	0.04	0.04	0.0	0.04	0.04	0.0	0.04	0.0
Subtotal	100.17	100.02	100.06	99.98	100.10	100.17	100.07	100.06	100.20	100.02
less O	0.02	0.0	0.02	0.02	0.0	0.02	0.02	0.0	0.02	0.0
Total	100.15	100.02	100.04	99.96	100.10	100.15	100.05	100.06	100.18	100.02
0.9 Fe_2O_3 / 0.9 Fe_2O_3 + FeO	.112	.115	.112	.119	.120	.114	.109	.101	.100	.107

B. 1965–66 Melt samples, T >1,070°C

Sample	M1–7	M21–24B	M21–24T	M21–25	M21–26S	M21–26T	M21–27S	M21–27T	M23–21	M24–3
SiO_2	50.24	49.83	49.59	50.28	50.16	50.14	50.11	50.22	50.47	50.42
Al_2O_3	13.31	13.29	13.04	13.35	13.51	13.36	13.23	13.34	13.54	13.58
Fe_2O_3	0.51	1.29	1.32	1.15	1.10	1.01	1.32	0.93	1.37	1.54
FeO	11.12	10.90	11.16	10.16	10.22	10.39	10.06	10.44	10.33	10.45
MgO	7.92	7.81	8.37	8.19	8.12	8.22	8.29	8.24	7.16	6.85
CaO	10.83	10.82	10.61	10.85	10.85	10.83	10.76	10.86	10.64	10.55
Na_2O	2.33	2.33	2.30	2.37	2.32	2.30	2.31	2.33	2.45	2.46
K_2O	0.51	0.51	0.50	0.52	0.53	0.52	0.52	0.53	0.61	0.61
H_2O	0.04	0.03	0.0	0.02	0.05	0.03	0.20	0.06	0.05	0.06
TiO_2	2.63	2.65	2.61	2.63	2.61	2.62	2 63	2.64	2.93	3.01
P_2O_5	0.28	0.28	0.27	0.28	0.28	0.28	0.27	0.28	0.29	0.30
MnO	0.21	0.18	0.18	0.17	0.18	0.18	0.17	0.18	0.17	0.18
CO_2	0.01	0.01	0.02	0.01	0.01	0.01	0.0	0.01	0.0	0.0
Cl	0.0	0.0	0.0	0.0	0.0	0.0	0.0	0.0	0.01	0.02
F	0.0	0.0	0.0	0.0	0.0	0.0	0.0	0.0	0.04	0.05
Subtotal	99.94	99.93	99.97	99.98	99.94	99.89	99.87	100.06	100.06	100.08
less O	0.0	0.0	0.0	0.0	0.0	0.0	0.0	0.0	0.02	0.03
Total	99.94	99.93	99.97	99.98	99.94	99.89	99.87	100.06	100.04	100.05
.9 Fe_2O_3 / .9 Fe_2O_3+FeO	.047	.096	.096	.092	.088	.081	.106	.075	.106	.117

C. 1965–66 Drill core, T <1,070°C

Sample	M1–6	M2–4	M3–2	M4–1	M5–9	M10–10	M11–9	M11–10	M11–11	M11–12	M11–14	M13–11	M13–12	M13–13	M13–14	M21–12	M22–10
SiO_2	50.44	50.51	50.20	50.19	50.40	50.42	50.40	50.34	50.27	50.36	50.29	50.41	50.39	50.43	50.45	50.40	50.44
Al_2O_3	13.48	13.45	13.22	13.23	13.49	13.25	13.44	13.34	13.36	13.38	13.26	13.30	13.36	13.25	13.31	13.26	13.31
Fe_2O_3	1.30	1.31	3.50	3.57	1.33	1.20	2.70	3.01	3.89	1.91	1.31	1.35	1.24	1.30	1.29	1.31	1.26
FeO	9.98	9.94	8.04	7.95	9.83	10.03	8.65	8.46	7.60	9.37	10.08	9.99	10.08	10.09	10.04	10.06	10.00
MgO	7.93	7.79	8.43	8.45	8.01	8.25	7.85	7.99	8.14	8.18	8.30	8.00	8.08	8.17	8.06	8.10	8.09
CaO	10.92	10.97	10.76	10.70	10.99	10.87	10.94	10.88	10.85	10.94	10.80	10.87	10.86	10.80	10.91	10.81	10.88
Na_2O	2.33	2.37	2.07	2.12	2.33	2.33	2.33	2.32	2.32	2.32	2.31	2.34	2.38	2.33	2.36	2.37	2.36
K_2O	0.52	0.53	0.50	0.52	0.51	0.52	0.52	0.52	0.51	0.51	0.52	0.53	0.52	0.52	0.52	0.52	0.52
H_2O	0.01	0.03	0.11	0.12	0.06	0.04	0.03	0.03	0.02	0.03	0.02	0.03	0.04	0.01	0.02	0.06	0.04
TiO_2	2.62	2.68	2.60	2.62	2.63	2.60	2.65	2.68	2.61	2.60	2.65	2.69	2.67	2.67	2.63	2.68	2.64
P_2O_5	0.28	0.28	0.28	0.28	0.27	0.28	0.28	0.28	0.28	0.27	0.28	0.29	0.28	0.28	0.28	0.28	0.28
MnO	0.18	0.17	0.17	0.17	0.17	0.18	0.17	0.17	0.17	0.17	0.17	0.18	0.18	0.17	0.17	0.17	0.17
CO_2	0.01	0.01	0.01	0.01	0.01	0.01	0.01	0.01	0.01	0.0	0.01	0.01	0.01	0.01	0.01	0.01	0.01
Cl	0.0	0.0	0.0	0.0	0.0	0.0	0.0	0.0	0.0	0.0	0.0	0.0	0.0	0.0	0.0	0.0	0.0
F	0.0	0.0	0.0	0.0	0.0	0.0	0.0	0.0	0.0	0.0	0.0	0.0	0.0	0.0	0.0	0.0	0.0
Subtotal	99.98	100.04	99.89	99.93	100.03	99.98	99.97	100.03	100.03	100.04	100.00	99.99	100.09	100.03	100.05	100.03	100.00
less O	0.0	0.0	0.0	0.0	0.0	0.0	0.0	0.0	0.0	0.0	0.0	0.0	0.0	0.0	0.0	0.0	0.0
Total	99.98	100.04	99.89	99.93	100.03	99.98	99.97	100.03	100.03	100.04	100.00	99.99	100.09	100.03	100.05	100.03	100.00
.9 Fe_2O_3 / .9 Fe_2O_3+FeO	.105	.106	.282	.288	.109	.097	.219	.243	.315	.155	.105	.108	.100	.104	.104	.105	.102

D. Segregation veins

Sample	M23–19A	68–2–10	68–1–17.7	68–1–28	68–1–44.5	69–1–55.5
SiO_2	49.57	50.77	50.17	50.07	50.96	52.66
Al_2O_3	13.05	12.27	13.57	12.05	13.41	12.29
Fe_2O_3	1.90	4.26	1.26	2.41	1.83	1.85
FeO	12.69	10.45	9.92	12.92	10.90	13.14
MgO	4.60	4.23	7.99	4.30	5.55	3.26
CaO	8.70	8.47	10.95	8.49	9.77	7.59
Na_2O	2.91	2.75	2.27	2.73	2.69	3.09
K_2O	0.88	1.11	0.56	1.02	0.80	1.38

TABLE 10.—*Major element chemical analyses, Makaopuhi lava lake samples collected in 1965–66*—Continued

D. Segregation veins—Continued

Sample	M23–19A	68–2–10	68–1–17.7	68–1–28	68–1–44.5	69–1–55.5
H_2O	0.01	0.34	0.06	0.0	0.05	0.16
TiO_2	4.84	4.49	2.78	5.26	3.57	3.49
P_2O_5	0.43	0.52	0.25	0.52	0.39	0.70
MnO	0.21	0.20	0.16	0.21	0.18	0.20
CO_2	0.0	0.0	0.01	0.01	0.01	0.03
Cl	0.02	0.02	0.01	0.02	0.02	0.04
F	0.06	0.08	0.04	0.06	0.06	0.10
Subtotal	99.87	99.96	100.00	100.07	100.19	99.98
less O	0.03	0.04	0.02	0.03	0.03	0.05
Total	99.84	99.92	99.98	100.04	100.16	99.93
$\frac{.9\ Fe_2O_3}{.9\ Fe_2O_3+FeO}$	.112	.268	.102	.144	.131	.112

TABLE 11.—*Major element chemical analyses, Makaopuhi lava lake: samples collected in 1968–69*

Sample	68–1–1	68–1–2	68–1–3	68–1–4	68–1–5	68–1–6	68–1–7	68–1–8	68–1–9	68–2–10	68–1–11	68–1–12	68–2–13
SiO_2	50.27	50.21	50.18	50.31	50.23	50.26	50.24	50.32	50.43	50.34	50.50	50.48	50.72
Al_2O_3	13.59	13.38	13.45	13.51	13.52	13.44	13.46	13.43	13.53	13.62	13.65	13.55	13.53
Fe_2O_3	1.56	1.42	1.33	1.24	1.25	1.25	1.20	1.21	1.24	1.32	1.32	1.22	1.43
FeO	9.67	9.88	9.92	9.99	9.99	9.99	10.08	10.08	10.26	10.01	10.24	10.34	10.17
MgO	7.72	8.21	8.12	7.99	8.10	8.11	8.10	8.02	7.42	7.78	6.99	7.24	6.74
CaO	10.96	10.78	10.90	10.92	10.90	10.90	10.90	10.90	10.82	10.88	10.79	10.78	10.70
Na_2O	2.33	2.30	2.31	2.31	2.30	2.31	2.30	2.31	2.39	2.37	2.46	2.41	2.43
K_2O	0.53	0.53	0.52	0.52	0.54	0.53	0.53	0.53	0.55	0.55	0.57	0.57	0.60
H_2O	0.19	0.14	0.13	0.04	0.05	0.02	0.01	0.0	0.01	0.01	0.01	0.01	0.02
TiO_2	2.71	2.67	2.68	2.66	2.68	2.69	2.70	2.69	2.82	2.69	2.93	2.89	3.08
P_2O_5	0.26	0.27	0.26	0.26	0.26	0.26	0.27	0.27	0.29	0.28	0.29	0.28	0.30
MnO	0.17	0.17	0.17	0.17	0.17	0.18	0.18	0.18	0.18	0.17	0.18	0.18	0.18
CO_2	0.01	0.01	0.01	0.01	0.0	0.0	0.0	0.0	0.01	0.0	0.0	0.0	0.0
Cl	0.01	0.01	0.01	0.01	0.01	0.01	0.01	0.01	0.02	0.01	0.01	0.01	0.01
F	0.04	0.04	0.04	0.03	0.03	0.03	0.03	0.04	0.04	0.04	0.04	0.04	0.04
Subtotal	100.04	100.00	100.03	99.97	100.03	99.98	100.01	99.99	100.01	100.07	99.98	100.00	99.95
less O	0.02	0.02	0.02	0.01	0.01	0.01	0.01	0.02	0.02	0.02	0.02	0.02	0.02
Total	100.02	99.98	100.01	99.96	100.02	99.97	100.00	99.97	99.99	100.05	99.96	99.98	99.93
$\frac{.9\ Fe_2O_3}{.9\ Fe_2O_3+FeO}$	.127	.115	.108	.101	.102	.102	.097	.098	.098	.106	.104	.096	.113

Sample	68–1–14	68–2–15	68–1–16	68–1–17	68–1–47	68–1–18	68–1–19	68–2–20	68–1–21	68–1–57	68–2–59	69–1–24.7	69–1–25.6	69–1–41.0	69–1–42.0	69–1–22
SiO_2	50.65	50.58	50.54	50.65	50.59	50.60	50.79	50.75	50.71	50.62	50.58	50.32	50.39	49.98	50.16	50.90
Al_2O_3	13.56	13.45	13.30	13.45	13.65	13.29	13.14	13.35	13.35	13.41	13.41	13.73	13.69	13.77	13.60	12.97
Fe_2O_3	1.32	1.51	1.47	1.49	1.33	1.47	1.49	1.51	1.59	1.65	1.45	2.79	2.23	4.93	1.51	1.65
FeO	10.18	10.31	10.42	10.41	10.55	10.42	10.71	10.53	10.67	10.63	10.51	8.42	9.18	6.20	9.80	11.70
MgO	6.96	6.82	6.74	6.55	6.62	6.71	6.47	6.39	6.13	6.29	6.83	7.66	7.33	7.67	8.00	5.18
CaO	10.81	10.61	10.56	10.45	10.47	10.53	10.19	10.33	10.19	10.25	10.44	11.20	10.95	11.14	10.96	9.38
Na_2O	2.46	2.46	2.46	2.50	2.50	2.45	2.51	2.54	2.58	2.51	2.48	2.24	2.40	2.19	2.30	2.73
K_2O	0.58	0.59	0.60	0.63	0.60	0.60	0.67	0.66	0.69	0.71	0.62	0.54	0.62	0.48	0.54	0.80
H_2O	0.01	0.0	0.0	0.02	0.07	0.03	0.06	0.0	0.07	0.10	0.09	0.04	0.06	0.49	0.04	0.12
TiO_2	3.00	3.10	3.26	3.24	3.14	3.27	3.33	3.31	3.39	3.30	3.09	2.60	2.77	2.49	2.68	3.89
P_2O_5	0.29	0.31	0.31	0.32	0.32	0.30	0.34	0.32	0.36	0.34	0.33	0.25	0.29	0.24	0.24	0.41
MnO	0.18	0.19	0.19	0.19	0.18	0.19	0.19	0.19	0.18	0.18	0.18	0.16	0.17	0.16	0.17	0.20
CO_2	0.0	0.0	0.0	0.0	0.02	0.01	0.0	0.0	0.0	0.02	0.02	0.01	0.01	0.02	0.02	0.0
Cl	0.01	0.01	0.01	0.02	0.02	0.02	0.02	0.02	0.02	0.02	0.02	0.02	0.02	0.11	0.01	0.03
F	0.04	0.04	0.04	0.04	0.05	0.04	0.05	0.05	0.05	0.05	0.05	0.05	0.04	0.23	0.04	0.06
Subtotal	100.05	99.98	99.90	99.96	100.11	99.93	99.96	99.95	99.98	100.08	100.10	100.03	100.15	100.10	100.05	100.02
less O	0.02	0.02	0.02	0.02	0.03	0.02	0.03	0.03	0.03	0.03	0.03	0.03	0.02	0.12	0.02	0.03
Total	100.03	99.96	99.88	99.94	100.08	99.91	99.93	99.92	99.95	100.05	100.07	100.00	100.13	99.98	100.03	99.99
$\frac{.9\ Fe_2O_3}{.9\ Fe_2O_3+FeO}$	.105	.117	.112	.114	.102	.112	.111	.114	.118	.123	.110	.230	.180	.417	.114	.122

be subdivided into the following categories:

1. Samples collected during the eruption
   a. pumice
   b. melt samples dipped from the rising lava lake
2. Drill core
   a. Subsolidus: T <1.000°C before drilling
   b. partially molten: 1,000°<T<1,070°C before drilling
3. Melt samples (T>1,070°C) collected in drill holes
4. Segregations collected either as veins (solidified or partially molten) found during drilling or as melt that flowed into open drill holes and was subsequently drilled out.

Most samples were collected before September 1966 at depths of less than 4.6 m (core) or less than 7.6 m (melt). Core from 68–1 and 68–2 was obtained to 15.8 m, melt samples from 16.5 to 18.3 m.

The overall chemical variation is portrayed on magnesia variation diagrams (fig. 15), which show the compositions of all samples collected during the eruption, all samples analyzed from drill holes 68–1 and 68–2, one sample of melt from the hole 69–1, and all segregations. Analyses of drill core collected during 1965–66 are not plotted separately but overlap on all plots with the composition of samples collected during the eruption.

Group 1 above comprises a set of analyses that defines the composition of the erupted magma. Intersample variation may be largely described in terms of small differences in olivine content and amount of oxidation. The melt samples are somewhat reduced and also depleted in olivine relative to the pumice, representing, respectively, oxidation of pumice during fountaining (Swanson and Fabbi, 1973) and gravitational settling of olivine during filling of the lake. The sample of quenched glassy crust on the final lava lake surface (M1–1G) is as rich in MgO as the pumice, suggesting that olivine was locally concentrated upward by turbulence accompanying crustal foundering (Wright and others, 1968, fig. 10d, p. 3191 and 3197).

The analyses of pumice, dipped melt, and quenched glassy crust together define a uniform batch[7] of magma. This considerably simplifies the description of interpretation of differentiation in the lake, because we assume a constant (± olivine) initial composition for the lake, unlike, for example, the situation during the 1959 eruption that formed Kilauea Iki lava lake (Wright, 1973; Murata and Richter, 1966). The average composition of the four pumice samples, designated MPUMAV, is shown in table 12.

By considering the uniform initial composition of the lava and the concept of magma batch, we can examine the analyses of all samples collected subsequent to the eruption. We solve the following mixing equation, using the computer method and weighting of Wright and Doherty (1970).

Unknown = MPUMAV ± olivine (Fo_{90} + Fo_{70}, each with 1.5 weight percent included Cr-spinel)

The residuals (expressed as absolute weight percent) in each calculation are inspected to see if they exceed twice the estimated precision of analysis (Wright, 1971, p. 6). If not, then the analysis is considered to differ from that of the initial erupted magma only by addition or removal of olivine. Otherwise, the pattern of residuals that exceed twice the precision levels is used to evaluate various differentiation and contamination effects in the lava lake.

One of the first applications of this procedure was to identify iron contamination in melt samples collected in or near steel casings (M21–24, 21–26, 21–27 in table 10). Samples collected in steel core barrels had FeO residuals of 0.5–1.3 weight percent, indicating that iron was introduced into the melt by reaction with the steel casing. Collection in stainless steel was accompanied by much less reaction, and FeO residuals are correspondingly better (0.1–0.2 weight percent). Nonetheless, some reaction is unavoidable, and interpretation of trace-element distribution in these melt samples would be compromised by the contamination. When FeO is used as an additional mixing component in equation (4), the residuals are all reduced to precision levels. Hence one can conclude that these samples of melt, although contaminated, were not otherwise differentiated within the lake.

Samples of core were not contaminated during drilling and, down to a depth of 8.5 m, are equivalent in composition to the erupted magma minus differing amounts of olivine (fig. 15).

Below 8.5 m, the magnesia content decreases, and the residuals in equation (4) become significant. Addition of augite and plagioclase to the mixing equation reduces the residuals to precision levels, suggesting that these minerals, in addition to olivine, were partly removed from the liquid. In drill holes 68–1 and 68–2, the most differentiated sample analyzed, which has a MgO content of 6.13 percent, is melt trapped in the bit at 54.0 feet (68–1–21); the mixing calculation indicates separation of about 5 percent olivine, 10 percent augite, and 10 percent plagioclase from MPUMAV to yield the composition of 68–1–21. A sample of melt that flowed into the core barrel at the end of drilling hole 69–1 is even more differentiated, having a MgO content of 5.18 percent and a calculated separation of 7 percent olivine, 15 percent augite, and 16 percent plagioclase. Compositions of segregation veins are more differentiated yet, similar to veins from other lava lakes (see Wright and Fiske, 1971, appendix 2). The differentiation is interpreted in a later part of this paper.

Water (H_2O) content of the pumice (table 10) is relatively high (0.10–0.17 percent) compared with that of the dipped melt samples (0.02–0.09 percent) reflecting degassing during the eruption. The Makaopuhi eruption evidently had a higher initial water content then the later Mauna Ulu eruption described in Swanson and Fabbi (1973, fig. 1). The surface glass also has a high water content (M1–1G, 0.37 percent H_2O+), an observation for which we have no explanation. The water content of solidified crust decreases rapidly at first, then more slowly with depth until it is below detection levels (7.9 m; 68-1–7, table 11). Samples of melt collected through drill holes at depths of about 4–6 m

[7]These samples fit the definition of magma batch given by Wright, Swanson, and Duffield (1975, p. 111 ff).

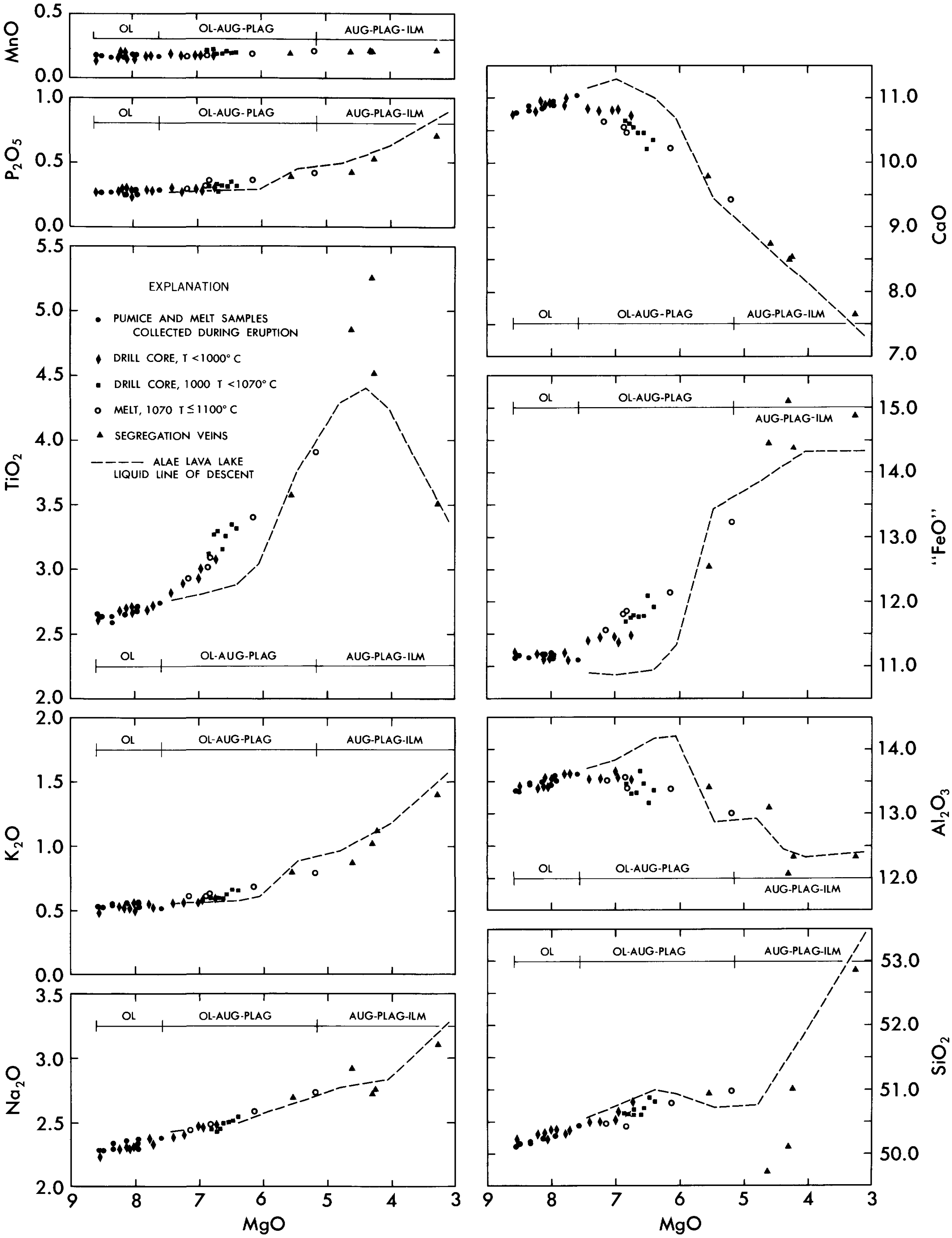
MnO
P_2O_5
TiO_2
K_2O
Na_2O
CaO
"FeO"
Al_2O_3
SiO_2
MgO
OL
OL-AUG-PLAG
AUG-PLAG-ILM
EXPLANATION
PUMICE AND MELT SAMPLES COLLECTED DURING ERUPTION
DRILL CORE, T <1000° C
DRILL CORE, 1000 T <1070° C
MELT, 1070 T ≤1100° C
SEGREGATION VEINS
ALAE LAVA LAKE LIQUID LINE OF DESCENT

have water contents of 0.03–0.05 percent comparable with that of solidified crust collected later at similar depth. The deep-melt samples collected in 1968 and 1969 have higher H_2O contents than solidified and partially molten samples collected at shallower depths. These virtually nonvesiculated melt samples have water contents of 0.07–0.12 percent (68–1–21; 68–2–59; 69–1–22 in table 11) which are probably near equilibrium solubilities at the respective pressures (4–5 bars calculated from their depth and the bulk density of the overlying crust).

Oxidation ratios ($0.9Fe_2O_3/(0.9Fe_2O_3+FeO)$, tables 10–11) are somewhat higher in the pumice (M–1, M–20, M–26) than in either melt samples quenched in water (M–18, M–22) or the least oxidized core samples, reflecting oxidation during fountaining (Swanson and Fabbi, 1973). Samples collected in contact with steel (M1–7, M21–26T, M21–27T) are reduced, evidently by reaction with the steel. Oxidation ratios of more than 0.11 are presumably a function of crystal liquid differentiation and (or) exposure to high oxygen fugacity values during subsolidus cooling.

PETROGRAPHY

All samples consist of varying amounts of olivine and included spinel, clinopyroxene, plagioclase, Fe-Ti oxides, apatite, and glass. Phenocrysts of olivine (common) and augite (rare) are present in most samples.

Modal analyses, done in transmitted light, are summarized in table 13. Modal data on samples of fine-grained core from holes drilled in 1965 and 1966 are in error, the dark minerals (pyroxene and opaques) being overestimated relative to plagioclase and glass. This can be proven by comparing the average mode of samples collected below 1,000°C, after converting from volume percent to weight percent, with a chemical mode (Wright and Doherty, 1970) calculated from MPUMAV (table 14).[8]

Modal data for coarser grained samples collected from drill holes 68–1 and 68–2 are more nearly correct in terms of pyroxene/plagioclase ratio, but opaque minerals are still systematically overestimated.

Modal data for samples collected both during the eruption and to a depth of 8.5 m in the lake may be used to define a mineral paragenesis along the liquid line of descent for MPUMAV. The mineral percentages plotted against glass content are shown in figure 16. Volume percent glass as estimated optically is shown as a function of temperature in figure 17. The errors in modal analysis make it difficult, if not impossible, to quantify precisely the amount of crystallization as a function of temperature, although limits can be placed by using the following procedure. Starting with mineral percentages given by the chemical mode, we drew curves of weight-percent mineral against weight-percent glass (fig. 16), assuming that the volume-percent glass is determined correctly and that the glass density varies linearly with refractive index

[8]Rittmann (1973) describes this masking effect and provides an empirical correction factor for opaque minerals based on grain size and thin-section thickness. The correction factor for Makaopuhi, (0.6, fig. 17) agrees well with that estimated from Rittman (0.65, 1973, fig. 35, p. 79).

TABLE 12.—*Average composition of pumice (MPUMAV) erupted into Makaopuhi lava lake; March 1965*

	Original	Dry weight[1]
SiO_2	50.18	50.28
Al_2O_3	13.26	13.28
Fe_2O_3	1.48	
FeO	9.86	11.21[2]
MgO	8.27	8.29
CaO	10.82	10.84
Na_2O	2.32	2.32
K_2O	.54	.54
H_2O+	.12	----
H_2O-	.01	----
TiO_2	2.64	2.65
P_2O_5	.27	.27
MnO	.17	.17
CO_2	.01	----
Cl	.02	----
F	.04	----
Subtotal	100.01	
less O	.02	
Total	99.99	99.85[2]

[1]Composition used in mixing and differentiation calculations.
[2]"FeO" = FeO +0.9 Fe_2O_3 *after* normalization to 100 percent. The total differs from 100 percent by the amount of Fe_2O_3 converted to FeO.

FIGURE 15.—MgO variation diagrams, Makaopuhi lava lake plotted in weight percent. Symbols are explained in the MgO-TiO_2 Box. O1=olivine; aug=augite; plag=plagioclase; ilm=ilmenite. The dashed line is the liquid line of descent for Alae lava lake (Wright and Fiske, 1971, fig. 4). Plotted samples include all core and melt samples from drill holes 68–1 and 68–2 (table 11), pumice and melt samples collected during the eruption (table 10A), and all segregation veins (table 10D). Most of the 1965–66 drill core (tables 10C) would plot at MgO contents greater than 7.5 percent with values of other oxides that fall within the scatter shown for the later drill core and eruption samples. These are not shown to avoid overcrowding of data points. Many melt samples (table 9, 10B) are contaminated from being collected in drilling steel or stainless steel. They would plot with slightly higher values of "FeO"/MgO than the samples shown. These are also not plotted.

The horizontal line indicates what minerals are crystallizing over different ranges in MgO content. Chemical data are illustrated further in figures 22 and 23; data on the origin of segregation vein compositions, many of which lie off the Alae liquid line of descent, are shown in table 21. See text for further discussion of interpretation of chemical data.

TABLE 13.—*Modal data, Makaopuhi lava lake*

[Modal data were obtained in transmitted light. Data are reported in volume percent. *Glass* comprises pools of isotropic material, usually light to dark brown, interstitial to mineral grains. *Quench* comprises microcrystalline material resulting from partial devitrification of glass during quenching. Fibrous extensions of larger crystals into glass are also included under quench. Together, glass and quench comprise material inferred to represent liquid at the temperature of collection. Temperatures of samples were not obtained at the time of collection. Rather the reported temperatures are read from the reconstructed temperature data given in figure 10 using the depth and date of collection. Starred (*) values for Fe-Ti oxide represent oxidation during collection of the sample]

A. Samples collected during the eruption

Sample	M-3	M-7	M-8	M-12	M-18	M-22	M1-1G	M60-B
Depth (ft)	surface of rising lava lake						Skin[1]	Flow[2]
T(°C)	----	----	----	----	≤1,160	----	1,140	----
Number of points (0.3×0.3 mm grid)	2,000	2,000	2,000	3,000	790	1,323	4,687	1,247
Olivine	4.4	4.0	3.7	3.1	5.3	4.9	4.4	6.8
Pyroxene	15.4	16.4	13.6	6.0	6.2	7.5	12.3	4.7
Plagioclase	8.3	10.1	6.6	0.5	0.4	0.4	4.1	0.3
Fe–Ti oxide	----	----	----	----	----	----	----	----
Glass	60.9	50.8	71.1	89.1	86.4	81.2	75.5	79.6
Quench	11.0	18.7	5.1	1.4	1.7	6.0	3.7	8.6

B. Melt samples collected through Drill holes (sample data in table 10)

		M21–21		M21–24				M21–26			M21–27		
Sample	M20–13	Bottom	Top	Bottom	Middle	Top	M21–25	Sampler	Bottom	Top	Sampler	Bottom	Top
Depth (ft)	20–23	17–18		19–22			15.4–16.1	25–26.75			29–30.5		
T(°C)	1,130–1,135	1,075–1,105		1,110–1,125			1,065–1,075	~1,130			~1,135		
Number of points (0.3×0.3 mm grid)	1,229	678	1,284	2,456	1,500	1,907	1,478	1,000	2,000	1,500	1,862	2,000	2,000
Olivine	3.0	3.7	4.5	3.0	2.9	3.4	3.4	5.0	2.8	3.3	3.3	4.4	4.5
Pyroxene	16.1	9.5	8.0	12.2	7.2	8.9	62.1	17.7	13.6	11.8	13.4	15.1	11.5
Plagioclase	10.7	6.7	8.6	9.1	6.2	8.8	19.8	9.0	7.9	10.0	7.1	9.9	10.2
Fe–Ti oxide	----	----	----	----	----	1.7*	15.2	----	----	----	----	----	----
Glass	6.2	----	0.2	6.2	2.8	----	----	56.8	58.8	----	60.6	43.0	37.1
Quench	64.0	80.4	78.7	69.3	81.0	77.2	1.1	11.5	17.0	74.9	15.6	27.6	36.7

B. Melt samples collected through drill holes—(Continued)

		M22–18				M23–24				
Sample	M22–15	Bottom	Center	Top	M23–21	Bottom	Top	M23–25	M24–2	M24–3
Depth (ft)	21	21–23			24	24		24	27–29	29–30
T(°C)	1,095	1,095–1,110			1,095	1,090			1,060–1,085	1,085–1,100
Number of points (0.3×0.3 mm grid)	1,004	1,400	1,633	1,500	984	1,235	1,720	1,246	953	800
Olivine	4.9	2.6	2.2	1.9	1.7	1.8	2.0	2.1	0	.4
Pyroxene	22.2	18.3	13.8	19.7	12.2	8.2	7.7	7.4	24.9	15.5
Plagioclase	13.3	11.9	11.7	15.4	6.3	6.9	7.3	8.7	23.6	16.0
Fe–Ti oxide	0.5*	----	----	----	----	----	----	----	----	----
Glass	----	64.5	65.0	7.5	72.5	82.0	78.2	77.6	4.2	3.9
Quench	59.1	2.7	7.3	55.6	7.3	1.1	4.8	4.2	47.3	64.2

C. Drill core, partially molten 1,070 >T >980°

Sample	M1–6	M2–4	M5–13	M7–7	M9–13	M10–12	M10–13
Depth (ft)	6.1–7.1	6.1–7.1	10.1–11.0	7.9–8.9	10–10.5	8.0–9.0	9.0–10.0
T(°C)	1,040–1,100	1,040–1,100	1,060–1,070	1,030–1,085	1,055–1,070	955–1,010	1,010–1050
Number of points (0.3×0.3 mm grid)	1,500	1,404	1,500	1,848	2,000	1,281	1,500
Olivine	1.4	2.7	1.6	4.2	2.3	1.9	1.0
Pyroxene	35.7	33.6	45.4	32.3	40.4	52.0	49.5
Plagioclase	20.1	21.6	29.4	19.6	23.5	31.4	28.3
Fe-Ti oxide	1.1	.5	5.5	----	3.7	11.4	6.7
Glass	38.4	37.9	18.1	34.9	24.2	3.3	15.4
Quench	2.3	3.9	----	9.0	5.9	----	----

TABLE 13.—*Modal data, Makaopuhi lava lake*—Continued

C. Drill core. Partially molten—Continued

Sample	M10–14	M11–15	M11–16 a	M11–16 b	M11–16 c	M13–12	M13–13	M13–14	M21–17
Depth (ft)	10.0–10.6	11.0–11.9		11.9–12.9		8.1–9.1	9.1–10.1	10.1–11.1	15.9–16.9
T°C)	1,050–1,070	980–1,030		1,025–1,070		915–980	980–1,025	1,025–1,080	1,065–1,085
Number of points (0.3×0.3 mm grid)	4,000	1,254	2,000	2,000	1,500	1,500	2,000	2,000	1,436
Olivine	2.8	2.8	2.2	2.9	1.8	2.3	2.6	2.4	1.6
Pyroxene	37.7	40.8	39.4	49.1	46.0	51.1	50.3	42.3	29.7
Plagioclase	25.4	24.0	25.0	28.8	29.6	30.7	30.7	26.3	19.6
Fe–Ti oxide	3.3	3.7	3.8	9.1	4.6	11.3	8.3	4.4	----
Glass	30.8	28.7	29.6	10.1	17.1	3.5	7.2	24.3	29.0
Quench	----	----	----	----	0.9	1.1	1.0	0.3	20.2

C. Drill core. Partially molten—Continued

Sample	M22–12 Bottom	M22–12 Middle	M22–12 Top	M22–13	M23–15 Bottom	M23–15 Top	M23–16	M23–17 Bottom	M23–17 Top	M23–18 Bottom	M23–18 Top
Depth (ft)		16.0–17.0		18.0–19.0	15.9–16.9		16.9–17.9	17.9–18.65		19.7–20.9	
T(°C)		975–1,010		1,035–1,060	950–975		975–990	990–1,005		1,060–1,085	
Number of points (0.3×0.3 mm grid)	2,000	2,000	2,500	1,404	1,424	1,000	1,500	1,500	1,413	1,424	1,000
Olivine	1.5	2.2	2.5	1.4	0.9	1.4	1.2	0.7	1.2	1.8	1.4
Pyroxene	48.1	51.8	47.8	46.1	54.3	53.8	50.0	48.6	51.5	34.4	31.5
Plagioclase	31.7	30.0	34.2	25.6	28.5	31.0	27.1	32.6	31.7	24.1	26.8
Fe-Ti oxide	6.0	5.5	5.2	3.7	11.9	9.3	14.3	4.4	6.7	1.4	?
Glass	12.2	10.6	10.1	16.0	3.5	3.3	2.1	13.7	9.9	38.3	----
Quench	.6	----	.1	7.2	1.1	1.1	5.3	----	----	----	40.3

D. Drill core, subsolidus, T<980°C

Sample	M9–1	M9–2	M9–3	M9–4	M9–6	M9–7	M9–8	M9–10	M9–11	M2–1	M7–1
Depth (ft)	0–0.2	0.2–0.4	0.4–0.65	0.65–0.8	1.0–2.0	2.0–3.0	3.0–4.0	5.0–6.0	6.0–7.0	0–1.0	0–1.0
T(°C)	<100°	100–140	140–190	190–210	240–385	385–510	510–625	720–805	805–885	0–310	30–100
Number of points (0.3×0.3 mm grid)	1,500	820	1,500	1,500	1,500	1,000	1,500	1,500	1,185	1,343	1,000
Olivine	3.0	0.7	3.0	2.4	2.1	1.7	1.1	2.4	1.9	3.0	4.7
Pyroxene	29.4	38.8	42.0	45.1	46.1	46.6	50.4	51.4	54.4	34.7	25.6
Plagioclase	9.4	15.6	16.9	18.6	22.2	28.3	25.1	24.0	27.8	24.1	15.4
Fe-Ti oxide	----	1.2	2.4	5.1	8.6	9.7	12.0	13.9	11.1	8.6	2.8
Glass	----	----	----	----	----	1.5	0.9	2.0	2.5	29.6	----
Quench	58.2	43.7	35.7	28.8	21.0	12.2	10.5	6.3	2.3	----	51.6

D. Drill core, subsolidus—Continued

Sample	M7–6	M10–11	M11–13	M11–14	M13–11	M22–10	M22–11	M23–6	M23–9
Depth (ft)	4.9–5.45	7.0–8.0	9.0–10.0	10.0–11.0	7.1–8.1	11.0–12.0	14.0–15.0	4.9–5.9	8.9–9.9
T(°C)	725–800	885–955	865–920	920–980	845–915	780–820	900–935	360–425	600–670
Number of points (0.3×0.3 mm grid)	1,000	1,500	1,000	2,000	2,000	1,732	1,791	1,500	1,500
Olivine	1.8	2.2	2.5	2.0	2.0	0.7	1.1	1.2	1.9
Pyroxene	52.5	45.9	48.5	52.6	52.8	51.6	50.6	53.4	50.4
Plagioclase	21.1	28.4	31.4	30.8	30.6	33.8	32.6	24.8	29.0
Fe–Ti oxide	15.0	12.8	11.6	10.4	9.3	7.9	9.0	13.9	14.3
Glass	----	----	2.7	3.3	2.7	5.0	5.6	2.3	1.7
Quench	9.4	10.7	3.3	0.9	2.6	1.0	1.3	3.8	2.7

(sp gr=5.13 R.I−5.41)[9]. The results of such a construction are shown in figures 16, 17, and 18. The S-shaped curves of figures 17 and 18 show that the crystallization rate is fastest at temperatures close to the crust-melt interface, far exceeding the rates at near-liquidus or near-solidus temperatures.

The order of crystallization of minerals and their temperatures of first appearance are summarized in

[9]R. T. Okamura, unpub. data, Hawaiian glasses.

TABLE 13.—*Modal data, Makaopuhi lava lake*—Continued

68–1, 68–2, 69–1

Sample	69–1–22	68–2–59	68–1–21	68–2–20	68–1–19	68–1–18	68–1–17	68–1–16	68–2–15	68–1–14	68–1–7
Depth (ft)	60–66	59	54	51.5	49.5	48.0	46.1	44.2	42.0	39.8	26.0
T(°C)	1,100–1,105	1,100	1,082	1,060	1,055	1,043	1,029	1,011	<1,000	<1,000	<1,000
Number of points (0.4×0.5 mm grid)	1,616	956	1,996	1,673	1,816	1,828	2,000	1,376	1,901	1,859	1,934
Olivine	0	0.3	1.4	0.7	0.5	0.8	0.7	0.1	0.2	0.8	2.1
Pyroxene	0	7.3	9.5	15.7	20.4	25.3	31.1	34.2	32.5	36.5	43.1
Plagioclase	0.2	5.8	9.7	21.1	24.3	35.9	41.3	43.7	48.3	43.0	41.9
Fe-Ti oxide	0	0	0	1.3	1.8	4.1	6.6	5.8	6.2	7.3	6.5
Glass	99.8	83.6	76.9	50.0	----	27.2	14.4	11.8	9.3	7.3	3.0
Quench	0	3.0	2.5	11.2	53.0	6.7	5.9	4.4	3.5	5.1	3.4
Vesicles											
Volume percent	0	0.1	0.2	3.7	4.9	13.2	12.8	12.8	12.3	10.5	8.1
Size (mm) (median)	----	.15×.15	.35×.35	.3×.3	≤.3×.3	.5×1	1×1.5	.6×.85	.5×7	.5×5	.5×.5
(maximum)				(.7×.7)	(1×.5)	(1.2×1.2)	(1.5×2)	(1.5×2)	(1×2)	(1×1)	(1×2)

[1]Glassy skin, surface of lava lake near Drill hole #1.
[2]Small flow from original line of vents in Makaopuhi crater. Erupted March 5, 1965.

TABLE 14.—*Chemical mode for MPUMAV, Makaopuhi lava lake*

[Calculated by methods described in Wright and Doherty (1970). Mineral compositions are not all unique but are chosen to be reasonable for the bulk rock composition. MPUMAV—average composition of erupted pumice, table 12]

	As is	Corrected to 2 percent olivine[1]
Olivine (Fo_{70})	6.5	2.0
Augite ($En_{43}Fs_{23}Wo_{34}$)	33.4	41.7
Pigeonite ($En_{51}Fs_{39}Wo_{10}$)	6.4	
Plagioclase (An_{57})	42.5	44.5
Ilmenite	4.2	5.5
Titanomagnetite	1.0	
Apatite	0.6	6.3
Glass	5.4	

[1]These values of olivine, *total* pyroxene, plagioclase, *total* Fe-Ti oxide, and glass + apatite are used as a reference to correct optical modes (See fig. 16 and text, p. 31).

table 15, after Wright and Weiblen (1967).[10] Pigeonite, magnetite, and iron-rich rims on olivine, not distinguished optically, have been identified by the electron microprobe.

Melt samples that flowed into drill casings lost crystals during flow and appear to have lost augite relative to plagioclase and olivine. The latter effect can be seen in table 13, comparing samples collected at the top of a casing and those at the bottom (M21–26 top and bottom). The evidence for total amount of crystals lost is shown in table 16. The temperature of each sample is estimated from its crystallinity (glass content) using figure 17. This is compared with the actual temperature of collection derived from figure 10. Loss of crystals during flow into the casing results in a tempera-

[10]The glass percentages given as volumes in Wright and Weiblen (1967) are given as weight percent here.

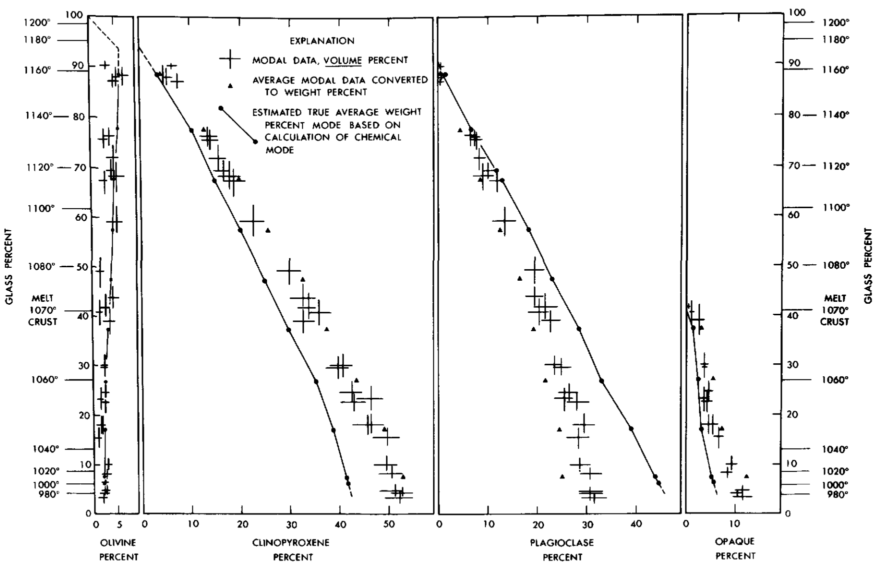

FIGURE 16.—Modal data (transmitted light—table 13) plotted as percent minerals versus percent glass. Temperatures (from fig. 17) are interpolated on the vertical axis. Data are converted to weight percent and compared with theoretical curves that pass through the mode calculated from the bulk chemistry (table 14). In all samples the pyroxene and opaque minerals are overcounted and plagioclase is undercounted due to masking effects promoted by the fine grain size (table 18). The true variation of olivine with temperature and glass is not known because of possible crystal settling.

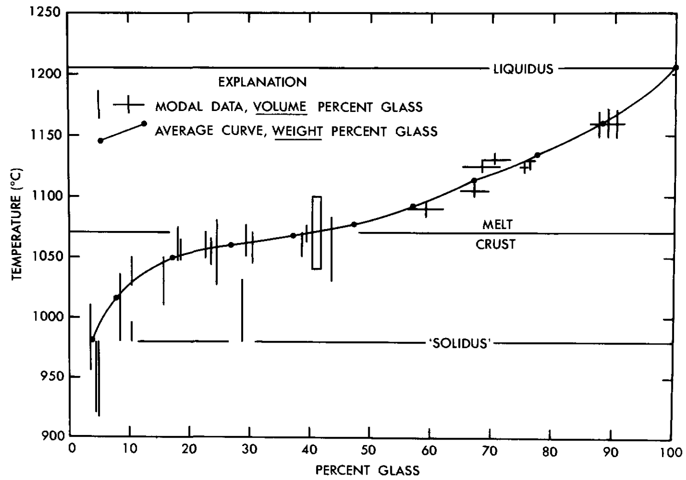

FIGURE 17.—Percent glass plotted against collection temperature. This is an updated version of figure 12 of Wright, Kinoshita, and Peck (1968). Length of bars show uncertainties in both temperature and modal composition. All samples used to define curve were collected above 8.5 m depth and were neither contaminated nor flow-differentiated. Liquidus is estimated from the MgO/FeO ratio (Tilley, and others, 1964; see also Wright and others, 1968, table 5), and solidus is drawn where residual glass content becomes approximately constant. The interface between crust and melt is defined from the drilling to be at a temperature of 1,070°C (fig. 10). Crystallization rate (percent crystallization per unit drop in temperature) is higher near the interface than at temperatures closer to either solidus or liquidus.

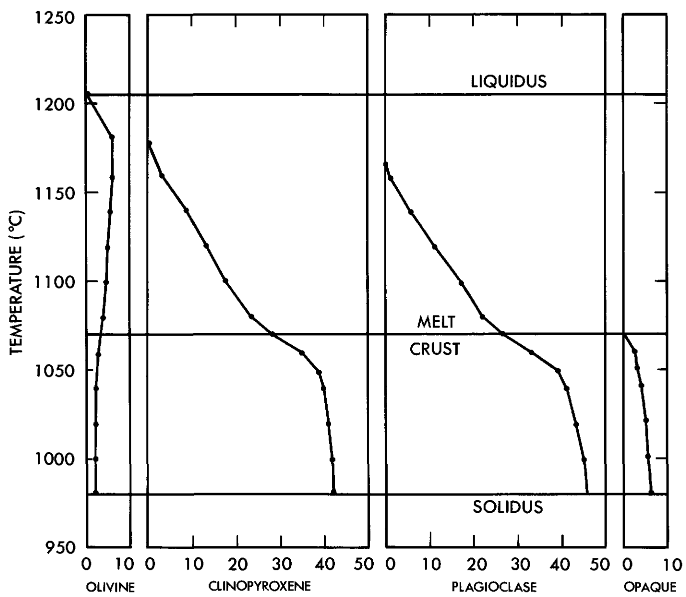

FIGURE 18.—Weight-percent minerals plotted against temperature. These are the solid lines of figure 16 plotted with temperature instead of glass content as the ordinate. This figure emphasizes, as does figure 17, the increased rates of crystallization across the crust-melt interface.

ture estimate that is higher than the true temperature of collection. This is confirmed for two chemically analyzed samples (M23–21 and M24–3) which show a large temperature discrepancy and have differentiated bulk compositions.

TABLE 15.—*Mineral paragenesis, Makaopuhi lava lake*
[After Wright and Weiblen (1967)]

Mineral	Composition	Temperature (°C±10°)	Glass (weight percent)
Olivine	Fo_{80-85}	1,205	100
Augite	$En_{47}Fs_{13}Wo_{40}$	1,185	94
Plagioclase	An_{67}	1,180	92
Ilmenite	$Ilm_{89}Hem_{11}$	1,070	44
Olivine	Fo_{55}	1,050	17
Pigeonite	$En_{61}Fs_{32}Wo_{7}$	1,050	17
Magnetite	$Usp_{63}Mag_{37}$	1,030	9
Apatite	----	1,020	7
Solidus	----	980	4 (residual glass)

One sample (M20–13) shows a lower temperature (higher crystallinity) then the temperature of collection. This sample was collected on the stainless-steel rotor used to measure viscosity in the melt (Shaw and others, 1968). The sample probably crystallized somewhat during the several hours it took to pull out rotor and casing.

Samples collected during the eruption show a range of temperatures, all of which are probably lower than the temperature of the main body of the lake because of cooling near the exposed edge of the lake before collection. The higher temperature samples were collected when the eruption rate was accelerating and the lake surface was visibly hotter (Wright and others, 1968).

The petrography of the core changes as a function of increasing depth in the following ways:

1. Olivine decreases both in size and amount; large (>1 mm diam) phenocrysts are absent below 10.1 m.
2. Grain size of all minerals increases with depth to a maximum in partially molten core collected at 13.4 m, then decreases as the amount of liquid increases in core collected at higher temperatures and greater depth.
3. Vesicle size and amount increase in the same way as grain size, reaching a maximum at about 14.0 m.
4. The amount of residual glass apparently increases with increasing depth. Modal counts given about 12 percent by volume at subsolidus temperatures near 12.2 m compared with 4–6 percent at depths less than 4.6 m.

Compositions of two residual glasses, determined by electron microprobe by R. L. Helz are given in table 17 compared with residual glass from Alae lava lake. The Alae glass was initially analyzed by wet-chemical methods, then used as a standard for probe calibration. The two Makaopuhi glasses differ significantly from the Alae glass only in iron content. All are mimimum melting calc-alkaline rhyolite compositions having about 3 percent admixture of mafic components. From mixing calculations (Wright and Doherty, 1970), the calculated amount of residual glass should be only

TABLE 16.—*Temperature (°C) of melt samples estimated in two different ways*

[T (measured) gives the temperature of collection read from the reconstructed temperature data of figure 10 using the date and depth of collection. T (modal) is the temperature inferred from the crystallization of the collected sample using figures 16 and 17. Where T (measured) exceeds T (modal) the sample is inferred to have crystallized to some extent during slow quenching. Where T (modal) exceeds T (measured), the sample is inferred to have lost crystals during flow differentiation. This effect is evident for two analyzed samples (M23–21 and M24–3) both of which have differentiated chemical compositions]

Sample no.	Date of collection	Depth of collection (ft)	T (measured) (°C)	T (modal) (°C)	Comment
M–3	March 7, 1965	surface	not known	1,125	Sample collected from the rising lava lake on ceramic tubes pushed into the melt. Quenched in air.
M–7	March 8, 1965	---- do ------	not known	1,120	Do.
M–8	March 11, 1965	---- do ------	not known	1,135	Do.
M–12	March 12, 1965	---- do ------	not known	1,165	Do.
M–18	March 14, 1965	---- do ------	[1]≥1,160	1,160	Do. quenched in water.
M–22	March 15, 1965	---- do ------	not known	1,160	Do.
M1–1G	April 19, 1965	0.0	[2]1,140	1,140	Glassy skin on lava-lake surface adjacent to drill hole 1.
M60–1B	April 1, 1965	surface	not known	1,160	Small flow from early, short-lived, vent.
M20–13	August 3, 1965	21–23	1,130–1,135	1,120	Melt in casing used to emplace viscometer (see Shaw and others, 1968). Probably crystallized during recovery of viscometer and casing.
M21–21	August 17, 1965	17–18	1,095–1,105	1,135–1,140	Flowed into drill steel. Probably differentiated.
M21–24	August 30, 1965	19–22	1,110–1,125	1,135–1,145	Lost augite relative to plagioclase during steam-impelled flow into drill steel.
M21–25	September 16, 1965	15.4–16.05	1,065–1,075	<980	Pyroxene-rich residue (see table 13) left in hole after collection of 21–24.
M21–26	September 16, 1965	25–26.75	1,130	1,115–1,130	Collected on ceramic and by flow into stainless steel casing. Probable loss of some crystals during flow.
M21–27	September 27, 1965	29–30.5	1,135	1,120–1,130	Do.
M22–15	November 9, 1965	21.0	1,095	1,095	Collected on ceramic.
M22–18	November 9, 1965	21.0–23.0	1,095–1,110	1,100–1,125	Collected in flow into stainless steel casing. Probably lost some crystals during flow.
M23–21	January 19, 1966	24.0	1,095	1,140	Flowed into drill bit. *Differentiated composition* (table 10)
M23–24	February 3, 1966	24.0	1,090	1,145	Melt in drill bit.
M24–2	July 28, 1966	27.0–29.0	1,060–1,085	1,085	Flowed into core barrel, bottom sampler.
M24–3	July 28, 1966	29.0–30.0	1,085–1,100	1,115	Do. Top sample *Differentiated composition* (table 10).

[1]Thermocouple reading during collection.
[2]Minimum temperature inferred from profile obtained on April 21, 1965 (table 3) is consistent with finite element modeling and heat flow calculations related to loss of heat during crustal foundering March 15–19, 1965 (H.R. Shaw, written commun. 1974).

about 10–20 percent greater for differentiated samples. Thus part of the difference in modal glass content is probably not real but instead due to grain-size-related counting errors.

DISTRIBUTION OF OLIVINE

The distribution of large (>1 mm) phenocrysts crystals of olivine in drill holes 68–1 and 68–2 is shown schematically in figure 19 as determined from megascopic examination of drill core. The largest olivine phenocryst observed measured 7 by 8 mm, but most do not exceed 5 mm in diameter. There is a good correspondence between the MgO content and amount of observed olivine; samples in which MgO is less than about 7.8 percent contain no large olivine phenocrysts.

The distribution of olivine is not the same in the two drill holes. Relative to 68–1, the upper part of 68–2 is depleted in olivine, and the zone from 9.1 to 10.1 m has visible olivine, missing in 68–1.

VARIATION IN GRAIN SIZE

Maximum, minimum, and median grain diameters have been estimated from thin sections for each analyzed sample in holes 68–1 and 68–2 (table 18), and median grain volumes were computed (fig. 20, table 19). Grain size remains nearly constant to about 6.1 m, then increases irregularly, reaching a maximum in the partially molten sample 68–1–17 collected at 13.4 m. The grain size then decreases downward as the percent of melt increases.

CORE DENSITY AND VESICLE DISTRIBUTION

The vesicle distribution in the lake was studied by inspection of drill core from holes 68–1 and 68–2 and by measurements of abundance and maximum and median diameters in thin sections (tables 13 and 19). Bulk core densities were measured on large pieces of core (table 20; fig. 2). Core densities vary irregularly with depth, and the variation is different in the two drill

TABLE 17.—*Composition of residual glass from Makaopuhi and Alae lava lakes*

	Makaopuhi lava lake		Alae lava lake	
	68–1–7 Depth 26.0'[1]	68–1–14 Depth 39.8'[1]	A12–9 (probe)[1]	A12–1011 (wet chemical)[2]
SiO_2	75.0	75.1	75.9	75.8
Al_2O_3	12.6	12.6	11.9	12.2
FeO	.76	1.64	1.1	1.6
MgO	.03	.05	.05	.2
CaO	.40	.43	.54	.6
Na_2O	3.25	3.44	3.37	3.4
K_2O	5.82	5.64	5.99	5.5
TiO_2	.45	.33	.24	.7
P_2O_5	----	----	----	----
MnO	----	----	----	----
Total	98.2	99.2	99.2	100.0

[1]Electron microprobe analyses by R. T. Helz.
[2]Recalculated from analyses of four impure separates after correcting for feldspar and apatite. Analyst: R. Meyerowitz and J. Marinenko.

holes, as is evident in the photographs of the two cores (figs. 24, 25).

Megascopic inspection of core from holes 68–1 and 68–2 shows that the vesicle distribution is irregular in the upper part of the lake. Down to a depth of 3.0 m, the vesicles are large (as much as 15 mm diam, median diam=4–6 mm) and abundant. Their abundance in 68–1 decreases to a minimum around 6.1 m, corresponding to the location of the maximum core density (fig. 21). Large single vesicles persist to a depth of 6.1 m in both drill holes; the largest observed measures 20×16 mm at 2.5 m. Below 7.6 m the vesicle distribution is quite regular.

Below 3.0 m, vesicle cylinders and sheets are common although poorly formed in both drill holes. These concentrations of vesicles are always associated with a greater amount of glass than is in the host rock, and where they are well formed, the rock breaks along them and blades of ilmenite line the vesicle walls. The glass and ilmenite suggest that the cylinders and sheets mark zones of low pressure into which relatively late-stage liquid was beginning to segregate.

Thin-section study shows that median vesicle size increases with depth in the lake similar to the changes in grain size, reaching a maximum at about 14.0 m (fig. 20). The vesicularity of partly molten samples is greater than that of the solidified rock immediately above, although the deepest partly molten samples in drill hole 68–2 are quite dense. Melt samples collected between depths of 16.5 and 18.3 m are dense, containing 1–2 vesicles per thin section. The specific gravity of sample of melt containing only traces of crystals or vesicles (69–1–22) is 2.78±0.02. This contrasts with samples of melt collected in 1965–66 from depths of 4.6–6.1 m, which had many long tubular vesicles and a low bulk density.

The relation between core density and depth are different for the small pieces of drill core collected in

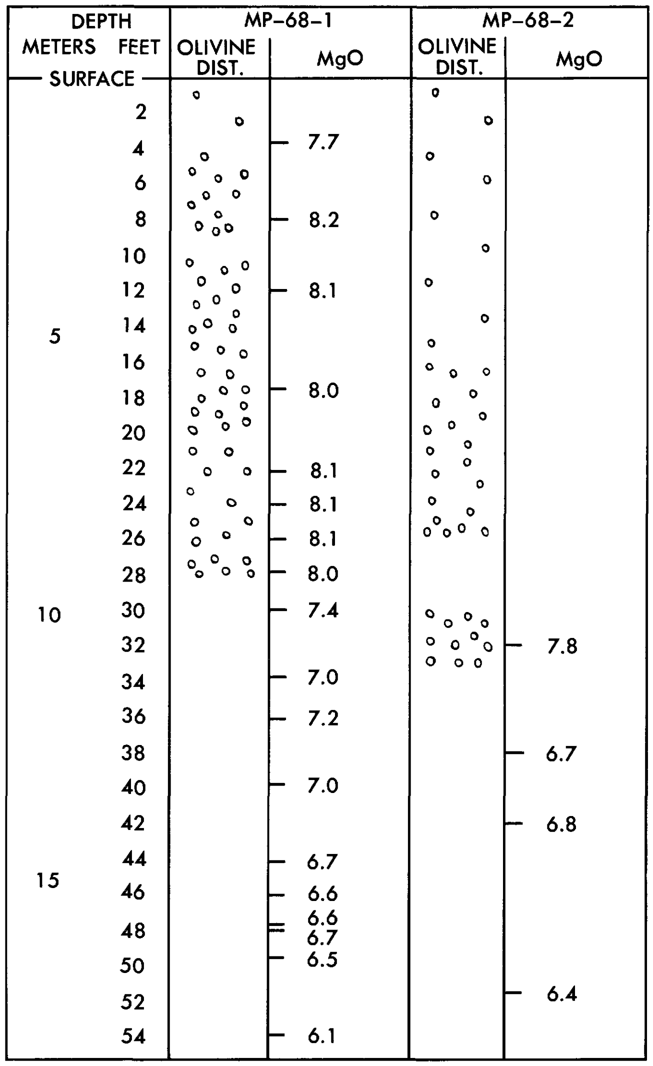

OLIVINE CONCENTRATION WITH DEPTH, MAKAOPUHI LAVA LAKE DRILL HOLES

FIGURE 19.—Schematic distribution of large (>1 mm diam) olivine crystals in drill holes 68–1 and 68–2. Note the different distribution in the two drill holes and the correlation between MgO content and the incidence of large olivine. Samples below 8.5 m depth are flow differentiated (fig. 22).

1965–66, compared with the large pieces collected in 1968 (fig. 21). For a given depth, bulk core densities are lower in the larger core reflecting the irregular distribution of vesicles and the presence of some large vesicles. Drilling without a core spring reduces recovery and biases it toward denser pieces of rock.

DISCUSSION

All of the data summarized under "Observations" contribute to our understanding of the cooling and crystallization of basaltic lava in Makaopuhi lava lake. Unfortunately none of the sets of measurements forms

TABLE 18.—*Summary of grain-size measurements for analyzed samples from drill holes 68–1 and 68–2.*
[Grain size (mm)]

Sample	Depth[1] (ft)	T (°C)[2]	Olivine median	Olivine min/max	Augite median	Augite min/max	Plagioclase median	Plagioclase min/max	Ilmenite median	Ilmenite min/max	
68–1–2	8.0	<100	0.15–0.3× .15–.3	0.1×0.1 .6×.6	0.015×0.015	<.015 .15×.15	0.03×0.15	<.015 .06×.35	0.03×0.15	0.015 .07×.2	
68–1–3	12.0	<100	.3×.3	.1×.1 1×1	.015–.03 ×.015–.03	<.015 .25×.25	.015 to .04 ×.15–.2	<.015 .07×.5	.015–.04 ×.15–.3	.015 .07×.3	
68–1–4	17.5	<100	.2–.35 ×.2–.35	.1×.1 .6×.1	.015–.03 ×.015–.03	<.015 .35×.35	.015–.04 ×.15–.2	<.015 .1×.4	.03× .15–.20	.015 .07×.35	
68–1–5	22.0	>120	.2–.3 ×.2–.3	.07×.07 .4×1	.015–.03 ×.015–.03	<.015 .15×.15	.015–.04 ×.15–.2	<.015 0.1×0.9	.03–.04 ×.2	.015 .15×.4	
68–1–6	24.0	>180	.3×.3	.1×.1 1×2	.015–.03 ×.015–.03	<.015 .15×.20	.015–.04 ×.5–.2	<.015 .3×.3	.04–.07 ×.15–.2	.015 .15×.3	(rare)
68–1–7	26.0	>250	.2×.3	.1×.1 .8×1.1	.015–.04 ×.015–.04	<.015 .3×.4	.015–.04 ×.15	⩾.015 .5×.5	.04–.07 ×.15–.3	.015 .2×.5	(rare
68–1–8	28.0	>330	.3×.3	.1×.1 .6×.7	.015–.04 ×.015–.04	<.015 .35×.35	.015–.04 ×.15	⩾.015 .15×.5	.04–.07 ×.15–.3	.015 .2×.4	(rare)
68–1–9	30.0	>410	.35×.35	.2×.2 .4×.6	.03–.06 ×.03–.06	<.015 .2×.65	.04–.07 ×.2–.4	.02 .15×1	.06–.08 ×.2–.45	.02 .15×.4	
68–2–10	32.0	>480	.3×.3	.1×.1 .35×1.2	.015–.04 ×.015–.04	<.015 .2×.2	.015–.04 ×.15	⩾.015 .5×.5	.03–.06 ×.2	.015 .2×.3	(rare)
68–1–11	33.8	>545	.3×.3	.7×.7	.03–.07 ×.03–.07	⩾.015 .3×.3	.07 ×.2–.3	.025 .35×.5	.07–.10 ×.3–.45	.02 .2×.7	(rare)
68–1–12	36.0	>620	.2×.2	.75×.75	.03–.07 ×.03–.07	⩾.015 .25×.25	.07 ×.2–.3	.02 .1×.7	.07–.10 ×.3–.45	.03 .15×.4	
68–2–13	38.0	>690	.15–.35 ×.15–.35	.8×.8	.04–.07 ×.04–.07	.025 .2×.2	.04–.07 ×.2–.3	.02 .15×.8	.07–.15 ×.3–.45	.03 .2×1	
68–1–14	39.8	>750	.2×.2	1.2×.25	.04–.07 ×.04–.07	.02 .25×.25	.03–.07 ×.2–.35	.03 .15–.7	.07–.15 ×.3–.5	.03 .2×.5	(rare)
68–2–15	(41.0) 42.0	990	.2×.2	.25×.25	.07–.14 ×.07–.14	.03 .4×.4	.05–.1 ×.4–.7	.03(rare) .3×.6	.07–.15 ×.3–.5	.03 .15×.7	(rare)
68–1–16	44.2	1,011	none		.07–.15 ×.07–.15	.04 .3×.45	.07–.15 ×.3–.45	.03 .35×.8	.07–.15 ×.3–.55	.02 .3×.6	(rare)
68–1–17	46.1	1,029	.3×.3	.5×.5	.07–.15 ×.07–.15	.03 .15×.6	.06–.10 ×.3–.4	.03 .4×.6	.07–.15 ×.25–.55	.015 .35×.6	
68–1–18	48.0	1,043	rare .2×.2	.4×.4	.06–.10 ×.06–.1	.03 .15×.3	.04–.07 ×.2–.4	.03 .2×.7	.04–.09 ×.3–.55	.02 .2×.7	(rare)
68–1–19	49.5	1,055	rare .2×.2	.2×1	.04–.10 ×.04–.1	.03 .15×.3	.03–.07 ×.15–.35	.02 .1×.6	.07×.4	cannot tell	
68–2–20	(50.5) 51.5	1,060	.2×.2	.35×.6	.03–.07 ×.03–.07	.02 .2×.2	.03–.06 ×.15–.30	.015 .25–.5	.04 ×.25–.45	.01 .07×.9	
68–1–21	54.0	1,082	rare .2×.2	.3×.5	.03–.07 ×.03–.07	.02 .2×.4	.03–.06 ×.15–.20	.015 .15×.3		not present	

[1]Samples collected in drill hole 68–2 were slightly cooler at the same depth than samples collected in drill hole 68–1. For consistency in comparing data from the two drill holes, the value in parenthesis is the estimated depth in 68–1 that fits the temperature of collection. The 2d value is the actual depth of collection.
[2]Temperatures are estimated from the last temperature profile measured. The crust-melt interface was assumed to be at 1,070°C, and the solidus was assumed to be at 980°C. The position of the 1,000° isotherm was estimated from the glass content of the core using figure 17. The temperature data are subject to uncertainties in these assumptions.

TABLE 19.—*Volumes* ($mm^3 \times 10^6$) *of crystals and vesicles; samples from drill holes 68–1 and 68–2*

Sample No.	Depth (ft)	Augite Median	Augite Maximum	Plagioclase Median	Plagioclase Maximum	Ilmenite Median	Ilmenite Maximum	Vesicles Median	Vesicles Maximum
68–1–2	8	0.00005	3.4	0.13	4.2	0.13	1.9	wide range	15625
1–3	12	.0013	15.6	.13	9.8	.11	3.9	20.8	5832
1–4	17.5	.0013	42.9	.13	10.0	.16	5.1	20.8	125
1–5	22	.0013	3.4	.13	45.0	.25	16.5	76.8	1953
1–6	24	.0013	4.5	.13	27.0	.53	10.1	76.8	1000
1–7	26	.022	36.0	.11	125.0	.68	35.0	144.7	236
1–8	28	.022	42.9	.11	3.0	.68	24.0	231.2	729
1–9	30	.091	26.0	.91	86.3	1.59	16.5	301.8	800
2–10	32	.022	8.0	.11	125.0	.41	15.0	74.4	512
1–11	33.8	.125	27.0	1.23	73.5	2.71	63.0	231.2	625
1–12	36.0	.125	15.6	1.23	28.0	2.71	16.5	130.0	452
2–13	38	.166	8.0	.76	57.0	4.54	120.0	480	729
1–14	39.8	.166	15.6	.69	44.6	4.84	35.0	166.6	452
2–15	41.0	1.16	64.0	3.09	81.0	4.84	44.6	195.3	875
1–16	44.2	1.33	16.2	4.53	161.0	5.14	81.0	421.9	5832
1–17	46.1	1.33	13.5	2.24	120.0	4.84	99.8	693	14976
1–18	48.0	.512	6.8	.91	63.0	1.80	63.0	421.9	5832
1–19	49.5	.343	6.8	.63	21.0	1.96		19.7	729
2–20	50.5	.125	8.0	.46	46.9	1.06	30.6	144.7	1000
1–21	54	.125	17.6	.35	10.1	----	----	64.0	125

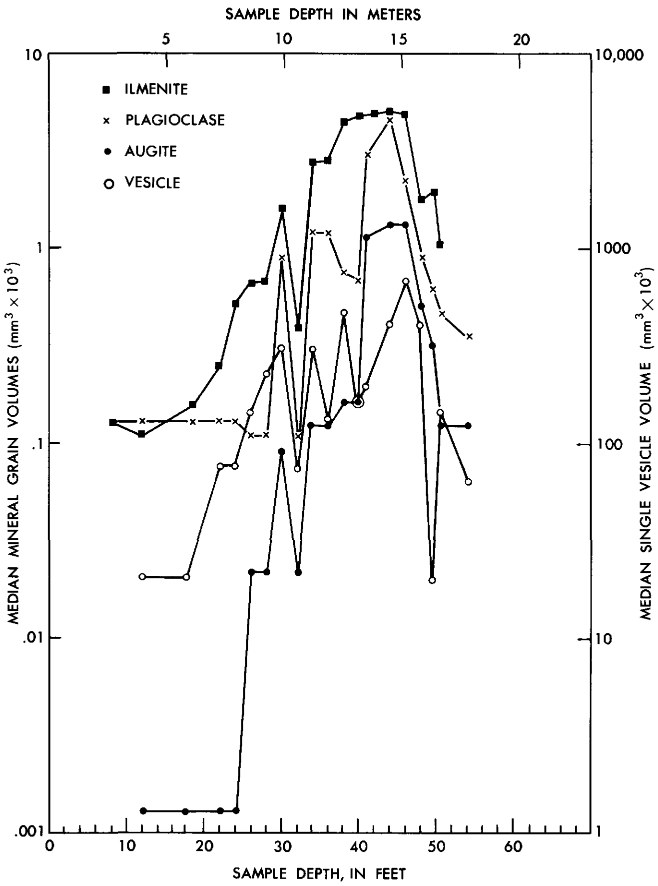

FIGURE 20.—Median volumes of augite, plagioclase, ilmenite, and vesicles plotted against depth (note different scale for vesicles). Data are given in table 19, calculated from grain size data given in table 18. Grain size is nearly constant between 1.8 m and 6.1 m. Between 1.8 m and the surface, the core shows increasing amounts of devitrified glass and fine-grained quench intergrowths of the mineral phases. Below 6.1 m, grain size increases and reaches a maximum in partially molten core collected at 13.4–14.0 m. Grain size decreases below 14.0 m correlated with decreasing crystallinity of the partially molten samples.

TABLE 20.—*Density of drill core from holes 1–23, 1965–66, and 68–1, 68–2, 1968*

Core no.	Depth (ft)	Weight (grams)	Density (g/cc)	
M–3–5	0–1.08	8.832	2.03	
M–3–5	0–1.08	12.503	2.03	
M–3–6	1.08–1.87	11.028	2.39	
M–4–3	0–1.0	7.161	1.63	
M–5–4	0–1.0	9.595	1.60	
M–5–5	1.0–2.1	8.043	2.33	
M–5–6	2.1–3.1	9.404	2.36	
M–5–7	3.1–4.1	5.042	2.51	
M–5–9	6.1–7.1	9.979	2.45	
M–5–11	8.1–9.1	15.448	2.43	} 2.505
M–5–11	8.1–9.1	15.148	2.58	
M–5–13	10.1–10.3	13.568	2.66	
M–7–5	3.5–4.9	33.872	2.48	
M–9–7	2.0–3.0	6.840	2.44	
M–9–8	3.0–4.0	4.141	2.37	
M–9–9	4.0–5.0	7.942	2.42	
M–10–14	10.0–10.6	5.367	2.61	
M–11–4	0–1.0	19.558	2.03	
M–11–4	0–1.0	16.481	2.03	
M–11–5	1.0–2.0	12.724	2.24	

TABLE 20.—*Density of drill core from holes 1–23, 1965–66, and 68–1, 68–2, 1968*—Continued

Core no.	Depth (ft)	Weight (grams)	Density (g/cc)	
M–11–6	2.0–3.0	11.032	2.20	
M–11–8	4.0–5.0	20.139	2.30	
M–11–9	5.0–6.0	14.907	2.26	
M–11–10	6.0–7.0	13.358	2.30	
M–11–12	8.0–9.0	9.794	2.38	
M–11–13	9.0–10.0	8.268	2.57	
M–11–14?	10.0–11.0	5.751	2.48	
M–11–16	11.9–12.9	27.868	2.64	} 2.65
M–11–16	11.9–12.9	26.554	2.66	
M–13–14?	10.1–11.1	4.862	2.54	
M–13–15	11.0–11.8	6.902	2.60	
M–13–13	9.1–10.1	16.141	2.54	
M–13–14	10.1–11.1	25.356	2.65	} 2.655
M–13–14	10.1–11.1	10.047	2.66	
M–16–3	0–1.8	10.334	1.75	
M–16–6	3.85–4.8	11.808	2.47	
M–16–8?	5.92–6.92	6.288	2.58	
M–16–9	6.92–7.92	13.379	2.65	
M–16–11	8.92–9.92	7.060	2.57	
M–16–14	11.92–12.92	7.460	2.72	
M–17–4	0.9–1.5	14.915	2.26	} 2.255
M–17–4	0.9–1.5	14.620	2.25	
M–17–10	13.5–14.5	6.498	2.40	
M–20–6	5.1–6.1	10.303	2.55	
M–20–9?	12.1–13.1	3.371	2.50	
M–20–10	13.1–14.1	9.688	2.59	} 2.595
M–20–10	13.1–14.1	8.819	2.60	
M–21–14	12.95–13.95	7.245	2.66	
M–22–10 ?	11.0–12.0	4.531	2.27	
M–23–1	0–1.2	20.244	1.76	
M–23–2	1.2–2.2	10.848	2.14	
M–23–3	2.2–3.2	8.339	2.51	
M–23–7	5.9–7.9	7.664	2.55	
M–23–8	7.9–8.9	12.345	2.59	
M–23–9	8.9–9.9	6.558	2.47	
M–23–13	12.9–13.9	16.070	2.66	
M–23–15	15.9–16.9	3.638	2.62	

Drill hole 68–1: Depth (ft)	Weight (grams)	Density (g/cc)	Drill hole 68–2: Depth (ft)	Weight (grams)	Density (g/cc)
1.0	350.9	1.95	0.5	35.2	1.94
1.0	104.2	1.91	2.0	63.5	2.32
1.9 –2.8	416.0	2.46	3.7	284.8	2.51
3.7	597.0	2.44	3.9	135.8	2.47
6.6	193.0	2.42	8.8	388.0	2.48
7.3	6.27	2.54	9.0	385.0	2.34
8.8	484.2	2.76	9.2	782.5	2.59
9.0	1003.5	2.38	9.8	500.0	2.68
9.5	1102.9	2.46	10.0	812.2	2.61
10.0	1372.5	2.55	10.6	1154.5	2.66
10.8	898.5	2.65	11.4	310.08	2.71
11.4	681.2	2.57	11.7	495.5	2.67
12.2	432.3	2.61	12.2	218.2	2.66
12.5	2560.0	2.52	12.6	271.5	2.66
14.8	1176.5	2.60	12.8	284.2	2.61
15.5	1946.0	2.60	13.1	242.6	2.68
16.3	222.3	2.84	13.5	1170.3	2.78
16.5	241.9	2.73	14.4	268.5	2.73
17.0	931.3	2.75	14.7	298.7	2.80
17.8	291.4	2.74	17.5	189.6	2.69
18.0	419.0	2.76	17.9	211.9	2.72
18.3	486.7	2.71	18.2	155.8	2.66
18.6	1700.0	2.78	18.3	2150.0	2.67
20.0	1211.0	2.78	19.5	955.0	2.68
20.6	2980.0	2.74	20.0	968.5	2.66
22.3	773.0	2.73	22.1	1385.0	2.75
23.0	2276.0	2.72	22.9	1257.0	2.74
24.2	1054.0	2.72	23.6	2880.0	2.73
25.0	1650.0	2.76	25.3	239.5	2.69
25.9	932.0	2.68	25.5	302.0	2.72
26.5	1094.0	2.69	26.0	680.0	2.62
27.4	1280.0	2.71	27.3	249.0	2.56
28.3	508.0	2.65	27.6	275.2	2.56
29.35	943.0	2.67	27.9	545.3	2.65
30.7	484.7	2.69	30.9	263.2	2.76
31.0	179.0	2.69	31.2	289.1	2.78
33.5	206.7	2.58	31.5	404.2	2.70
34.6	108.5	2.57	33.0	382.5	2.59
37.2	131.0	2.63	34.1	301.0	2.63
38.5	111.0	2.57	35.0	384.7	2.63
45.1	344.7	2.43	37.0	71.5	2.58
45.5	481.0	2.52	38.8	193.5	2.47
45.8	557.2	2.54	39.3	258.6	2.53
46.2	646.0	2.53	45.7	240.1	2.59
46.8	423.5	2.57	45.9	723.1	2.66
47.1	647.0	2.52	47.0	80.05	2.52
47.5	241.5	2.46	47.1	196.85	2.51
47.6	181.7	2.50	49.0	132.6	2.53
48.0	513.5	2.48	49.1	207.0	2.56
48.5	703.0	2.50	50.0	204.0	2.57
49.0	192.0	2.52	50.2	928.5	2.74
			50.7	1179.0	2.83

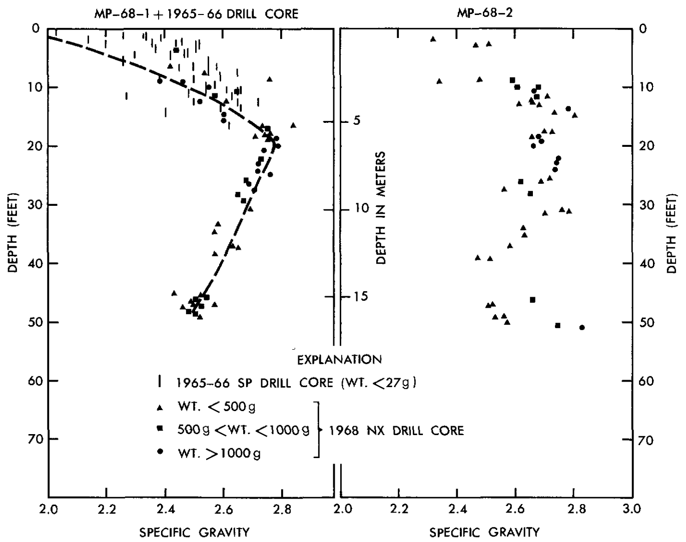

FIGURE 21.—Bulk density of drill core plotted against depth. The left-hand plot compares the density of 1-cm drill core collected in 1965–66 with that of 6-cm drill core collected from drill hole 68–1 in 1968. The incidence of large vesicles and vesicular zones recovered in the larger core explains the somewhat lower bulk density of this core at similar depths compared with the 1-cm core where only the denser pieces were recovered.

The right-hand plot shows the density profile of drill hole 68–2 drilled only a few metres away. The scatter is much greater although both holes show a maximum density of 2.78 g/cc at depths of 5–6 m. Densities of partially molten core reach minimum values of 2.5 g/cc at a depth of 15 m before increasing again below the crust-melt interface (DH 68–2). Density of crystal- and vesicle-free glass that flowed into the core barrel during drilling of hole 69–1 is 2.78 g/cc for comparison (sample 69–1–22), tables 9 and 11).

a complete record, because of the difficulties of measurement and the premature burial of the lava lake. The following sections discuss only those topics for which information is sufficient to form reasonable inferences about processes that took place in the lake. Final answers will come only from study of other bodies of molten basalt and from experimental studies and scale modeling of cooling and crystallization processes. We hope that the following sections will stimulate others to pursue topics of use in refining the hypotheses presented in this paper.

CHEMICAL DIFFERENTIATION IN THE LAVA LAKE

Three differentiation processes were observed in the lava lake.

1. Gravitative settling of large olivine crystals.
2. Removal of augite, plagioclase, and smaller olivine crystals from melt, possibly during convective flow.
3. Formation of liquid segregations by flow into open fractures in the partly molten crust.

These processes are seen on a small scale in the lava lake, but they are also important on a larger scale in explaining the overall variation in composition of Kilauea lavas, for they are inferred to take place in the conduits and magma reservoirs of the volcano (Wright and Fiske, 1971).

GRAVITATIVE SETTLING OF OLIVINE

The incidence of large olivine phenocrysts decreases markedly, if erratically, with increasing depth in the lava lake (fig. 19). We infer that many of the large olivine phenocrysts settled through the melt and became concentrated near the bottom of the lake. Support for this inference comes from the study of the prehistoric Makaopuhi lake, which has a zone of high olivine concentration about three quarters of the way from the top (Moore and Evans, 1967).

Is the presence of large olivine phenocrysts at the observed depths in the 1965 lava lake consistent with a simple crystal settling model? To answer this question, we assume that Stokes law is obeyed and make the additional simplifying assumption that the olivine settles at a constant rate at temperatures of more than 1,100°C. If the settling rate exceeds the rate at which the 1,100° isotherm moves downward, olivine will be lost to the bottom part of the lake. The slope of the 1,100° isotherm, taken from figure 10, as a function of depth is as follows:

Depth (m)	1.52	3.05	4.57	6.10	7.62
Slope $\times 10^5$ (cm/sec)	6.64	3.55	2.40	1.82	1.46

Viscosities of melt at 1,100°, 1,110°, and 1,130°C were estimated from glass analyses (table 11, analysis 69–1–22; Weiblen and Wright, unpub. data) using the method described by Shaw (1972, table 2 and equation 3, p. 873).

Results are as follows:

Sample No	69–1–22	M22–18GL	M21–26G1
Temperature (°C)	1,100°	1,110°	1,130°
Viscosity (poises)	1,148	1,072	832

If we use the maximum viscosity value (1,148 poises) and assume a density difference of 0.6 (g/cc) between olivine and liquid, the Stokes law equation can be solved for the radius (r) of a crystal whose settling rate would equal the rate of movement of the 1,100° isotherm.

$$V=\frac{2gr^2\Delta\rho}{9\eta} \tag{5}$$

where

V = velocity of the particle
$\Delta\rho$ = difference in density between olivine and liquid
η = viscosity of the liquid in poises
g = gravitational constant

Solving for a velocity equal to the rate of depression of the 1,100° isotherm at a depth of 1.52 m, we get:

$$6.64\times10^{-5} = \frac{2\times980\times0.6\times r^2}{9\times1{,}148}$$

$$r=0.0242 \text{ cm}$$

Thus olivine crystals of a diameter greater than 0.5 mm that crystallized at a temperature of more than 1,100°C should not be found at depths greater than about 1.5 m. This result, however, is contradicted by the data of figure 19, indicating that there were factors that inhibited the settling of olivine. Two obvious possibilities are: (1) interference of settling olivine crystals by upward-moving gas bubbles or (2) inhomogeneities caused by movement of foundered crust or by currents or turbulence in the upper part of the lake. We cannot offer a quantitative explanation on the basis of present knowledge.

FLOW DIFFERENTIATION OF OLIVINE-AUGITE-PLAGIOCLASE

The grain size of augite (table 18) and the low density of plagioclase preclude the gravitative settling of these minerals, based on consideration of Stoke's law. Yet analyzed samples of core from depths of more than 8.5 m have differentiated compositions explainable by removal of these minerals plus olivine. The amount and composition of the minerals removed has been estimated by mixing calculations (Wright and Doherty, 1970), using the average composition of Makaopuhi pumice (MPUMAV in table 12) as a parent (figs. 22, 23.) Figure 22 shows the total amount of the three silicates removed as a function of depth. Superimposed on the overall trend are reversals amounting to 1–3 percent total crystals. The maximum number of crystals removed from the crust from 68–1 and 68–2 is 25 percent at 16.5 m. A melt sample collected at 18.0 m (68–2–59) shows less differentiation, possibly because it was collected at a high temperature when crystal removal was still going on. Three samples of melt that flowed into drill-hole casings plot off the main trend in figure 22. All of these have fewer crystals (by modal count) and are more differentiated than samples collected in place at equivalent depths. The shallowest sample was collected at a depth where subsequently drilled core was found to be undifferentiated. These samples are inferred to have lost crystals during flow into the casings and thus confirm that this type of differentiation can indeed happen during flow.

Mineral percentages derived from the mixing calculations and calculated mineral compositions (fig. 23), were both plotted as a function of the amount of liquid remaining, according to the calculation:

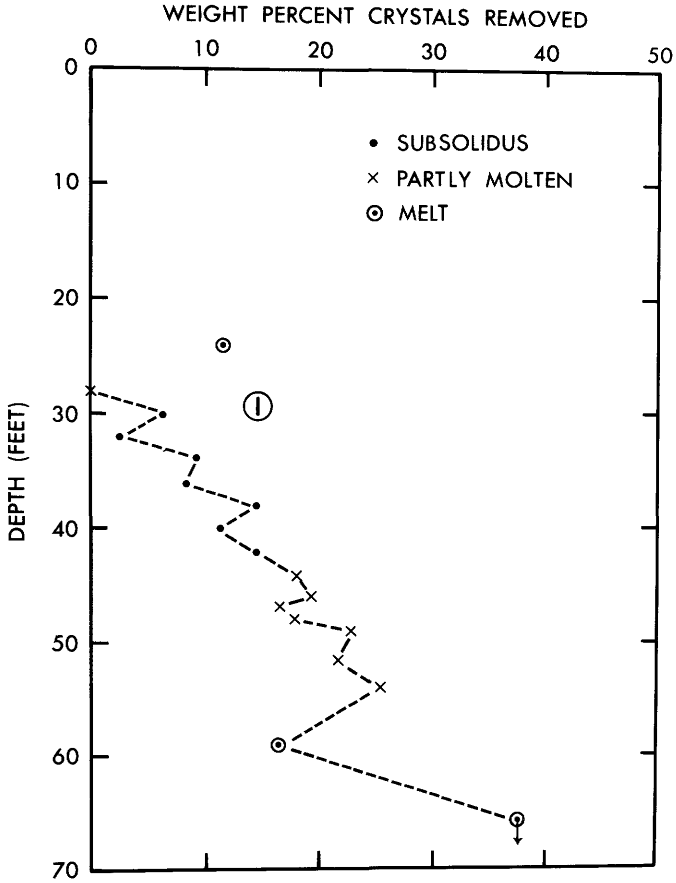

FIGURE 22.—Results of differentiation calculations, Makaopuhi lava lake. The following mixing equation was solved by the method of Wright and Doherty, 1970) for each sample collected in 1968. (Chemical analyses are given in table 11 and plotted in figure 15.)

MPUMAV (table 12) (parent) = a × composition of 1968 drill core (differentiate) + b × olivine + c × augite + d × plagioclase + e × ilmenite where a+b+c+d+e=1

Samples collected shallower than 8.5 m show only a small value for b (a is near 1 and c, d, and e are 0); below 8.5 m the sum of b+c+d+e (=crystals removed from parent to give composition of differentiate) are plotted on the abscissa at the depth at which each sample was collected. Symbols are explained in the figure. The broken line traces a pattern of erratically increasing amount of differentiation with depth. The two samples that plot off the line (M23–21 and M24–3 of table 16) were differentiated artifically by flow into the core barrel or bit during sampling. The vertical bar inside the circle indicates uncertainty in the depth of collection of the melt.

$$\text{Parent (MPUMAV)} = x \text{ percent olivine} + y \text{ percent augite} + z \text{ percent plagioclase} + a \text{ percent liquid} \qquad (6)$$

where

$x + y + z + a = 100$ percent.

Two sets of assumptions were tested to derive mineral compositions. The first assumed that olivine com-

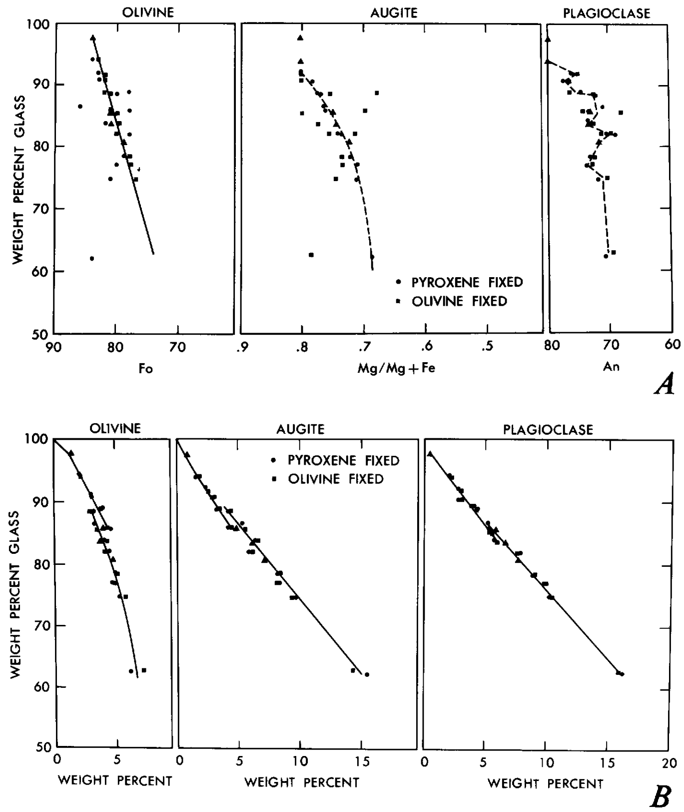

FIGURE 23.—Results of differentiation calculations, Makaopuhi lava lake. *A*, Composition of minerals removed as a function of amount of differentiation (see mixing equation in caption for fig. 22). The squares represent the results of calculations that assume regular increase in Fe/Mg ratio of olivine with increased amount of differentiation; Fe/Mg ratios of augite are determined by calculation and scatter widely. The dots represent the results of calculations that assume a regular increase of Fe/Mg ratio of augite with increased amount of differentiation; Fe/Mg ratios of olivine are determined by calculation and scatter widely. Plagioclase compositions are obtained by calculation and show slight differences related to assumptions regarding composition of mafic phases. Triangles represent selected points on the curves of weight percent mineral plotted against weight percent glass calculated from modal data of undifferentiated samples (fig. 16). *B*, Weight percent of olivine, augite, and plagioclase lost as a function of the amount of differentiation (refer to mixing equation in caption for fig. 22). Coefficients b (olivine), c (augite), and d (plagioclase) are plotted against a (amount of differentiate). Symbols as in *A*. The calculated amounts of crystallizing phases are little affected by assumptions regarding composition of augite and olivine (see above). There is a break at about 87 percent glass where both the absolute amount of the rate of crystallization of augite and plagioclase increase at the expense of olivine.

position varied regularly and linearly as a function of liquid content, becoming more iron-rich with decreasing amount of liquid; the composition of the augite was not specified. The other assumption was that augite varied in composition from an assumed magnesian augite ($En_{47}Fs_{13}Wo_{40}$, according to Wright and Weiblen, 1967) to more iron-rich compositions with decreasing liquid content; the composition of the olivine was not specified. In either case the compositions of the mineral whose composition was not initially assumed scatter widely (fig. 23), indicating that the olivine and pyroxene were not removed in precisely the proportions present in the melt. Plagioclase compositions were calculated from two extreme compositions, An_{80} and An_{60}, and show a general trend of increasing soda in plagioclase with decreasing amount of liquid. The plagioclase compositions are affected to a small (<2 An percent) extent by the assumptions regarding the mafic minerals.

The amounts of minerals crystallizing (fig. 23) are not affected significantly by assumptions regarding mineral compositions. Both augite and plagioclase show an increase in the rate of crystallization at a liquid content of about 85 percent, and olivine shows a corresponding decrease. The curves of figure 23, relating percent of minerals crystallizing to the amount of liquid remaining show a general agreement with similar curves drawn from modal data for undifferentiated samples shown in figure 16. The principal difference is the prolonged cyrstallization of iron-rich olivine in the differentiated samples which may be related to crystallization at a slightly higher water pressures prevailing at greater depths in the lake.

The temperature at which differentiation took place may be estimated in two ways. A minimum temperature is obtained directly from the temperature profiles extrapolated at the depth and date of collection. The temperature of differentiation may also be calculated by taking the mode of a differentiated sample, adding back the crystals lost during differentiation, and applying the recalculated glass content to figure 17 to obtain temperature. Table 21 summarizes these results for three different samples of melt. Minimum temperatures of differentiation range from 1,080° to 1,110°C.

SEGREGATION VEINS

A feature common to all the studied lava lakes in Hawaii is the presence of zones of relatively coarse grained, glassy, vesicular rock (segregation veins) that appear to fill fractures and have, on analysis, a highly differentiated composition. These are distinct from vesicle cylinders and sheets which are more vesicular and somewhat more glassy than adjacent crust but which do not have sharp contacts or a differentiated composition. Liquids of bulk composition similar to that of the segregation veins filled holes drilled into the crust at depths where the temperature before drilling exceeded 1,030°. By analogy, the segregation veins are presumed to represent liquids injected at temperatures between 1,030°C and 1,070°C, the temperature below which a rigid crust is present. The liquid fraction of the basalt at these temperatures ranges from about 15 to 45 per-

TABLE 21.—*Adjusted modal data for differentiated melt samples from drill holes 68–1, 68–2, and 69–1*

[Modes of differentiated samples collected at temperatures of more than 1,070°C are reconstructed by replacing crystals lost during differentiation. Steps in the reconstruction are given in the following columns. A=Mode in volume percent; B=Volume percent crystals lost from sample by differentiation; C=Reconstructed volume percent mode after exchanging crystals lost for an equal volume of liquid; D=Column C converted to weight percent. E=Original mode (Column A) converted to weight percent. T (observed) is the temperature estimated from figure 10 using sample depth and date of collection. T (reconstructed) is the temperature read from figure 17 using the weight percent glass calculated in column D]

Sample No. 69–1–22
Depth (ft) 60–66
T (observed, °C) ~1,100
T (reconstructed, °C) 1,100

Modal Data	A	B	C	D	E
Olivine		5.9	5.9	7.1	--
Augite		13.3	13.3	15.3	--
Plagioclase	0.2	16.8	17.0	15.9	0.2
Ilmenite		.1	.1	.2	--
Glass	99.8	--	63.7	61.5	99.8

Sample No. 68–2–59
Depth (ft) 59
T (observed, °C) ~1,100
T (reconstructed, °C) 1,110

Modal Data	A	B	C	D	E
Olivine	0.3	3.1	3.4	4.1	0.4
Augite	7.3	5.3	12.6	14.6	8.4
Plagioclase	5.8	6.9	14.7	13.9	5.5
Ilmenite	--	--	--		
Glass	86.6		69.3	67.4	85.7

Sample No. 68–1–21
Depth (ft) 54
T (observed, °C) 1,082
T (reconstructed, °C) 1,085

Modal Data	A	B	C	D	E
Olivine	1.4	4.6	6.0	7.1	1.7
Augite	9.5	8.2	17.7	20.0	10.9
Plagioclase	9.7	10.7	20.4	18.7	9.1
Ilmenite	--	--			--
Glass	79.4		56.9	54.2	78.4

cent by weight (fig. 17). The crystal framework of the crust behaves as a filter, through which the liquid fraction moves into the open fracture. The efficiency of the filtration process is variable. Some segregations carry in crystals, so that the bulk composition of the segregation does not lie on the liquid line of descent for the lake as a whole, whereas other segregations are virtually free of early-formed crystals.

Figure 15 shows the composition of analyzed segregations (table 10D) in Makaopuhi lava lake compared with a derived liquid line of descent for Alae lava lake (Wright and Fiske, 1971, figure 3).[11] The compositions of two of the segregations are too poor in silica and too rich in FeO and TiO_2 to correspond to a pure liquid fraction, even taking into account the difference in starting composition between the Alae and Makaopuhi lava (Wright and Fiske, 1971, table 4a). We can evaluate the amount and composition of crystal contamination for all segregations by combining minerals and liquids representative of the Alae liquid line of descent in the following mixing calculation:

Segregation composition = Alae glasses + augite + plagioclase + ilmenite + (pigeonite + magnetite at lower temperatures)

The compositions of Alae glasses are chosen to bracket the MgO content of the segregation.

Solutions are shown in table 22, from which we infer that the two segregations with high FeO and TiO_2 formed at temperatures below which pigeonite and magnetite were crystallizing, that M23–19A was segregated at a lower temperature than 68–1–28, and that in both cases the smaller crystals (iron-rich pyroxene, sodic plagioclase, and newly crystallized pigeonite and opaques) were brought in with the liquid in significant quantities. One segregation (M68–2–10.0) fit closely the liquid line of descent and thus was nearly 100 percent liquid after segregation. M68–1–44–5 was segregated at the highest temperature judging from its MgO content; it was segregated with some crystals of augite and plagioclase.

One analyzed sample (68–1–17–7), included in table 10D, contains a thin vesicular zone which has some concentration of glass and ilmenite. Its composition fits

[11] We use wet chemical analyses from Alae in preference to electron microprobe analyses of Makaopuhi (P. W. Weiblen, unpub. data, 1968) which are less precise and may have biases in some oxides related to the standards used in the analysis.

TABLE 22.—*Results of mixing calculations for segregation veins*

[Compositions of glass from Alae lava lake analyzed by wet chemical methods (Peck and others, 1966) are used in preference to electron probe analyses from Makaopuhi lava lake, for which there are problems of standardization]

A. Dry-weight composition of liquids, Alae lava lake

	DPH 77 GL	A–4–12	A–6–30	A–6–29	A–5–20
SiO_2	51.02	50.80	51.50	52.01	53.54
Al_2O_3	14.22	12.90	12.47	12.35	12.43
FeO	11.32	13.47	14.14	14.35	14.35
MgO	6.08	5.47	4.41	4.06	3.11
CaO	10.72	9.45	8.46	8.19	7.31
Na_2O	2.57	2.66	2.81	2.84	3.27
K_2O	.61	.89	1.08	1.17	1.58
TiO_2	3.05	3.75	4.41	4.26	3.37
P_2O_5	.30	.46	.57	.63	.89
MnO	.18	.21	.21	.22	.21

B. Solutions

	M23–19A	68–2–10.0	68–1–28	68–1–44.5	69–1–55.5
Liquid					
DPH 77GL				7.7	
A–4–12				84.5	Solution unsatisfactory (high residuals).
A–6–30		80.2			
A–6–29		18.7	78.6		
A–5–20	51.7		5.5		
Crystals					
Augite ($En_{37}Fs_{28}Wo_{36}$)	12.5	.6	6.1	2.8	
Pigeonite ($En_{52}Fs_{37}Wo_{11}$)	7.0		.5		
Plagioclase	22.1 (An_{51})		5.6 (An_{50})	4.7 (An_{50})	
Ilmenite (Hm_{10})	5.9	.5	3.3	.3	
Titanomagnetite (Usp_{70})	.7		.4		

that of undifferentiated core near the same depth with the exception of a slightly higher TiO_2 content. Thus the vesicular zone does not represent a true segregation but perhaps marks the beginning of segregation of liquid into zones of lower pressure.

The conditions that cause fracturing in partly molten crust are poorly understood. The large segregations described by Moore and Evans (1967) from prehistoric Makaopuhi lava lake are subhorizontal fillings that pinch and swell along the strike. These are found at depths of 6.2–38.1 m, and are most common between 15.2 and 30.5 m. The Makaopuhi fracture fillings, by contrast, are smaller and generally not horizontal. Dips 30°–70° are common (table 23). A discrete, disk-shaped segregation was found in Makaopuhi at 3.1 m (68–2–10.0), although the obvious segregations are found only below 8.5 m. Between 3.1 and 8.5 m, vesicle sheets and cylinders are always associated with glass and, where the rock breaks along these structures, plates of plagioclase and ilmenite are seen coating the fracture.

We suggest that there is a continuous process of liquid segregation associated with fracturing and degassing of the lava and partly molten crust. The earliest segregations occur along zones of low pressure accompanying upward streaming of gas through the partly molten crystal framework. Later, discrete fractures open, perhaps in response to cooling surfaces related to gas escape. Finally, large horizontal fractures may form when the upper crust becomes more or less supported by the walls of the crater and fails to track the lens of melt as it cools and solidifies.

TABLE 23.—*Attitudes of segregation veins, Makaopuhi lava lake*

Drill hole No.	Depth (ft)	Thickness (in.)	Angle to horizontal (°) as seen in drill core
MP 68–1	28.0	2.0	55
	30.2	.5	45
	34.3	1.5	65
	34.5	2.8	60
	34.7	6.0	0
	44.7	1.5	45
MP 68–2	28.6	4.0	20
	32.8	1.5	60
	36.8	1.0	35

CONVECTIVE COOLING IN THE LAVA LAKE

Convection has long been considered a potentially important process in the cooling history of the lava lakes. However, there has heretofore been no direct evidence of thermal convection, and arguments can be made that convection would not be expected during the early part of the cooling history. In this section we evaluate the conditions under which convection might take place and indicate the evidence that supports convective transfer of heat in Makaopuhi lava lake.

The condition for classical thermal convection to take place is that a relatively dense, cold body of liquid overlies a less dense, warmer body of liquid. The gravitational instability that results will tend to set up a circulation in which the denser liquid moves downward and displaces lighter liquid. In a pure liquid a decrease in temperature will cause a corresponding increase in liquid density; cooling from the top and sides of a container of liquid can initiate convection of the entire volume of liquid. Cooling of the lava lake is more complex, in that the presence of crystals and gas bubbles must be taken into account. Crystallization of olivine and pyroxene would tend to enhance the density contrast between the cooler, more crystal-rich liquid, and the hotter, crystal-poor, liquid, assuming that the crystal-liquid suspension behaves as a uniform material (Bradley, 1965, 1969). Crystallization of plagioclase, which has a density equal to or less than that of the liquid, would suppress only slightly, if at all, the tendency for convection. Bubbles of gas, much lighter than the melt from which they exsolved, would rise and tend to offset or even eliminate convection.

The high vesicularity of all drill core attests to the presence of gas bubbles at some time during cooling of the melt. The presence of vesicle sheets and cylinders is evidence of upward movement and entrapment of gas bubbles, presumably at high melt temperatures when the fluidity was relatively high. The high vesicularity of melt samples collected in September and October 1965 is direct evidence of the presence of gas bubbles in the liquid at temperatures as high as 1,130° and depths as great as 9.1 m. Thus, during the early stage of cooling, gas bubbles were rising and expanding in the melt, effectively offsetting the density gradient produced by cooling, and we think it unlikely that thermal convection could occur at this stage.

Presumably much of the early degassing of the lake was related to the supersaturation of the magma in volatiles at the time of eruption, as evidenced both by fountaining accompanying the eruption and by observed outgassing of fractures and open drill holes for several months after the eruption. This outgassing abruptly diminished during July 1965 and was correlated with a sharp decrease in the less soluble components (SO_2, CO_2; Finlaysen and others 1968); this may represent the time at which the lake became saturated with respect to H_2O (P about 1 atm). If so, then all subsequent gas evolution probably reflected the decreased solubility on cooling.

The melt samples collected in December 1968-January 1969 at temperatures of 1,070–1,100°C and depths of 16.5–18.3 m are dense, of low crystallinity, and virtually free of vesicles (table 14). The core density profile (fig. 21) suggests that from 6.2 m to 16.5 m the melt was becoming progressively more dense relative to the crust. If these samples are representative, then a strong tendency toward thermal convection existed at the time of last drilling and probably for some time previous. Unfortunately we have no melt samples collected between October 1965 and December 1968, so the time at which vesiculation declined to a point where convection might have begun is not closely bracketed.

The reason for the decrease in the amount of gas exsolution at a given temperature, as shown by the contrast in vesicularity of melt samples in 1965–66 and 1968–69, is not definitely known. One possibility is that the increase in total pressure beneath the thickening upper crust may have increased the solubility of water in the melt, thus lowering the temperature at which vesiculation could begin.

Further supporting evidence for convection is provided by the thermal profiles (fig. 10); specifically the occurrence of transient "shelves" on the 1,100° and 1,118° isotherms, the erratic fluctuations of the 1,130° and 1,140° isotherms, and the flattening of the 1,070° isotherm from its initial slope during the period March-September 1966. The melt beneath the crust generally became hotter in this time period relative to what a conductive cooling model predicts. In contrast, the last drilling of the lake showed depression of the 1,070° isotherm from its initial conductive slope, indicating cooling beyond that predicted by the conduction model. Short-term heating and longer term net cooling would be expected if the melt were convecting. If so, then convection presumably began in March 1966, when the crust was approximately 7.6 m thick.

A third indication of possible convection comes from the observation that basalt cored below 8.5 m is differentiated by removal of augite and plagioclase in addition to olivine. Evidence is given above that this type of differentiation occurs during flow, and we hypothesize that convective flow could cuase the observed crystal liquid fractionation. The timing of the convective differentiation agrees with the observed development of thermal anomalies in the melt if differentiation is assumed to have occurred above 1,100°C, as the 1,100° isotherm reached 8.5 m in March 1966, precisely when the flattening of the 1,100° and 1,118° isotherms was first observed.

HIGH-TEMPERATURE OXIDATION OF BASALT

Measurements of oxygen fugacity reported in this paper and by Sato and Wright (1966) place constraints on the interpretation of conditions under which primary oxidation of basaltic lava takes place. For Makaopuhi lava lake, the lava is oxidized at temperatures between 800° and 400° at fO_2 values as high as 10^{-2} atm. Samples collected within a short time after exposure to high fO_2 contain olivine and pyroxene that show incipient formation of hematite along fractures. High oxygen fugacities are apparently transient, however, persisting only for weeks or months, and the basalt is probably reduced to some extent during subsequent cooling.

The extremely high maximum oxygen fugacities deny any process in which fO_2 is controlled by the oxide mineralogy of the rock, homogeneous equilibria in the magmatic gas, or some combination of these. Rather the data suggest a nonequilibrium process by which either hydrogen is lost from, or oxygen introduced into the magmatic gas in equilibrium with the basalt. On the basis of preliminary data, Sato and Wright (1966, p. 3) proposed differential loss of hydrogen by diffusion: sion:

> A plausible mechanism to account for the zones of high fO_2 in Makaopuhi lake is one in which a certain horizon of the lake gradually cools to the temperature range in which oxygen and water molecules can no longer diffuse through the basalt freely, while hydrogen continues to escape toward the surface because of its greater diffusion rate. In other words, the basalt acts as a semipermeable membrane for hydrogen in this temperature range. This preferential escape of hydrogen includes further thermal decomposition of water and locally generates high oxygen fugacities, so that oxidation of the basalt occurs in the horizon . . . As the temperature of the horizon decreases further, even the diffusion of hydrogen becomes difficult, and the hydrogen ascending from underlying layers begins to react with, and possibly reduce, the previously oxidized basalt.

This hypothesis explains the shape of the observed profiles at a single time but does not fully explain the transient nature of the anomalies or why the basalt is not always subjected to high fO_2 between 800 and 400°C.

Contamination of the drill hole by atmospheric oxygen has been suggested by E. F. Heald, (written commun., 1966) and P. B. Barton, (oral commun., 1973). The consistency and reproducibility of the profiles suggest that contamination is not caused by air introduced during the measurement process or by erratic wind-forced air circulation in the drill holes.

Another possible source of contamination is oxygen-saturated rainwater, as suggested by H. R. Shaw (oral comm., 1973). This hypothesis requires convective circulation in which rainwater undergoes both boiling and condensation in a kind of miniature geothermal system within the upper crust. The excess oxygen in the circulating water could react to oxidize the hot basalt as the gases migrated to the surface. At lower temperature, the gas would again be in equilibrium with the unoxidized basalt, assuming the amount of atmospheric oxygen introduced is small compared with the volume of basalt reduced. The transient nature of the oxidation would be controlled by vagaries of the circulation process. The onset and duration of oxidation at any one place would depend in part on the volume of magmatic gas compared with the volume of evaporated rainwater. Early in the lake's history, visible degassing of drill holes and joint cracks attested to release of large volumes of magmatic gas. High fO_2 at this stage was found only in a drill hole near the edge of the lake, where the chance for oxidation was relatively high. The latest development of high fO_2 was over the deepest part of the lake where the chance for oxidation by raïnwater was probably least.

This oxidation hypothesis, by nature a disequilibrium process, is not a completely satisfactory explanation of all the data. However, given the possibility of deep circulation of water, it lacks the contradictions that make other hypotheses less tenable.

INTERPRETATION OF SURFACE ALTITUDE CHANGES

The most difficult lava-lake data to interpret unambiguously are the surface altitude changes (fig. 12). In fact, the pattern of surface-altitude changes is different for all three historic lava lakes that have been studied. The altitude changes are not directly explained in terms of simple contraction during crystallization and cooling (see earlier discussion) and probably are the net result of a variety of partly competing processes, the most important of which is vesiculation.

We believe that the behavior of Makaopuhi lava lake is tied to the pattern of gas release from the liquid. We do not have the necessary data to describe this pattern quantitatively; those data would come from a grid of drill holes that give a profile of core density from the surface of 1,100°C at evenly spaced times between 1965 and 1969. Nonetheless some principles may be set down that lead to the interpretation made on the basis of limited data.

We assume that gas is exsolved as bubbles that expand as they move upward in the melt (T>1,070°C) at velocities related to their size and the changing viscosity of the enclosing well. Some bubbles became frozen in position as they reach the crust-melt interface (T=1,070°C). The presence of inclined vesicle sheets and incipient vesicle cylinders, as well as direct observation of gas escape at the surface, indicates that some gas escapes through the crust, eventually connecting with fractures open to the surface.

A profile of core density versus depth principally reflects the relative amount of gas trapped by the crystallizing crust. The difference in core density from drill holes 68–1 and 68–2 (fig. 21) is an indication of the irregular nature of gas movement and entrapment.

We attach significance to the fact that the volume rate of subsidence of the lake surface (fig. 14) decreased abruptly about the time at which the crust attained its maximum density in late 1965 (figs. 10, 21, 14). Subsequently, the rate of subsidence continued to decrease in stepwise fashion, while core density decreased (vesicularity increased) in more regular fashion. The increased gas trapped in and immediately below the crust may have provided the increased buoyancy to offset the increase in crust density due to crystallization and thermal contraction. Continuation of this process eventually resulted in uplift of the lake surface. (fig. 12, 14).

We do not know why the amount of gas frozen in the crust differed from one time to another. This could be related to a thickening crust and to the decreased temperature of vesiculation postulated earlier from observation of glass density. When bubbles were freely moving in the melt, they could perhaps escape laterally along the crust-melt interface before being frozen into the permanent crust, as well as escaping upward through the cooling crust. As the beginning of vesiculation moved closer in temperature and distance to the interface between crust and melt, a lesser percentage of gas would be able to escape laterally until eventually, when the temperature of beginning of vesiculation was less than 1,070°, all of the exsolved gas entered, and most was trapped, in the growing crust. This is one way to relate the pattern of vesiculation to the changes in level of the lake surface.

In conclusion, we again emphasize that our interpretations are based on incomplete data on a model that assumes a similar pattern of solidification for all parts of the lake. Crustal foundering could have produced local points of gas concentration and inhomogeneities in the temperature distribution that might affect the vesiculation process. Possibly even factors external to the lake, such as tilting during intrusion into the upper east rift zone, (fig. 13) could also have affected the pattern of vesiculation. We hope that comparison of our data with data from other lava lakes can eventually resolve some of the factors that affect the altitude changes on the lake surface.

SUMMARY: COOLING AND SOLIDIFICATION HISTORY OF MAKAOPUHI LAVA LAKE

Our interpretations of the cooling, solidification, and differentiation of Makaopuhi lava lake are made in terms of several interrelated processes.

1. Density change on solidification. Where the crust is less dense than the melt from which it forms, there is a tendency to uplift the surface of the lake and vice versa.

2. Temperature of vesiculation. Vesiculation at temperatures between 1,190° and 1,070°C complicates the

density distribution in the melt as the bubbles will rise and become larger after vesiculation begins. Vesicles formed at temperatures less than 1,070° are trapped in place in the growing crust. This factor is at least as important as the change in density during crystallization in affecting the relative densities of crust and melt.

3. Convection of the melt. This is likely to occur in dense, nonvesiculated melts and is believed responsible for differentiation of the melt in which small crystals of iron-rich olivine, augite, and plagioclase are concentrated downward resulting in eventual cyrstallization of a differentiated melt.

We can trace these processes by looking at the changes of chemical composition, core density, temperature profiles, and surface-altitude changes through time as shown in figures 10, 14, 19, 21, and 22.

The earliest cooling regime extends from the time of formation of the permanent crust of March 19, 1965–January 1966 when the upper crust was 6.7 m thick. During this time we see evidence of the upper cooled layer of melt and infer conductive cooling of both melt and crust from the linear variation of isotherm depth with $\sqrt{t}$ (fig. 10). Finite-element calculations show that the initial thermal layering is largely eliminated during this period. Crustal isotherms are depressed near the close of this period because of the accumulative effect of rainfall on the surface. Crustal densities increase until near the end of this period when they reach a maximum value of 2.78g/cc, then begin to decrease again (fig. 21). Rates of subsidence of the surface are high at first because of initial degassing, then constant from July to December 1965 (fig. 14). The rates of subsidence abruptly decrease near the time of reversal of core densities. The chemistry and petrography of the upper crust is uniform except for the erratic decrease in olivine content with depth (fig. 19). Melt collected in this time period is frothy and of low bulk density and, apart from contamination effects introduced during sampling, is undifferentiated relative to the crust collected at the same or shallower depths.

A second stage of cooling extends from February through about December 1966, when the crust was 9.1 m thick. During this period the depth to isotherms in the melt (1,070°–1,140°C) fluctuates and the general slope of the isothermal surfaces in the melt is shallower than the slopes during stage 1 (fig. 10). Differentiation of solidified crust is observed in core collected near the end of this period (fig. 15, 22) and the density of crust shows distinct decrease with increasing depth (fig. 21). The rate of subsidence (fig. 14) decreases to less than half the rate observed during stage 1 near the end of the period. We interpret stage 2 as the time when the initial thermal layering in the lake was eliminated and when vesiculation of the lava was suppressed at temperatures of more than 1,070°C. Thermal convection was initiated at high temperatures leading eventually to differentiation of the solidified crust. (From fig. 10 it can be seen, on this model, that crystal-liquid differentiation was effective, beginning in February 1966 at temperatures more than about 1,118°C in order to cause the observed differentiated compositions below a depth of 8.5 m.) The increasing density of melt (lacking vesicles) compared with crust forming from it (fig. 21) is inferred to be responsible for the decreasing rate of subsidence (fig. 14).

The last time period is from 1967 to the last temperature measurements in February 1969. We know little about the thermal history except that the slope of the 1,070° isotherm steepens past the extrapolation of the slope during stage 1. Core density continues to decrease and, beginning in mid-1967 the central part of the lake shows net uplift which continues to the end of the period. The crust continues to become more differentiated with increasing depth during this period. The combined data imply that the convective regime was still operative and that the crust forming in the center of the lake was considerably less dense than was the melt.

None of the history can be exactly described in terms of any simple predictive model. Many of the changes we see and their timing may reflect inhomogeneities in either the initial temperature distribution or in terms of the presence of former foundered crust. Where we correlate the various aspects of the lake there are often timelags between one type of observation and another observation that is assumed to follow; for instance, the earliest evidence of differentiation in newly formed crust followed by several months the earliest evidence of convection in the melt. Nonetheless, we feel that there is sufficient information to present these ideas as best working hypotheses.

REFERENCES CITED

Bradley, W. H., 1965, Vertical density currents: Science v. 150, no. 3702, p. 1423–1428.

———1969, Vertical density currents: Limnology and Oceanography v. 14, p. 1–3.

Evans, B. W., and Moore, J. G., 1968, Mineralogy as a function of depth in the prehistoric Makaopuhi tholeiitic lava lake, Hawaii: Contr. Mineralology and Petrology, v. 75, no. 2, p. 85–115.

Evans, Bernard W. and Wright, T. L., 1972. Composition of liquidus chromite from the 1959 (Kilauea Iki) and 1965 (Makaopuhi) eruptions of Kilauea volcano, Hawaii: Am. Mineralogist, v. 57, no. 1–2, p. 217–230.

Finlayson, J. B., Barnes, I. L., and Naughton, J. J., 1968, Developments in volcanic gas research in Hawaii *in* The crust and upper mantle of the Pacific area: American Geophys. Union Geophys. Mon. 12, p. 428–438.

Grommé, C. S., Wright, T. L., and Peck, D. L., 1969, Magnetic properties and oxidation of iron titanium oxide minerals in Alae and

Makaopuhi lava lakes, Hawaii: Jour. Geophys. Research, v. 74, no. 22, p. 5277–5293.

Häkli, T. and Wright, T. L., 1967. The fractionation of nickel between olivine and augite as a geothermometer. Geochim. et Cosmochim. Acta, v. 31, p. 877–884.

Huebner, J. S., 1971, Buffering techniques for hydrostatic systems at elevated pressure *in* Research techniques for high pressure and high temperature, Gene C. Ulmer, ed.: New York, Springer Verlag, p. 123–177.

Huebner, J. S., and Sato, M., 1970, The oxygen fugacity-temperature relationships of manganese oxide and nickel oxide buffers. Am. Minerologist, v. 55, p. 934–952.

Moore, J. G., and Evans, B. W., 1967, The role of olivine in the crystallization of the prehistoric Makaopuhi tholeiitic lava lake, Hawaii: Contr. Mineralology and Petrology, v. 15, no. 3, p. 202–223.

Murata, K. J., and Richter, D. H., 1966, Chemistry of the lavas of the 1959–60 eruption of Kilaeua volcano, Hawaii: U.S. Geol. Survey Prof. Paper 537–A, p. 1–26.

Peck, D. L., Moore, J. G., and Kojima, George, 1964, Temperatures in the crust and melt of Alae lava lake, Hawaii, after the August 1963 eruption of Kilauea volcano—a preliminary report *in* Geological Survey research 1964: U.S. Geol. Survey Prof. Paper 501–D, p. D1–D7.

Peck, D. L., Wright, T. L., and Moore, J. G., 196 , Crystallization of tholeiitic basalt in Alae lava lake, Hawaii: Bull. Volcanol. v. 29, p. 629–656.

Richter, D. H., and Moore, J. G., 1966, Petrology of the Kilauea Iki lava lake, Hawaii: U.S. Geol. Survey Prof. Paper 537–B, 26 p.

Rittman, A., 1973, Stable mineral assemblages of igneous rocks—A method of calculation, in Minerals, rocks, and inorganic materials, v. 7: New York, Mendleberg, Berhn, Springer-Verlag, 262 p.

Robertson, E. C. and Peck, D. L., 1974, Thermal conductivity of vesicular basalt from Hawaii. Jour. Geophys. Research, v. 79, p. 4875–4888.

Sato, M., 1971, Electrochemical measurements and control of oxygen fugacity and other gaseous fugacities with solid electrolyte sensors, *in* Research techniques for high pressure and high temperature, Gene C. Ulmer, ed.: New York, Springer Verlag, 368 p.

Sato, M., 1971 M., and Moore, J. G., 1973, Oxygen and sulphus fugacities of magmatic gases directly measured in active vents of Mount Etna. Royal Soc. [London] Philos. Trans. A, v. 274, p. 137–146.

Sato, Motoaki, and Wright, T. L., 1966, Oxygen fugacities directly measured in magmatic gases: Science, v. 153, no. 3740, p. 1103–1105.

Shaw, H. R., 1972, Viscosities of magmatic silicate liquids: an empirical method of prediction: Am. Jour. Sci., v. 272, p. 870–893.

Shaw, H. R., Wright, T. L., Peck, D. L., and Okamura, R., 1968, The viscosity of basaltic magma: an analysis of field measurements in Makaopuhi lava lake, Hawaii: Am. Jour. Sci. v. 266, p. 225–264.

Shaw, H. R., Kistler, R. W., and Evernden, J. F., 1971, Sierra Nevada Plutonic Cycle: Part II Tidal energy and a hypothesis for orogenic-epeirogenic periodicities. Geol. Soc. America Bull. v. 82, p. 869–896.

Swanson, D. A., and Fabbi, B. P., 1973, Loss of volatiles during fountaining and flowage of basaltic lava at Kilauea volcano, Hawaii. U.S. Geol. Survey, Jour. Research, v. 1, p. 649–658.

Tilley, C. E., Yoder, H. S., and Schairer, J. F., 1964, New relations on melting of basalts; Carnegie Inst. Washington Yearbook 63, 1963–64, p. 114–121.

Wright, T. L., 1973, Magma mixing as illustrated by the 1959 eruption, Kilauea volcano Hawaii: Geol. Soc. America Bull. v. 84, no. 3, 849–858.

Wright, T. L., and Doherty, P. C., 1970, A linear programming and least squares computer method for solving petrologic mixing problems. Geol. Soc. America, Bull. v. 81, no. 7, 1995–2007.

Wright, T. L., and Fiske, R. S., 1971, Origin of the differentiated and hybrid lavas of Kilauea volcano, Hawaii, Jour. Petrology, v. 12, no. 1, p. 1–65.

Wright, T. L., and Weiblen, P. W., 1967, Mineral composition and paragenesis in tholeiitic basalt from Makaopuhi lava lake, Hawaii [abs]: Geol. Soc. America Program 1967 Annual Meeting, p. 242–243.

Wright, T. L. Kinoshita, W. T., and Peck, D. L., 1968, March 1965 eruption of Kilauea volcano and the formation of Makaopuhi lava lake: Jour. Geophys. Research, v. 73, no. 10, p. 3181–3205.

Wright, T. L., Swanson, D. A., and Duffield, W. A., 1975, Chemical compositions of Kilauea east-rift lava, 1968–1971. Jour. Petrology, v. 16, p. 110–113.

Wright, T. L., Peck, D. L., and Shaw, H. R., 1976, Kilauea Lava lakes: natural laboratories for study of cooling, crystallization, and differentiation of basaltic magma, *in* Sutton, G. H., Manghnani, M. H. and Moberly, Ralph, *eds*., The geophysics of the Pacific Ocean basin and its margin: Am. Geophys. Union Geophys. Mon. 19, p. 375–390.

FIGURES 24–28; TABLES 24–29

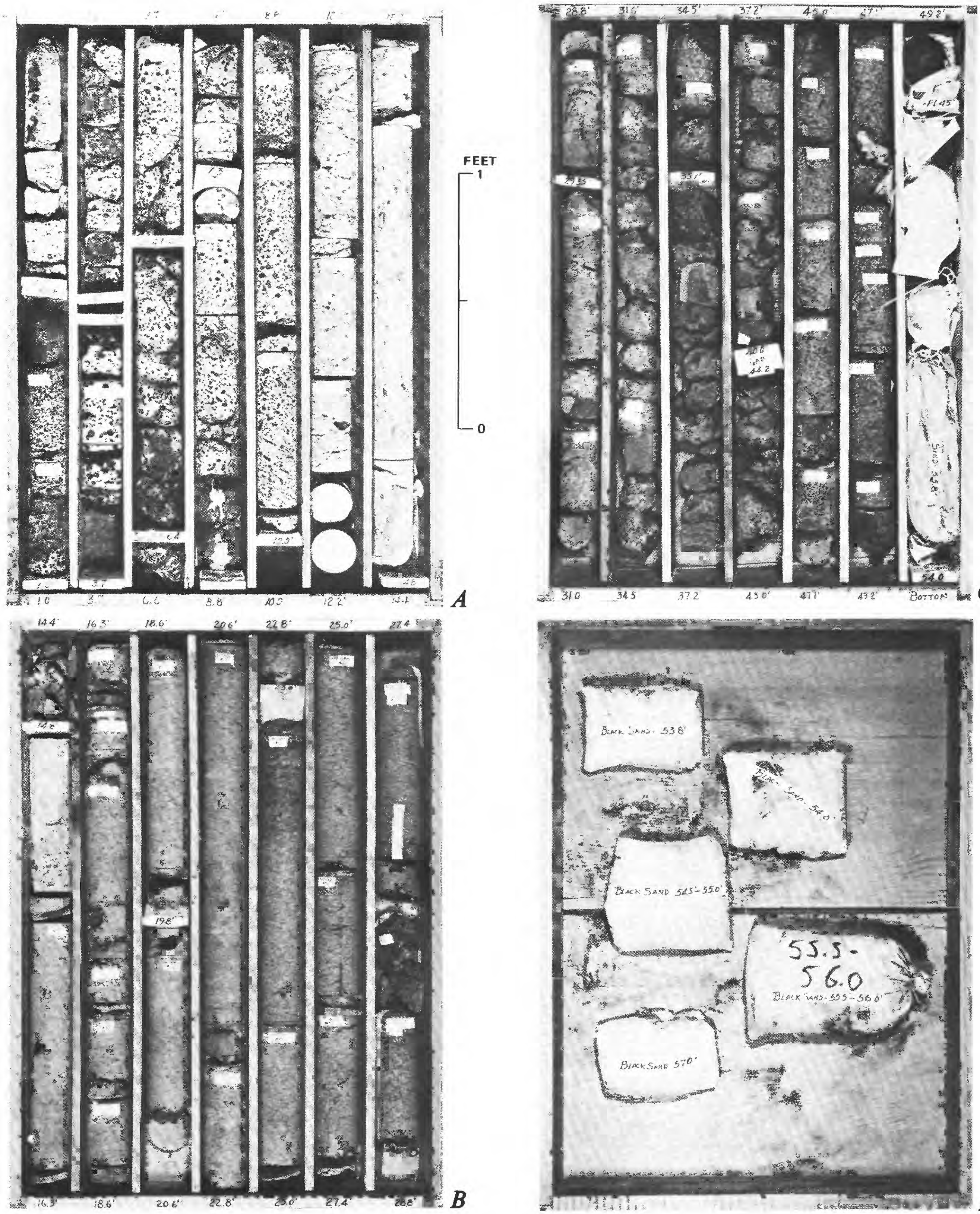

FIGURE 24.—Photographs of drill core for 68–1. *A*, 0–14.4 ft. *B*, 14.4–28.8 ft. *C*, 28.8–54.0 ft. *D*, Bags containing shattered glass (quenched melt) that came out around the drill hole collar while drilling between about 44 ft and 57 ft.

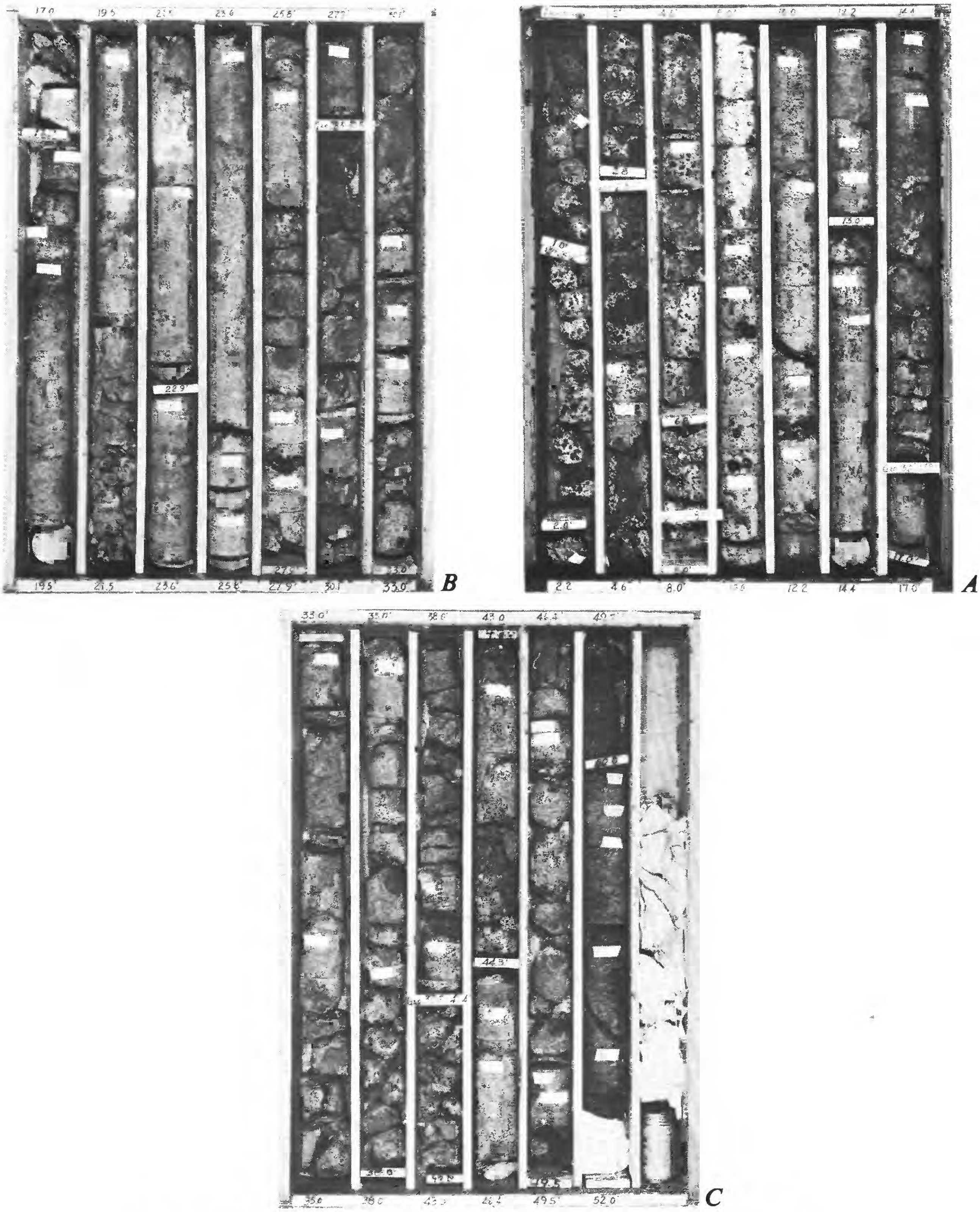

FIGURE 25.—Photographs of drill core for 68–2. *A*, 0–17.0 ft. *B*, 17.0–33.0 ft. *C*, 33.0–52.0 ft.

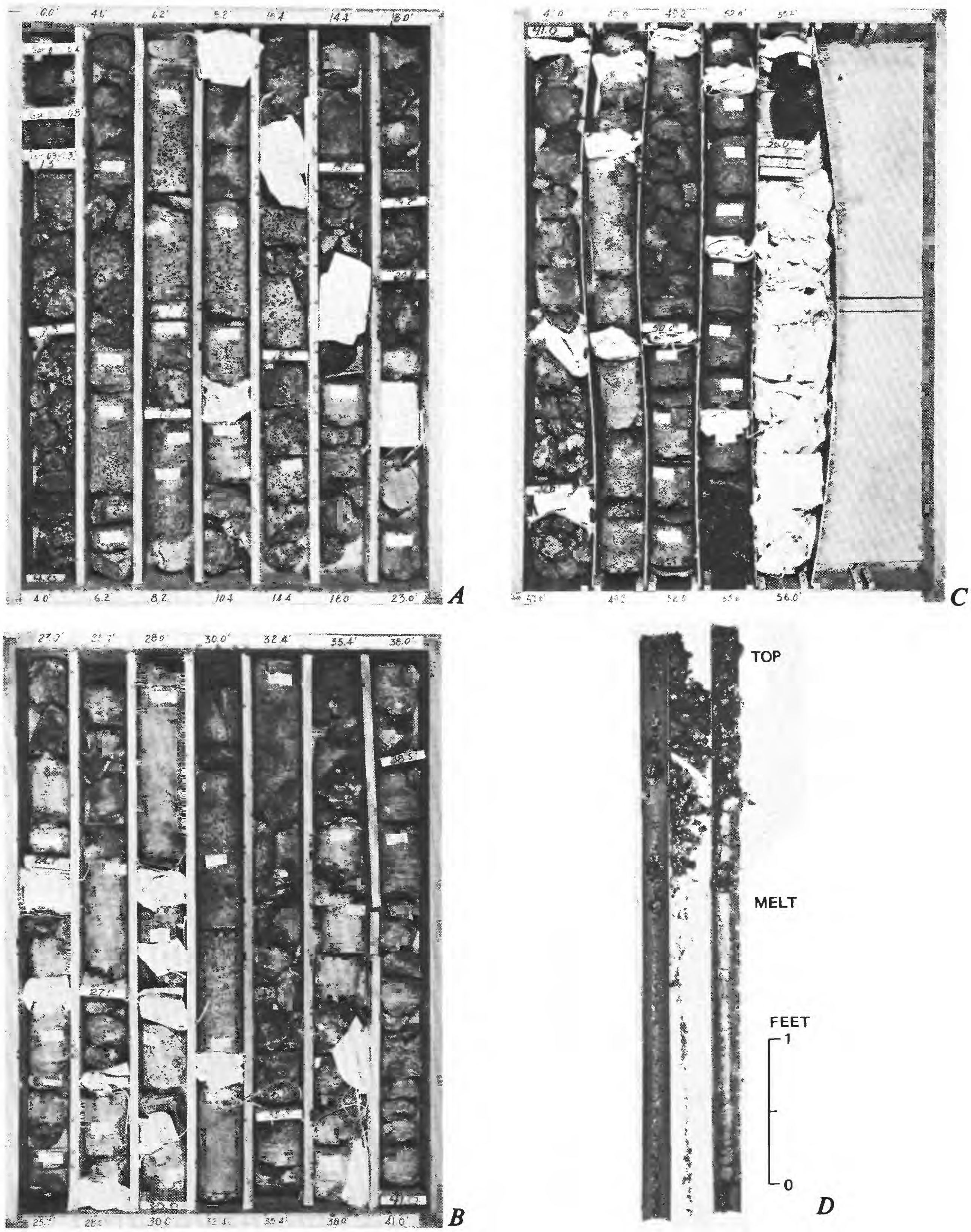

FIGURE 26.—Photographs of drill core for 69–1. *A*, 0–23.0 ft. *B*, 23.0–41.0 ft. *C*, 41.0–56.0 ft. *D*, Core barrel filled with glass (quenched melt) collected at approximately 61–66 ft.

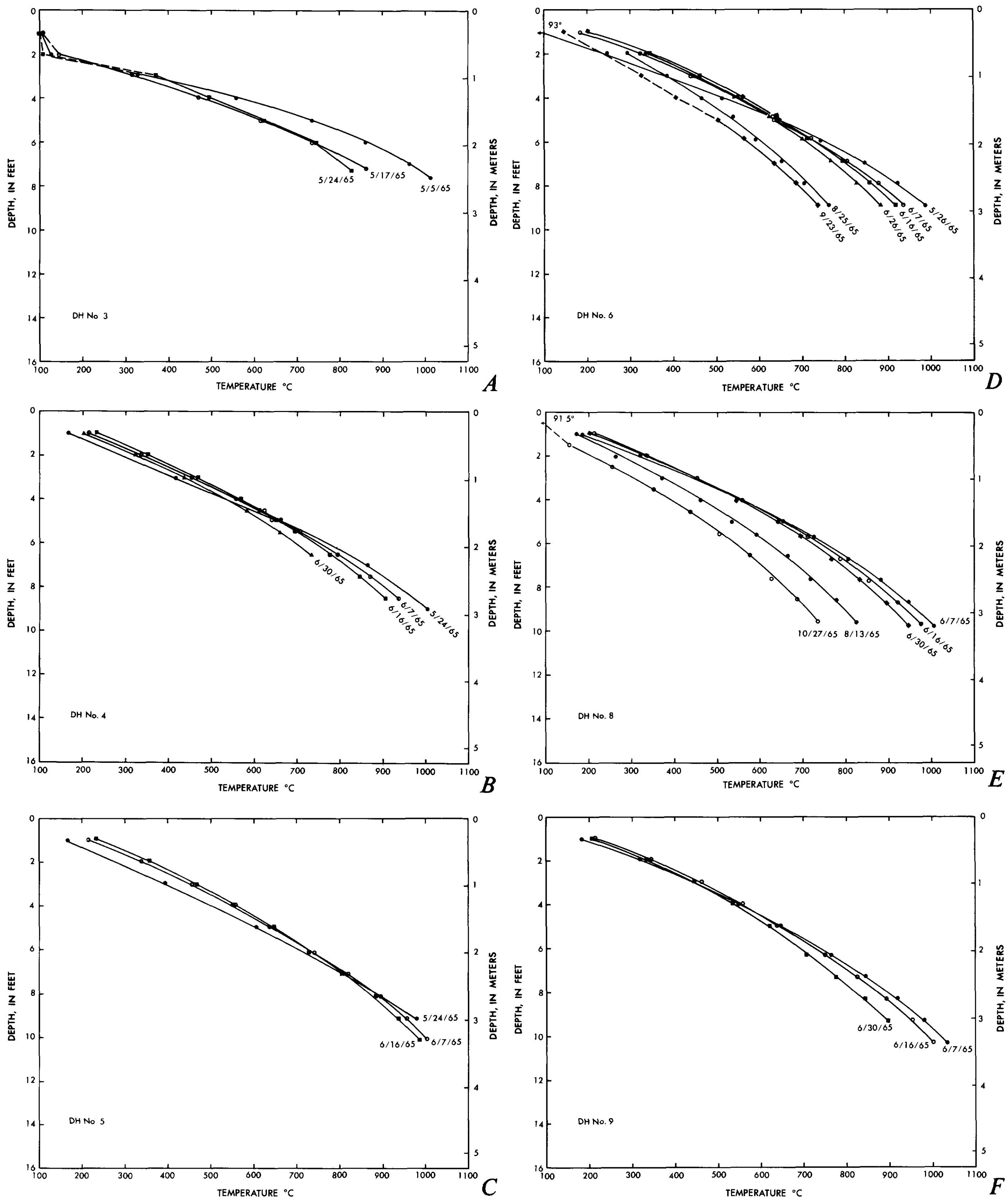

FIGURE 27.—Uncorrected temperature profiles. *A*, DH 3. *B*, DH 4. *C*, DH 5. *D*, DH 6. *E*, DH 8. *F*, DH 9. *G*, DH 10. *H*, DH 11. *I*, DH 12. *J*, DH 13, 14, and 16. *K*, DH 17. *L*, DH 20. *M*, DH 21. *N*, DH 22. *O*, DH 23. *P*, DH 23 uncorrected. *Q*, DH 24. *R*, DH 24 uncorrected. *S*, DH 68–1. Temperature in °C, depth in feet. Each profile is represented by a simple set of symbols.

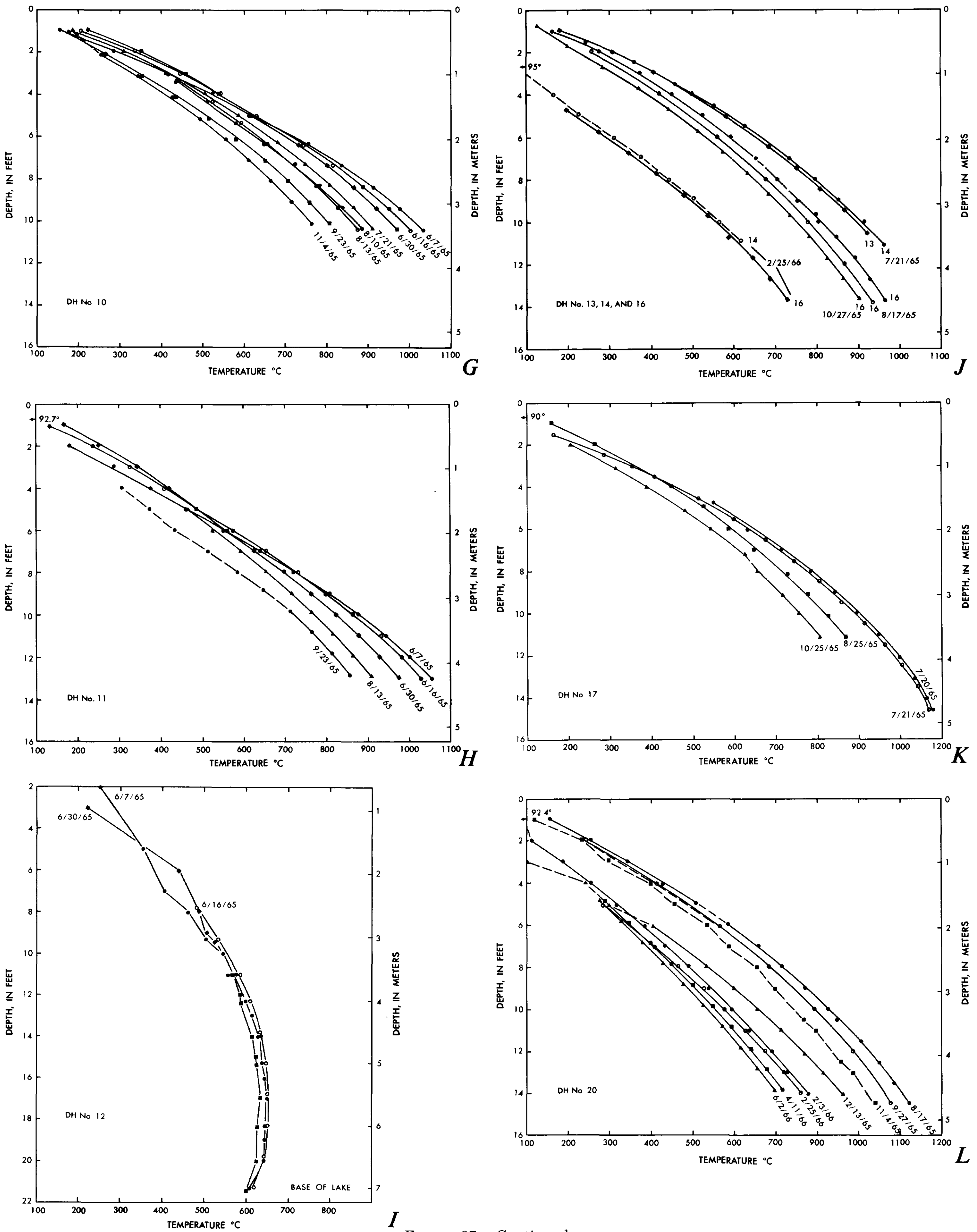

FIGURE 27.—Continued.

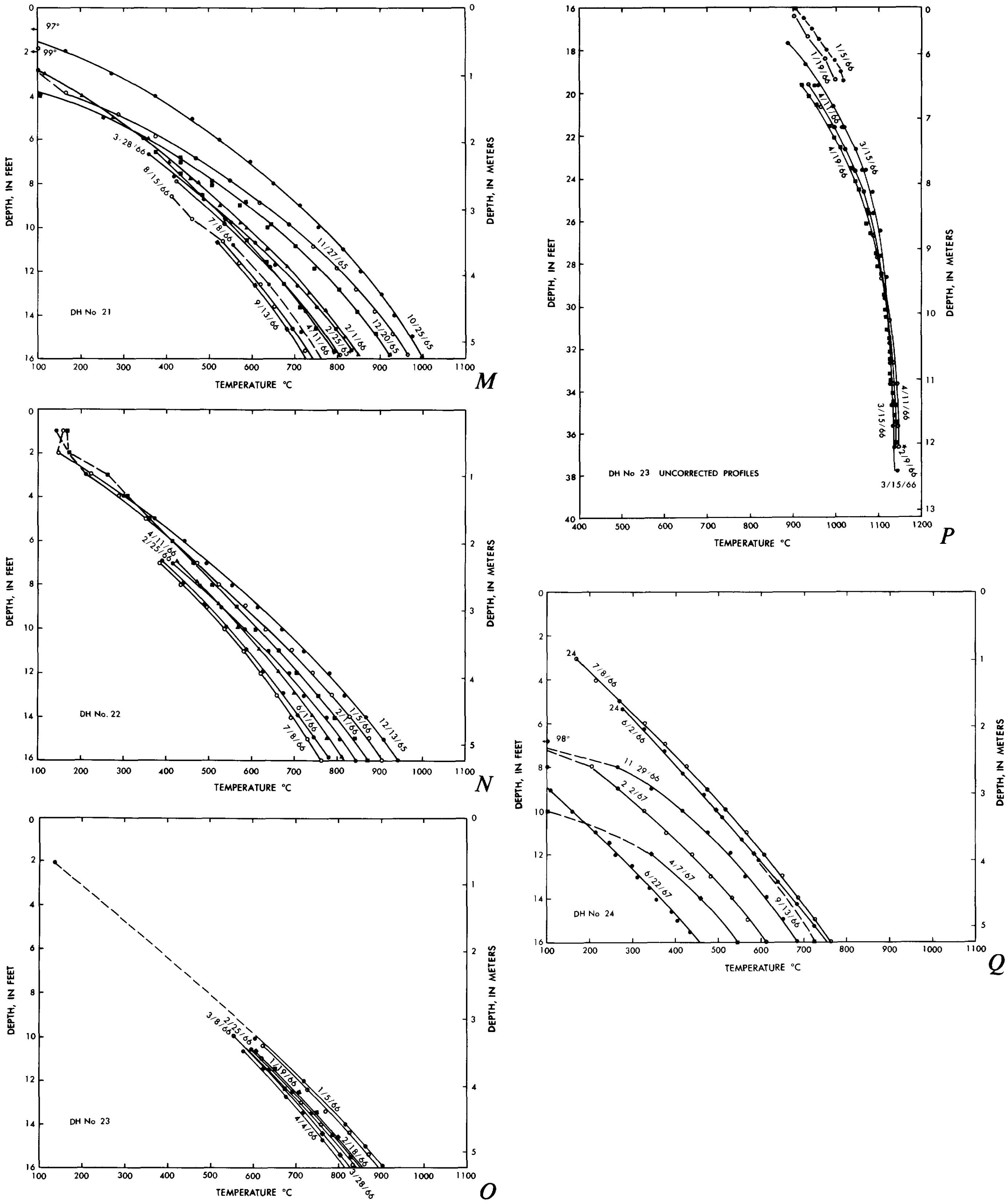

FIGURE 27.—Continued.

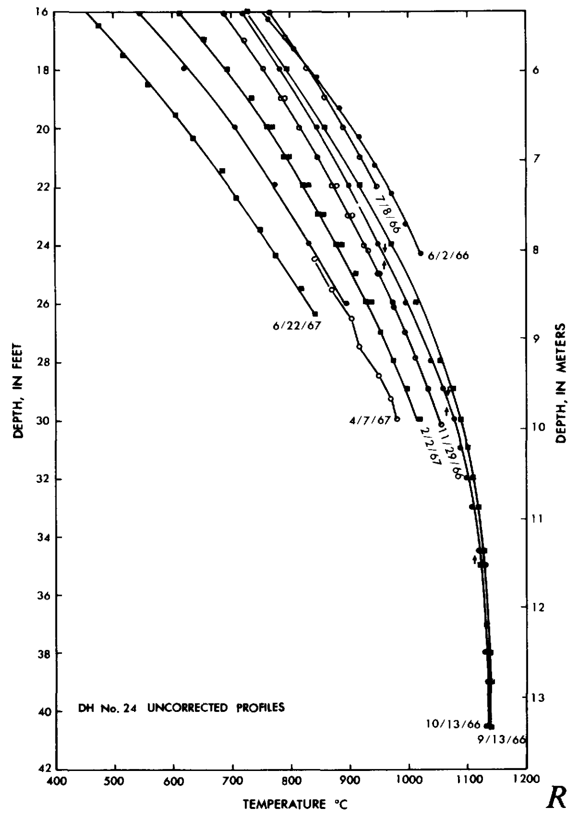

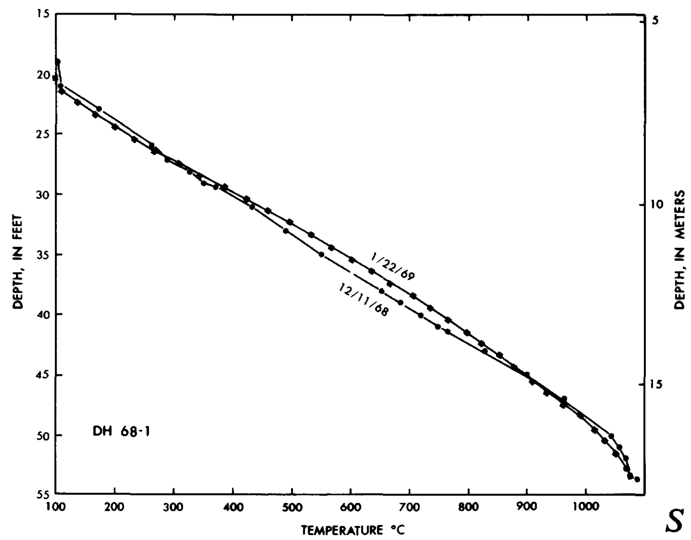

FIGURE 27.—Continued.

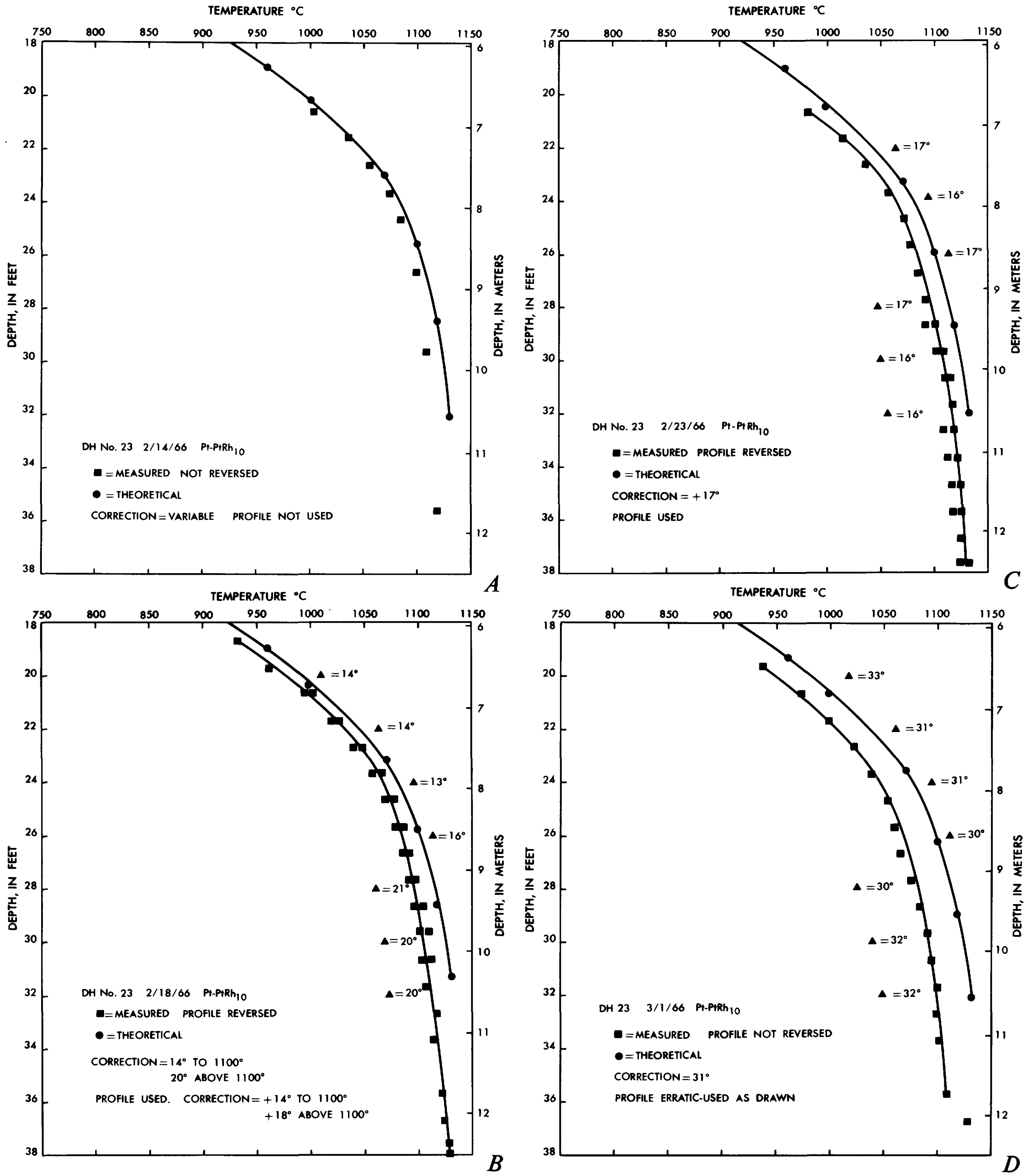

FIGURE 28.—Temperature profiles for DH 23 with correction for thermocouple contamination. *A*, 2/14/66. *B*, 2/18/66. *C*, 2/23/66. *D*, 3/1/66. *E*, 3/3/66. *F*, 3/8/66. *G*, 3/22/66. *H*, 3/28/66. *I*, 4/4/66. *J*, 4/25/66. *K*, 5/6/66. Temperature in °C, depth in feet.

■ = measured temperatures.

● = theoretical temperatures based on uncorrected profiles obtained before and after the measurement date.

▲ = difference between measured and theoretical temperature profile.

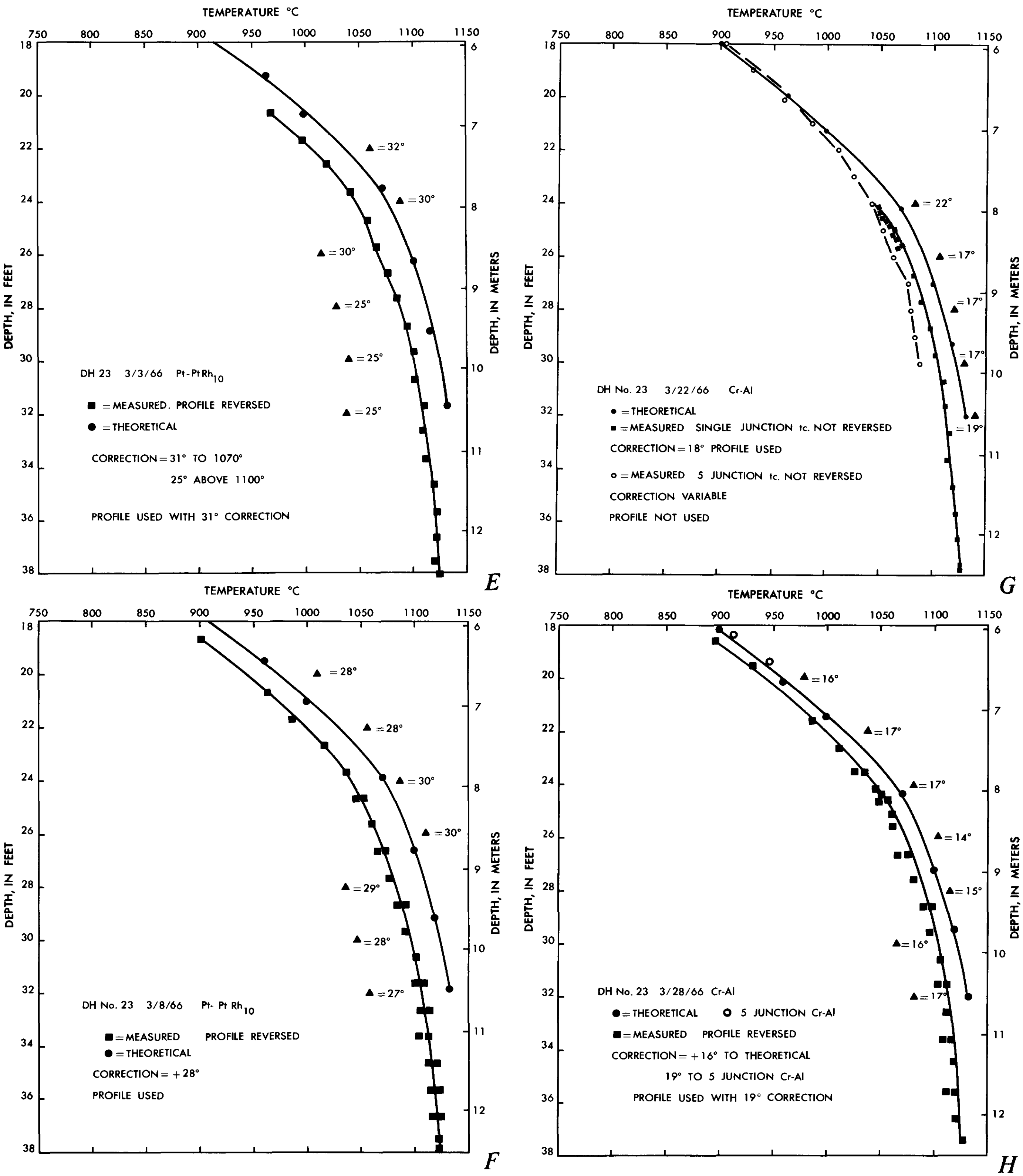

FIGURE 28.—Continued.

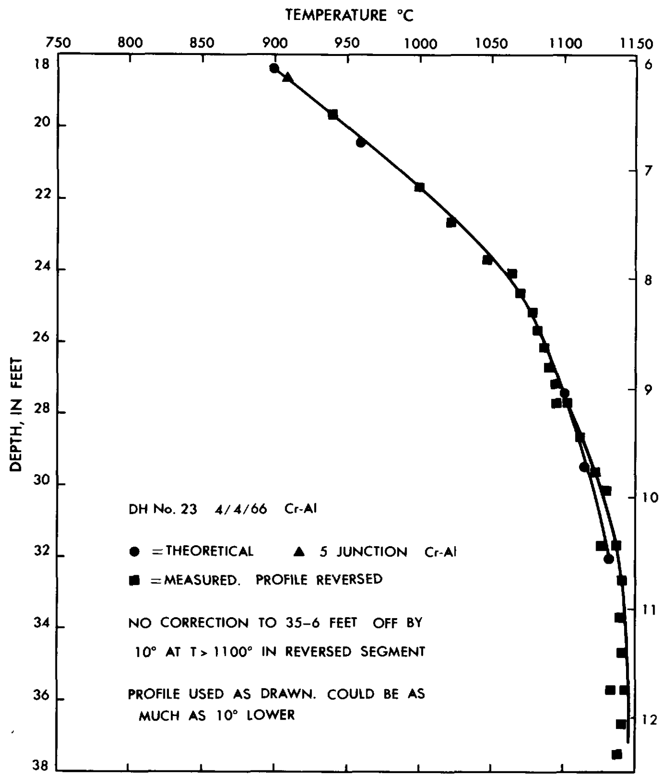

I

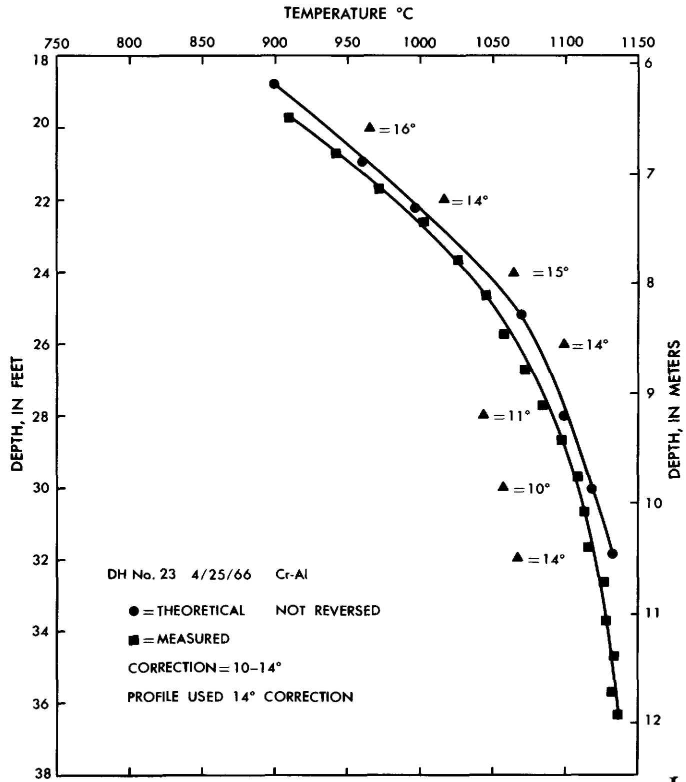

J

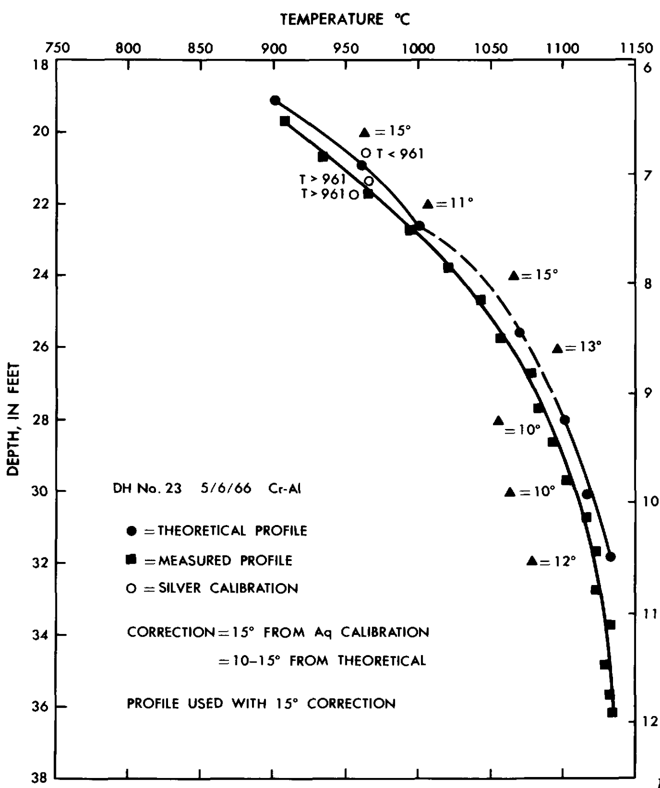

FIGURE 28.—Continued.

K

TABLE 24.—*Core logs for drill holes 1–24, 1965–66*

Drill hole No.	Date	Core interval (ft)	Temperature (°C)	Core recovery		Sample No.	Chemical analysis	Comment
				weight (g)	percent			
1	4–19–65	0–0.02				M–1–1	yes	Surface glass.
		0–0.8	0–260°	283	70	M–1–2		Mast hole, 1–1½ in. piece.
		0–1.4	0–400	28	25	M–1–3		
		1.4–2.9	400–655	49	20	M–1–4		Three ½ in. pieces.
		2.9–4.95	655–960		0			
		4.95–6.1	960–1,040	85	60	M–1–5		Two ½ in. pieces.
		6.1–7.1	1,040–1,100	47	25	M–1–6	yes	
	4–23–65	10.8–11.4	≈1,130			M–1–7	yes	Melt on bottom of steel rod.
2	4–19–65	0–1	0–310	56	45	M–2–1		One 3 in. piece.
		1–2	310–505	34	25	M–2–2		One 2 in. piece.
		2.0–5.1	505–940		0			
		5.1–6.1	940–1,040	68	50	M–2–3		
		6.1–7.1	1,040–≈1,100	18	20	M–2–4	yes	
	4–21–65	18	?			M–2–5		Ooze in drill pipe probe.
3	4–22–65	0–0.02				M–3–1		Glassy surface of lake.
		0.02–0.45	0–160	137	55	M–3–2	yes	Two ½ in. piece from top.
		0.45–0.7	160–240	98	50	M–3–3		
		0.7–0.9	240–280	93	60	M–3–4		
	4–27–65	0–1.08	0–300	96	80	M–3–5		One ½ in. piece from upper half of interval, 4>½ in.
		1.08–1.87	300–455	63	55	M–3–6		
		1.87–2.87	455–600	62	45	M–3–7		
		2.87–3.8	600–720		0			
		3.8–4.85	720–850	9	5	M–3–8		
		4.85–5.83	850–940	65	ca. 30	M–3–9		All small pieces.
		5.83–11	940–1,130±		0			
	4–28–65	11	1,130±	90		M–3–10		Melt sample oozed into base of stainless steel probe at 11 ft.; collected on old thermocouple steel at 9½ ft. Water quench.
4	4–22–65	0–0.45		179	70	M–4–1	yes	3 in. piece at top } Mast hole.
		0.45–0.8		162	75	M–4–2		One ½ in. piece-bottom } Mast hole.
	5–17–65	0–1.0	30–250	80	80	M–4–3		One 1 in. piece from upper 1½ ft. Three ½ in. pieces.
		1.0–2.0	250–410	96	80	M–4–4		
		2.0–3.0	410–540	33	20	M–4–5		
		3.0–4.0	540–650	19	10	M–4–6		
		4.0–5.0	650–750	61	40	M–4–7		One ½ in. piece.
		5.0–6.0	750–840	47	20	M–4–8		
		6.0–7.0	840–920	18	10	M–4–9		
		7.0–8.0	920–990	26	10	M–4–10		
		8.0–9.5	990–1,080	0	0			Crust melt interface at 9.3 ft.
5	4–22–65	0–.45	<180	216	95	M–5–1		2 in. piece—top, 1 in. piece—bottom, 1½ in. piece—middle.
		.45–.65	180–230	102	95	M–5–2		2 in. piece.
		.65–.85	230–280	127	95	M–5–3		2½ in. piece, one 1 in. piece from top.
	5–19–65	0–1.0	0–240	62	50	M–5–4		
		1.0–2.1	240–430	122	80	M–5–5		Three ½ in. pieces.
		2.1–3.1	430–560	96	75	M–5–6		One 1 in. piece.
		3.1–4.1	560–665	65	40	M–5–7		Two ½ in. pieces.
		4.1–5.1	665–760		0			
		5.1–6.1	760–850	152	80	M–5–8		One ½ in. piece.
		6.1–7.1	850–930	96	55	M–5–9	yes	One 1 in. piece, two ½ in. pieces.
		7.1–8.1	930–990	56	35	M–5–10		
		8.1–9.1	990–1,040	126	80	M–5–11		Three 1 in. pieces.
		9.1–10.1	1,040–≈1,060	18	10	M–5–12		One 1 in. piece.
		10.1–11.0	1,060–1,070	48	30	M–5–13		One 1 in. piece.
6	4–23–65	0–.4	<170	125	60	M–6–1		
		.4–.6	170–220	104	80	M–6–2		
		1.6–.75	220–250	92	90	M–6–3		1 in. piece from bottom.
	5–17–65	0–1.0	<240	109	85	M–6–4		1½ in. piece—top of hole; 2 in. piece—just below.
		1.0–1.9	240–400	58	55	M–6–5		One 3 in. piece.
		1.9–2.9	400–540	98	75	M–6–6		
		2.9–3.9	540–645	81	50	M–6–7		One ½ in. piece.

TABLE 24.—*Core logs for drill holes 1–24, 1965–66*—Continued

Drill hole No.	Date	Core interval (ft)	Temperature (°C)	Core recovery		Sample No.	Chemical analysis	Comment
				weight (g)	percent			
6–Con.		3.9–4.9	645–740	96	80	M–6–8		One ½ in. piece.
		4.9–5.9	740–830	109	60	M–6–9		
		5.9–6.9	830–915	21	25	M–6–10		
		6.9–7.9	915–980	88	70	M–6–11		
		7.9–8.9	980–1,035	30	20	M–6–12		
7	5–5–65	0–1	30–100	24	25	M–7–1		Much core left in hole; one ¾ in. piece.
		1–1.85	100–120	69	60	M–7–2		One ½ in. piece.
		1.85–2.85	120–275	60	50	M–7–3		One ¾ in. piece; top marked.
		2.85–3.5	275–460	35	50	M–7–4		One ½ in. piece; top marked.
	5–6–65	3.5–4.9	460–725	160	65	M–7–5		One 2½ in. piece; top marked; one 1 in. piece; top marked.
		4.9–5.45	725–800	30	50	M–7–6		All small pieces.
		5.45–7.9	800–1,030		0			
		7.9–8.9	1,030–1,085±	11	5	M–7–7		One good glassy piece.
		8.9–15	1,085±1,130		0			
	5–7–65	15–20	1,130–1,140			M–7–8		Melt oozed into steel probe for ball experiment. Collected on push rod.
8	5–24–65	0–.45	<180	47	25	M–8–1		
		.45–.7	180–195	47	20	M–8–2		
		.7–.8	195–210	58	50	M–8–3		
		0–1	<240	58	50	M–8–4		One 1 in. piece; one ½ in. piece.
		1–2	240–385	28	30	M–8–5		
		2–3	385–510	11	10	M–8–6		
		3–4	510–625	11	5	M–8–7		
		4–5	625–720	9	5	M–8–8		
		5–6	720–805		0			
		6–7	805–885	27	10	M–8–9		
		7–8	885–955	49	25	M–8–10		
		8–9	955–1,025	26	5	M–8–11		
9	5–24–65	0–.2	<100	62	70	M–9–1		One 1½ in. piece.
		.2–.4	100–140	93	75	M–9–2		One 2 in. split piece.
		.4–.65	140–190	156	100	M–9–3		One 2 in. piece.
		.65–.8	190–210	69	80	M–9–4		One 1 in. piece.
		0–1	<240	56	50	M–9–5		Three ¾ in. pieces.
		1–2	240–385	47	40	M–9–6		One ½ in. piece.
		2–3	385–510	39	30	M–9–7		Two ½ in. pieces.
		3–4	510–625	43	30	M–9–8		One ½ in. piece.
		4–5	625–720	121	80	M–9–9		One ½ in. piece.
		5–6	720–805	125	75	M–9–10		
	5–26–65	6–7	805–885	46	30	M–9–11		
		7–9	885–1,015		0			
		9–10	1,015–1,055	43	25	M–9–12		
		10–10.5	1,055–1,070	46	60	M–9–13		
10	5–26–65	0–.35	<130	134	75	M–10–1		2 in. piece. } Mast hole.
		.35–.55	130–165	98	85	M–10–2		2 in. piece } Mast hole.
		.55–.7	165–195	91	80	M–10–3		2 in. piece. } Mast hole.
		0–1.1	<260	42	50	M–10–4		One ½ in. piece.
		1.1–2.0	260–385	34	30	M–10–5		
		2.0–3.0	385–510	8	10	M–10–6		
		3.0–4.0	510–625	12	5	M–10–7		
		4.0–5.0	625–720	51	50	M–10–8		
		5.0–6.0	720–805	30	20	M–10–9		
		6.0–7.0	805–885	43	10	M–10–10	yes	
		7.0–8.0	885–955	45	40	M–10–11		
		8.0–9.0	955–1,010	13	5	M–10–12		
		9.0–10.0	1,010–1,050	65	50	M–10–13		
		10.0–10.6	1,050–1,070	63	70	M–10–14		Three ½ in. pieces.
11	5–26–65	0–.4	<80	130	90	M–11–1		Two 1½ in. pieces. } Mast hole.
		.4–.6	80–100	85	75	M–11–2		2 in. piece } Mast hole.
		.6–.8	100–130	90	80	M–11–3		
		0–1.0	<150	119	90	M–11–4		Numbered from top: two 1½ in. pieces; four 1 in. pieces; two ½ in. pieces.
		1.0–2.0	150–255	84	60	M–11–5		Four 1 in. pieces.
		2.0–3.0	255–360	43	30	M–11–6		One 1 in. piece.
		3.0–4.0	360–465	57	35	M–11–7		One ½ in. piece.

TABLE 24.—*Core logs for drill holes 1–24, 1965–66*—Continued

Drill hole No.	Date	Core interval (ft)	Temperature (°C)	Core recovery weight (g)	Core recovery percent	Sample No.	Chemical analysis	Comment
11–Con.		4.0–5.0	465–560	84	50	M–11–8		One 1½ in. piece.
		5.0–6.0	560–645	101	50	M–11–9	yes	Three 1 in. pieces.
		6.0–7.0	645–725	90	50	M–11–10	yes	One 1 in. piece.
		7.0–8.0	725–795	71	50	M–11–11	yes	
		8.0–9.0	795–865	95	40	M–11–12	yes	One ½ in. piece.
		9.0–10.0	865–920	80	50	M–11–13		Two ½ in. pieces.
		10.0–11.0	920–980	44	25	M–11–14	yes	One ½ in. piece.
		11.0–11.9	980–1,030	27	15	M–11–15		One ½ in. piece.
	6–1–65	11.9–12.9	1,025–1,070	203	100	M–11–16		Three 2 in. pieces, two ½ in. pieces.
12	6–1–65	0–0.2	[1]	22	30	M–12–1		
		.2–.5		26	30	M–12–2		
		0–.5		81	100	M–12–3		One 5½ in. piece.
		.5–1.05			0			
		1.05–2.3		82	50	M–12–4		Five ½ in. pieces.
		2.3–3.3		28	25	M–12–5		One ½ in. piece.
		3.3–4.3			0			
		4.3–6.3		225	75	M–12–6		One 1½ in. piece.
		6.3–8.3		109	40	M–12–7		One ½ in. piece.
		8.3–8.75		41	50	M–12–8		One ½ in. piece.
	6–4–65	8.75–9.7		67	20	M–12–9		Four ½ in. pieces.
		9.7–12.3		222	50	M–12–10		Seven 1 in. pieces, many ½ in. pieces.
		12.3–14.0		97	20	M–12–11		Two 1 in. pieces, many ½ in. pieces.
		14.0–15.9			0			
		15.9–17.0		65	50	M–12–12		Four ½ in. pieces.
		17.0–19.0		54	20	M–12–13		One 1 in. piece, one ½ in. piece.
		19.0–21.0			0			
		21.0–24.0		8	<5	M–12–14		One ½ in. piece and fragments (lava or talus?).
13	6–7–65	0–0.4	<120	71	40	M–13–1		
		0.4–0.65	120–170	99	75	M–13–2		Mast hole.
		0.65–0.85	170–210	110	95	M–13–3		2 in. piece.
		0–0.9	<220	92	80	M–13–4		Two 1 in. pieces, two ½ in. pieces.
		0.9–2.15	220–380	101	70	M–13–5		One 1 in. piece, One ½ in. piece.
		2.15–3.1	380–500	74	50	M–13–6		
		3.1–4.1	500–600	75	50	M–13–7		
		4.1–5.1	600–690	132	85	M–13–8		
		5.1–6.1	690–775	133	80	M–13–9		
		6.1–7.1	775–845	104	70	M–13–10		
		7.1–8.1	845–915	90	60	M–13–11	yes	
		8.1–9.1	915–980	48	30	M–13–12	yes	
		9.1–10.1	980–1,025	128	75	M–13–13	yes	One in. piece, two ½ in. pieces.
		10.1–11.1	1,025–1,080	133	75	M–13–14	yes	One 2 in. piece, three 1 in. pieces.
		11.0–11.8	1,080–1,100	51	40	M–13–15		Two ½ in. pieces from top of interval.
14	6–11–65	0–0.5	<160	92	40	M–14–1		Mast hole.
		0.5–0.8	160–200	94	50	M–14–2		
	6–16–65	0–0.85	<200	47	60	M–14–3		Two 1 in. pieces, three ½ in. pieces.
		0.85–2.0	200–350	42	35	M–14–4		Two ½ in. pieces.
		2.0–3.0	350–460	36	40	M–14–5		
		3.0–4.0	460–565	30	30	M–14–6		
		4.0–5.0	565–660	95	80	M–14–7		
		5.0–6.0	660–765	18	20	M–14–8		One ½ in. piece.
		6.0–7.0	765–815	72	60	M–14–9		
		7.0–8.0	815–885	82	70	M–14–10		One piece with large olivine crystal.
		8.0–9.0	885–950	58	50	M–14–11		
		9.0–10.0	950–1,010	92	60	M–14–12		
		10.0–11.0	1,010–1,060	26	20	M–14–13		
		11.0–11.9	1,060–1,070	17	10	M–14–14		
15	6–11–65	0–0.25	<100	62	60	M–15–1		Broken
		0.25–0.55	100–130	167	100	M–15–2		Irregular 3 in. pieces Mast hole.
		0.55–0.7	130–170	86	100	M–15–3		Good 2 in. pieces
	6–16–65	0–1.0	<210	35	30	M–15–4		One ½ in. piece.
		1.0–2.0	210–350	12	10	M–15–5		
		2.0–2.9	350–450	29	20	M–15–6		
		2.9–4.0	450–565	48	50	M–15–7		One ½ in. piece.
		3.85–4.85	550–645	92	70	M–15–8		One ½ in. piece.
		4.85–5.95	645–740	31	30	M–15–9		

TABLE 24.—*Core logs for drill holes 1–24, 1965–66*—Continued

Drill hole No.	Date	Core interval (ft)	Temperature (°C)	Core recovery weight (g)	Core recovery percent	Sample No.	Chemical analysis	Comment
16	6–30–65	0–0.4	<100	135	70	M–16–1		Mast hole.
		0.4–0.7	100–140	125	80	M–16–2		Mast hole.
		0–1.8	<300	75	45	M–16–3		2 in. piece, two 1 in. pieces.
		1.8–3.0	300–450	18	10	M–16–4		
		3.0–3.85	450–520	8	5	M–16–5		
		3.85–4.8	520–600	115	85	M–16–6		1 in. piece.
	7–12–65	4.8–5.92	600–670	78	55	M–16–7		½ in. piece.
		5.92–6.92	670–740	155	60	M–16–8		Two ½ in. pieces.
		6.92–7.92	740–800	76	60	M–16–9		1 ½ in. piece.
		7.92–8.92	800–860	84	60	M–16–10		
		8.92–9.92	860–910	128	80	M–16–11		Two ½ in. pieces.
		9.92–10.92	910–965	9	10	M–16–12		
		10.92–11.92	965–1,010	30	10	M–16–13		
		11.92–12.92	1,010–1,055	84	60	M–16–14		One 1 in. piece, one ½ in. piece.
	7–15–65	12.85–13.9	1,055–≈1,100	43	20	M–16–15		
17	7–12–65	0–0.48	<100	146	85	M–17–1		
		0.48–0.75	100–150	133	85	M–17–2		
	7–15–65	0–0.9	<190	106	95	M–17–3		One 1 in. piece, three ¼ in. pieces, three ½ in. pieces.
		0.9–1.5	190–270	104	90	M–17–4		Three 1¼ in. pieces, one 2 in. piece.
		1.5–2.5	270–370	49	25	M–17–5		One 1 in. piece.
		2.5–3.5	370–460	49	25	M–17–6		Two ½ in. pieces.
		3.5–4.5	460–560	13	10	M–17–7		
		4.5–5.5	560–640	50	20	M–17–8		Two ½ in. pieces.
		5.5–12.5	640–1,030		0			
		12.5–13.5	1,030–1,070	58	20	M–17–9		Three ½ in. pieces.
		13.5–14.5	1,070–1,100	23	5			
	7–16–65	14.5–16.1			0			
17A	7–28–65	0–1.0	<190	26	20	M–17A–1		
		1.0–2.0	190–300	94	75	M–17A–2		One ½ in. piece.
		2.0–3.0	300–400	38	30	M–17A–3		Two 2 in. pieces.
		3.0–4.0	400–500		0			
		4.0–5.0	500–580	90	70	M–17A–4		
		5.0–6.0	580–650	113	80	M–17A–5		Three pieces>½ in.
		6.0–7.0	650–710	98	70	M–17A–6		One piece>½ in.
		7.0–8.0	710–770	88	70	M–17A–7		
		8.0–8.85	770–820	54	40	M–17A–8		
		8.85–10.0	820–880	10	10	M–17A–9		
18	7–12–65	0–0.5		113	60	M–18–1		Mast hole. Site abandoned.
		0.5–0.57		39	90	M–18–2		
19	7–12–65	0–0.4		169	88	M–19–1		Mast hole. Site abandoned.
		0.4–0.8		226	88	M–19–2		
20	8–2–65	0–0.90	<190	17	15	M–20–1		
		0.9–1.9	190–300	35	30	M–20–2		
		1.9–3.1	300–410	10	10	M–20–3		
		3.1–4.1	410–500	24	10	M–20–4		
		4.1–5.1	500–570	102	70	M–20–5		One ½ in. piece.
		5.1–6.1	570–645	76	60	M–20–6		One 1 in. piece.
		6.1–7.1	645–700		0			
		7.1–8.1	700–770	45	40	M–20–7		
		8.1–9.1	770–830		0			
		9.1–10.1	830–880	81	50	M–20–8		
		10.1–12.1	880–970		0			
		12.1–13.1	970–1,010	82	60	M–20–9		
		13.1–14.1	1,010–1,045	104	70	M–20–10		One 1 in. piece, four ½ in. pieces.
		14.1–21			0			
		21–23	1,130–1,135			M–20–11		Melt on pusher rod above paddle.
		21–23	1,130–1,135			M–20–12		Melt on paddle wheel.
		21–23				M–20–13		Melt in stainless steel casing.
21	8–17–65	0–0.95	<175	112	95	M–21–1		Four ½ in. pieces, three 1 in. pieces, one 2 in. piece.
		0.95–1.95	175–280	113	90	M–21–2		Three ½ in. pieces, two 1 in. pieces.
		1.95–2.95	280–380	70	60	M–21–3		Five pieces>½ in.
		2.95–3.95	380–465	33	40	M–21–4		
		3.95–4.95	465–550	114	80	M–21–5		

TABLE 24.—*Core logs for drill holes 1-24, 1965-66*—Continued

Drill hole No.	Date	Core interval (ft)	Temperature (°C)	Core recovery weight (g)	Core recovery percent	Sample No.	Chemical analysis	Comment
21–Con.		4.95–5.95	550–620	104	80	M–21–6		
		5.95–6.95	620–685	94	80	M–21–7		Three ½ in. pieces.
		6.95–7.95	685–750	55	40	M–21–8		
		7.95–8.95	750–800		0			
		8.95–9.95	800–845	79	50	M–21–10		
		9.95–10.95	845–890	52	40	M–21–11		
		10.95–11.95	890–935	59	40	M–21–12	yes	
		11.95–12.95	935–980	101	80	M–21–13		One ½ in. piece.
		12.95–13.95	980–1,010	98	80	M–21–14		Three ½ in. pieces.
		13.95–14.95	1,010–1,040	5	3	M–21–15		
		14.95–15.95	1,040–1,064		0			
		15.95–16.95	1,065–1,085	8	3	M–21–17		Base of crust 160 ft.
		16.95–18.95	≈1,085–≈1,130		0			
		18.95–19.6	≈1,130–≈1,140	38	20	M–21–20		
		17–18	1,095–1,105	194	20	M–21–21		Ooze from drill steel, three 3-in. pieces, one 2 in. piece, one 1 in. piece.
		18	1,105	26		M–21–22		Ooze-end of stainless steel rod.
	8–30–65	20–22	1,115–1,125			M–21–23		Melt from outside of drill steel.
		19–22	1,110–1,125			M–21–24	yes	3 ft of melt in drill steel.
	9–16–65	15.4–16.05			55	M–21–25	yes	One 2 in. piece, good ooze sample.
	9–27–65	25–26.75				M–21–26	yes	Dense glassy melt surrounding long tubular voids—collected in ceramic tube and stainless steel casing. Four pieces >¾ in.
		29–30.5				M–21–27	yes	Melt in ceramic and in steel casing.
22	11–1–65	0–0.9		39	45	M–22–1		Two pieces>½ in.
		0.9–1.9		71	55	M–22–2		Three pieces>½ in.
		1.9–3.0			0			
		3.0–4.0		26	20	M–22–3		
		4.0–5.0		95	80	M–22–4		
		5.0–6.0	465–530	69	60	M–22–5		
		6.0–7.0	530–580	45	50	M–22–6		
		7.0–8.0	580–635	53	50	M–22–7		
		8.0–9.0	635–690		0			
		9.0–10.0	690–740	85	70	M–22–8		
		10.0–11.0	740–780	27	30	M–22–9		
		11.0–12.0	780–820	78	60	M–22–10	yes	One piece>½ in.
		12.0–14.0	820–900		0			
		14.0–15.0	900–935	132	80	M–22–11		Six pieces>½ in.
		15.0–16.0	990–1,020					
	11–9–65	16.0–17.0	975–1,010		100	M–22–12		
		17.0–18.0	1,010–1,035		0			
		18.0–19.0	1,035–1,060		50	M–22–13		
		19.0–20.0	1,060–1,075		20	M–22–14		Base of crust 19.7 ft.
		20.0–21.0	1,075–1,095		0			
		21.0	1,095			M–22–15		End of sampler.
		20.5–21.6	~1,095			M–22–16		Ooze on thermocouple.
		21.0	1,095			M–22–17		Plug at 21.0 ft (ooze).
		21–23	1,095–1,110			M–22–18		Melt in 2 ft stainless.
23	12–1–65	0–1.2	<100	85	80	M–23–1		Four pieces>½ in.
		1.2–2.2	<100	60	60	M–23–2		Two pieces>½ in.
		2.2–3.2	<100–150	83	65	M–23–3		Two pieces>½ in.
		3.2–3.6	150–250	28	40	M–23–4		
	12–6–65	3.5–5.0	250–360	130	80	M–23–5		One piece>½ in.
		4.9–5.9	360–425	95	80	M–23–6		One piece>½ in.
		5.9–7.9	425–540	195	75	M–23–7		Four pieces>½ in.
		7.9–8.9	540–600	110	80	M–23–8		Several>½ in.
		8.9–9.9	600–670	85	80	M–23–9		Two pieces>½ in.
		9.9–10.9	670–730	23	10	M–23–10		One piece>½ in.
		10.9–11.9	730–780	31	20	M–23–11		
		11.9–12.9	780–820	64	50	M–23–12		
		12.9–13.9	820–870	75	50	M–23–13		One large piece.
		13.9–15.9	870–950	41	20	M–23–14		
		15.9–16.9	950–975	80	60	M–23–15		Two pieces>½ in.
	12–13–65	16.9–17.9	975–990	60	60	M–23–16		

TABLE 24.—*Core logs for drill holes 1–24, 1965–66*—Continued

Drill hole No.	Date	Core interval (ft)	Temperature (°C)	Core recovery weight (g)	Core recovery percent	Sample No.	Chemical analysis	Comment
23–Con.		17.9–18.65	990–1,005	50	40	M–23–17		One piece>½ in.
		19.7–20.9	1,060–1,085	35	25	M–23–18		
	1–19–66	19.4–21.0	1,000–1,060		80	M–23–19	yes	Ooze drilled out as four separate pieces: a, b, c, d. May have come in from different horizons.
		24.0+	1,095+			M–23–21	yes	Small piece lodged in bit.
		23.5	1,090			M–23–22		Melt in bit and on stainless steel rod.
	2–3–66	21.0–22.0	1,030–1,060			M–23–23		Small piece in bit.
		24.0+	1,085+			M–23–24		Pushed 3–4 ft into melt which was collected in bit.
24	5–2–66	0–4.9	<290	400	51			
	5–23–66	4.9–7.0	280–390	90	38			
		7.0–9.0	390–480	150	80			
		9.0–11.0	480–580	140	80			
		11.0–13.0	580–670	60	40			
		13.0–15.0	670–740	170	60			
		15.0–17.0	740–815	145	50	[2]M–24–16.9		
		17.0–19.0	815–870	0	0			
		19.0–21.0	870–950	105	60	M–24–19.1		
						M–24–20.4		
		21.0–23.0	950–1,005	180	75	M–24–21.1		
						M–24–22.0		
						M–24–22.9		
		23.0–25.0	1,005–1,045	245	90	M–24–23.1		
						M–24–24.0		
						M–24–25.0		
		25.0–27.0	1,045–1,085	0	0			
	7–28–66	22.0–25.0	940–1,015	6	5	M–24–1		
		25.0–27.0	1,015–1,060	0	0			
		27.0–29.0	1,060–1,090	5		M–24–2	yes	Melt (in core barrel).
		29.0–30.0	1,090–1,100	6	5	M–24–3		Do.
		29.0–31.0	1,090–1,110					Hole cased to ~ 40 ft.
	11–29–66	30.0–30.2	1,053±3	8		M–24–4		Film of ooze on oxidized thermocouple sheath in cased hole.

[1]Hole near edge of lake. No way to extrapolate temperature back to the time of drilling.
[2]Analyzed or thin-sectioned samples from drilling dates 5/2/66 and 5/23/66 coded as follows: M–24–(depth in feet), for example, core collected at 21 feet is labeled M–24–21. Core fron redrilling in 7/28/66 numbered consecutively.

TABLE 25.—*Core logs for drill holes 68–1, 68–2 and 69–1; 1968–69*

Drill hole No.	Date	Core interval (ft)	Temperature[1] (c°C)	Core recovery percent	Core recovery intervals of no core (ft)	Sample Nos. for chemical analysis	Comment
68–1	11/6/68	0–1.0	<100	100			
		1.0–1.9	<100	100			Sublimates in vesicles.
		1.9–3.7	<100	50	1.9–2.8	68–1–1 (3.7 ft)	
		3.7–7.3	<100	81	4.7–4.9		
					5.9–6.4		
	11/12/68	7.3–10.0	<100	89	8.5–8.8	68–1–2 (8.0 ft)	
		10.0–14.8	<100	100		68–1–3 (12.0 ft)	Thin section (14.8 ft).
		14.8–19.8	~100	100		68–1–4 (17.5 ft)	
	11/15/68	19.8–23.0	100–200	100		68–1–5 (22.1 ft)	
		23.0–28.0	200–320	100		68–1–6 (24.0 ft)	Thin section (27.4 ft).
						68–1–7 (26.0 ft)	
						68–1–8 (27.9 ft)	
		28.0–28.8	320–350	100			Thin section (28.3 ft).
		28.8–29.35	350–390	100			
		29.35–35.1	390–590	71	scattered	68–1–9 (30.0 ft)	Thin section (33.5 ft).
						68–1–11 (33.8 ft)	
	11/18/68	35.1–40.0	590–770	57	scattered	68–1–12 (36.0 ft)	Core lost in drilling.
						68–1–14 (39.8 ft)	
		40.0–44.2	770–900	0	40.0–44.2		Probably drilled along vertical crack.
		44.2–49.5	900–1,030	100			
						68–1–16 (44.2 ft)	
						68–1–17 (46.1 ft)	
						68–1–47.5 (47.5 ft)	
						68–1–18 (48.0 ft)	
						68–1–19 (49.5 ft)	

TABLE 25.—*Core logs for drill holes 68–1, 68–2 and 69–1; 1968–69*—Continued

Drill hole No.	Date	Core interval (ft)	Temperature[1] (c°C)	Core recovery percent	Core recovery intervals of no core (ft)	Sample Nos. for chemical analysis	Comment
68–1	11/18/68	49.5–54.0	1,030–1,075	18	prob. 49.5–53.2	68–1–21 (54.0 ft)	Thin section (53.5 ft, 54.0 ft).
	11/20/68	47.9–57.0		--		----	Black sand erupted at top of drill hole throughout entire drilling interval. Collected in bags.
68–2	12/12/68	0–1.0	<100	100			
		1.0–2.0	<100	100			
		2.0–3.0	<100	80	2.8–3.0		
		3.0–8.0	<100	74	scattered in 5.9–8.0		5.9–8.0 ft: vertical fracture in core.
		8.0–13.0	<100	100			
	12/16/68	13.0–17.9	<100	84	scattered in 15.0–17.9		
		17.9–22.9	<100–200	100			
		22.9–27.9	200–320	100			
		27.9–33.0	320–500	84	scattered in 28.3–30.3	68–2–10 (32.0 ft)	
		33.0–38.0	500–720	88	36.5–37.1	68–2–13 (38.0 ft)	
		38.0–43.0	720–870	62	39.5–41.4	68–2–15 (42.0 ft)	
	12/18/68	43.0–44.3	870–900	100			
		44.3–49.1	900–1,010	0			Core spring left out of core barrel.
		44.3–49.5	900–1,020	56	not known		Redrilled—void to 46.0 ft.
		49.5–50.0	1,020–1,040	100			
		50.0–55.2	1,040–1,080	27	scattered 52.0–55.2	68–2–20 (51.5 ft)	Probably crossed crust-melt interface.
		55.2–59.0	1,080–1,100	low	not known	68–2–59 (59 ft)	Melt in bit, no core.
69–1	1/22/69	0–1.3		38	0.1–0.4, 0.7–0.8, 0.9–1.3		
		1.3–2.3		80	scattered		
		2.3–4.0		59	scattered		
		4.0–7.7		100			
		7.7–12.3		81	scattered		Thin sections (8.3 ft, 8.4 ft, 9.6 ft, 9.7 ft, 11.6 ft)
		12.3–15.0		52	scattered		Thin section (14.9 ft).
		15.0–19.2		52	scattered		
		19.2–20.0		38	scattered		
		20.0–24.7		55	scattered		Thin section (20.0–22.7 ft, 24.6 ft).
	1/28/69	24.7–27.1		83	scattered	69–1–24.7 (24.7 ft) 69–1–25.6 (25.6 ft)	Thin section (24.7 ft, 25.6 ft).
		27.1–30.0		100			Thin section (28.0 ft, 28.3 ft, 28.7 ft, 29.0 ft, 29.5 ft, 29.8 ft).
		30.0–35.0		90	scattered		Thin section (31.2 ft, 31.7 ft).
		35.0–38.5		100			Thin section (37.5 ft, 37.9 ft).
		38.5–41.0		80	scattered		Thin section (41.0 ft).
	1/31/69	41.0–46.0		30	not known	69–1–41.0 (41.0 ft) 69–1–42.0 (42.0 ft)	Thin section (exact depth not known).
		46.0–50.9		90	scattered		Thin section (47.3 ft, 47.6 ft, 48.3 ft, 49.5 ft).
		50.9–56.0		76	scattered	69–1–55.5 (55.5 ft)	Thin section (51.0 ft, 52.3 ft, 53.1 ft, 55.1 ft—segregation vein, 55.0 ft, 55.7 ft).
		56.0–61.0		0			In melt.
		61.0–66.0		0			In melt. Melt flowed into core barrel which was then recovered (fig. 26).

[1]Temperatures are not accurately known for drill holes 68–1 and 68–2 because the only temperature profiles showed effects of thermal depression from water introduced during drilling. No temperature data are obtained for 69–1. Where temperatures are given they are probably minimum values.

TABLE 26.—*Temperature profiles (°C) measured in drill holes 2–24, 68–1*

[Data for each drill hole given separately, with subheadings giving date (and hour for the earliest temperature profiles) followed in parenthesis by the square root of time in days since formation of the permanent crust on March 19, 1965. Example: 5/24/65 (8.11) 6/7/65 (8.93) 6/16/65 (9.42) 6/30/65 (10.14)]

Drill hole No. 2

Depth (ft)	4/19/65 (5.58) 09:55–10:45	14:09	4/21/65 (5.72) 14:45	15:13	15:32
1.0	137±				
2.0	334.7				
3.0	549.3				

TABLE 26.—*Temperature profiles (°C) measured in drill holes 2–24, 68–1*—Continued

Drill hole No. 2—Continued

Depth (ft)	4/19/65 (5.58) 09:55–10:45	4/21/65 (5.72) 14:09	14:45	15:13	15:32
3.1				441	449
4.0	734.9				
5.0	892.8				
6.1	1,016.6		954	1,031	963
9.1		1,131	1,109	1,088	1,116
12.1		1,134	1,110	1,088	1,115
15.1		1,128	1,103	1,083	
18.1		1,134	1,106		
21.1		1,136			

Drill hole No. 3

Depth (ft)	4/28/65 (6.31) 10:43–11:26	15:13–15:49	5/5/65 (6.83)	5/7/65 (6.98)	5/17/65 (7.67)	5/24/65 (8.11)
1.0	163.0		102.5		102.0	100.0
2.0	332.3	188.5	129.0		145.3	103.5
3.0	550.3		329.3		314.5	368.5
3.5				95		
4.0	715.3	685.1	561.1		470.0	496.8
5.0	849.8		738.0	484.4	615.3	618.0
6.0	955.5	899.0	860.8		741.8	748.3
6.5				787.8		
6.7	1,011.5					
7.0		993.8	964.3			
7.2					863.0	830.3
7.6			1,012.5			
8.0		1,056.3		961.0		
9.0		1,110.0		1,063.5		
9.5						

Drill hole No. 4

Depth (ft)	5/24/65 (8.11)	6/7/65 (8.93)	6/16/65 (9.42)	6/30/65 (10.14)
1.0	168.3	213.3	228.8	203.0
2.0		327.8	351.1	322.0
3.0	410.0	451.3	468.0	435.5
4.0		555.3	565.3	
4.5		620.0	611.8	581.0
5.0	661.1	645.0	651.3	
5.5		709.1	696.0	657.8
6.5		792.5	775.3	733.3
7.0	865.0			
7.5		867.5	845.0	
8.5		933.0	907.8	
9.0	1,003.8			

Drill hole No. 5

Depth (ft)	5/24/65 (8.11)	6/7/65 (8.93)	6/16/65 (9.42)
1.0	166.5	215.3	232.3
2.0		338.7	352.5
3.0	394.0	454.0	463.6
4.0		554.8	560.9
5.0	608.4	638.8	642.0
6.1		739.0	733.0
7.1	810.0	818.5	809.8
8.1		891.5	879.3
9.1	975.5	953.8	938.0
10.1		1005.8	987.8

Drill hole No. 6

Depth (ft)	5/26/65 (8.23)	6/7/65 (8.93)	6/16/65 (9.42)	6/26/65 (9.93)	7/25/65 (12.60)	9/23/65 (13.70)
1.0	93.1	182.0	203.8			146.0
2.0	249.3	325.8	349.5	338.9	293.0	
3.0	387.8	443.8	460.8	450.2		326.5
4.0	515.0	549.1	560.0	542.9	466.0	407.1
4.9		635.5	637.3	626.3	540.0	
5.0	641.6	637.3	644.5			503.1
5.9	736.0	720.7	716.5	699.6	594.2	565.5
6.9	835.0	802.8	792.3	769.3	652.5	627.8
7.9	918.2	874.5	859.5	828.7	705.8	686.0
8.9	982.5	936.8	919.3	883.6	761.0	737.3

Drill hole No. 7—No measurements made

Drill hole No. 8

Depth (ft)	6/7/65 (8.93)	6/16/65 (9.42)	6/30/65 (10.14)	Depth (ft)	8/17/65 (12.28)	Depth (ft)	10/27/65 (14.89)
1.0	184.8	212.3	202.5	1.0	170.8	0.5	91.5
2.0	320.8	335.3	337.8	2.0	265.0	1.5	156.8
3.0	449.3	456.3	453.8	3.0	371.6	2.5	258.5

TABLE 26.—*Temperature profiles (°C) measured in drill holes 2–24, 68–1*—Continued

Drill hole No. 8—Continued

Depth (ft)	6/7/65 (8.93)	6/16/65 (9.42)	6/30/65 (10.14)	Depth (ft)	8/17/65 (12.28)	Depth (ft)	10/27/65 (14.89)
4.0	559.0	559.3	546.0	4.0	436.3	3.5	351.8
5.0	649.5	643.5		5.0	536.0	4.5	437.1
5.7	724.0	710.8	697.8	5.6	591.8	5.5	505.8
6.7	805.8	787.8	769.3	6.6	660.7	6.5	573.8
7.7	881.8	858.0	835.0	7.6	720.0	7.5	629.8
8.7	948.3	920.3	891.8	8.6	776.8	8.5	686.8
9.7	1,004.8	974.0	941.8	9.6	824.0	9.5	734.0

Drill hole No. 9

Depth (ft)	6/7/65 (8.93)	6/16/65 (9.42)	6/30/65 (10.14)
1.0	184.3	219.3	205.3
2.0	320.8	344.0	332.8
3.0	448.0	462.0	446.0
4.0	554.5	559.3	538.2
5.0	643.8	638.8	620.1
6.3	760.5	749.3	707.3
7.3	840.7	822.8	776.0
8.3	915.0	892.3	842.0
9.3	977.4	952.3	895.3
10.3	1,031.8	1,004.0	

Drill hole No. 10

Depth (ft)	6/7/65 (8.93)	6/16/65 (9.42)	6/30/65 (10.14)	Depth (ft)	7/21/65 (11.13)	Depth (ft)	8/10/65 (11.99)	8/13/65 (12.11)	Depth (ft)	9/27/65 (13.85)	11/4/65 (15.16)
1.0	156.0	206.0	222.5	1.0	182.3	1.0			1.1	173.8	187.0
2.0	283.8	332.5	345.3	2.0	307.3	2.0			2.1	260.8	254.3
3.0	411.1	446.9	451.8	3.0	409.8	3.3	436.0	438.8	3.1	351.1	343.9
4.0	522.7	544.9	543.1	4.0	506.0	4.3	518.0	522.9	4.1	430.8	428.4
5.0	616.0	627.8	618.0	5.0	583.1	5.3	588.0	593.5	5.1	512.5	494.7
6.4	752.4	744.0	729.8	6.3	680.2	6.3	652.0	656.7	6.1	578.2	555.8
7.4	832.5	818.0	798.0	7.3	746.0	7.3	723.0	715.1	7.1	651.6	611.2
8.4	910.5	888.0	863.0	8.3	805.5	8.3	778.2	772.0	8.1	707.0	664.9
9.4	976.3	948.5	919.8	9.3	863.0	9.3	836.0	827.5	9.1	759.3	714.0
10.4	1,031.0	1,001.0	968.0	10.3	909.8	10.3	882.4	875.0	10.1	803.5	761.3

Drill hole No. 11

Depth (ft)	6/7/65 (8.93) 10:40–11:45	6/16/65 (9.42)	6/30/65 (9.93)	Depth (ft)	8/13/65 (12.11)	Depth (ft)	9/23/65 (13.70)
1.0	92.7	131.3	166.0				
2.0	180.3	235.8	250.3				
3.0	285.0	331.8	340.8				
4.0	376.8	410.6	413.5			4.0	309.3
5.0	466.0	487.0	486.8	5.0	465.3	5.0	373.0
6.0	552.3	573.3	557.1	6.0	525.5	6.0	433.1
7.0	640.4	652.2	624.8	7.0	590.5	7.0	512.0
8.0	724.2	730.3	692.6	8.0	654.3	8.0	586.2
9.0	804.8	801.5	762.5	9.0	713.5	8.8	648.8
10.0	877.0	864.5	822.0	9.9	767.3	9.8	711.0
11.0	947.3	931.0	878.0	10.9	815.5	10.8	762.0
12.0	1,006.5	984.0	929.4	11.9	862.3	11.8	811.0
13.0	1,052.3	1,027.0	976.9	12.9	909.3	12.8	854.0

Drill hole No. 12

6/7/65 (8.93)											
(ft)	10:53	(ft)	12:00	(ft)	12:25	(ft)	13:30	Depth (ft)	6/16/65 (9.42)	Depth (ft)	6/30/65 (9.93)
9.3	503.1	8.0	462.0	7.0	404.5	2.0	249.6	7.8	480.9	3.0	222.0
12.3	599.0	11.0	576.8	10.0	546.5	5.0	355.1	9.3	531.1	6.0	439.8
15.3	639.3	14.0	632.2	13.0	612.9	8.0	497.3	11.0	579.6	8.0	488.4
18.3	648.3	17.0	649.8	16.0	643.8	11.0	563.8	12.3	609.1	9.0	506.7
21.3	609.6	20.0	644.3	19.0	645.3	14.0	630.0	13.8	633.1	9.4	525.5
								15.3	646.4	11.0	569.8
								16.8	650.7	12.0	587.3
								18.3	649.8	12.4	585.8
								19.8	642.5	14.0	613.3
								21.3	615.5	15.0	621.6
										15.4	623.8
										17.0	632.4
										18.4	628.0
										20.0	627.3
										21.4	599.5

Drill hole No. 13

Depth (ft)	7/21/65 (11.13)
1.0	181.3
2.0	304.5
3.0	409.3
4.0	503.3

TABLE 26.—*Temperature profiles (°C) measured in drill holes 2-24, 68-1*—Continued

Drill hole No. 13—Continued

Depth (ft)	7/21/65 (11.13)
5.0	582.9
6.45	687.0
7.45	752.7
8.45	812.0
9.45	870.3
10.45	922.0

Drill hole No. 14

Depth (ft)	6/16/65 (9.42) 12:30	13:33	Depth (ft)	7/21/65 (11.13)	Depth (ft)	2/25/66 (18.51)
7.9	724.7	799.3	1.5	241.5	2.0	95
8.9	791.8	867.3	2.5	360.9	2.9	95
9.9	881.0	944.5	3.5	457.5	4.0	167.0
10.9	1,004.5	1,025.5	4.5	548.4	4.9	228.5
11.9	1,059.4	1,070.5	5.5	624.9	6.0	310.5
			7.05	736.5	6.9	377.0
			8.05	799.3	8.0	442.7
			9.05	857.1	8.9	502.0
			10.05	914.0	10.0	563.3
			11.05	960.5	10.9	617.6

Drill hole No. 15—No measurements made

Drill hole No. 16

Depth (ft)	8/17/65 (12.28)	Depth (ft)	9/27/65 (13.85)	Depth (ft)	10/27/65 (14.89)	2/25/66 (18.51)
1.0	161.8	2.0	257.1	0.7	122.8	
2.0	277.5	4.0	423.0	1.7	199.5	
3.0	375.6	6.0	560.2	2.7	282.3	
4.0	450.4	8.0	677.2	3.7	371.1	
5.0	523.3	10.0	779.1	4.7	445.0	199.0
6.0	591.3	12.0	866.8	5.7	515.8	275.7
7.0	651.4	13.8	931.7	6.7	574.5	347.5
8.0	703.0			7.7	631.4	414.5
9.0	758.0			8.7	684.9	480.2
9.7	798.8			9.7	734.6	539.1
10.0	807.8			10.7	781.8	589.1
10.7	848.3			11.7	824.0	641.4
11.7	892.5			12.7	865.8	687.3
12.7	929.0			13.7	901.8	735.1
13.7	966.5					

Drill hole No. 17

Depth (ft)	7/20/65 (11.08)	Depth (ft)	7/21/65 (11.13)	Depth (ft)	8/25/65 (12.60)	Depth (ft)	10/25/65 (14.82)
	Pt-$PtRh_{10}$						
4.8	546.0	0.5	90.3	1.0	159.5	2.0	203.3
6.0	637.1	1.5	160.8	2.0	259.8	3.15	310.8
7.0	714.3	2.5	287.1	3.0	351.0	4.0	389.1
8.0	783.0	3.5	408.4	4.0	447.8	5.15	480.4
9.0	842.1	4.5	514.3	5.0	524.3	6.0	541.3
10.0	897.3	5.5	599.8	6.0	588.0	7.15	621.6
11.0	949.1	6.5	675.3	7.0	646.7	8.0	656.4
12.0	995.2	7.5	743.8	8.15	722.8	9.15	716.3
13.0	1,032.4	8.5	806.4	9.15	776.5	10.0	752.3
14.0	1,064.3	9.5	856.9	10.15	822.5	11.15	807.8
14.6	1,076.2	10.5	911.0	11.15	868.5		
		11.5	961.3				
		12.5	1,006.0				
		13.5	1,043.0				
		14.5	1,064.0				

Drill hole No. 20

Depth (ft)	8/17/65 (12.28)	Depth (ft)	9/27/65 (13.85)	Depth (ft)	11/4/65 (15.16)	Depth (ft)	12/13/65 (16.38)	Depth (ft)	2/3/66 (17.91)	Depth (ft)	2/25/66 (18.51)	Depth (ft)	4/11/66 (19.70)	Depth (ft)	6/2/66 (20.97)
1.0	152.3	2.0	240.	1.0	116.3	1.0	94.5	1.0	92.4	5.0	282.0	4.85	284.5	4.8	274.0
2.0	252.8	4.0	413.3	2.0	237.0	2.0	98.7	2.0	110.0	5.95	340.5	5.85	340.3	5.8	327.5
3.0	342.3	6.0	563.6	3.0	295.1	3.0	101.0	3.0	188.3	7.0	408.5	6.85	392.5	6.8	378.0
4.0	424.0	8.0	684.8	4.0	399.3	4.0	245.0	4.0	254.8	7.95	462.7	7.85	446.4	7.8	428.0
5.0	504.5	10.0	792.3	5.0	454.3	5.0	292.0	5.0	315.1	9.0	526.2	8.85	497.0	8.8	478.0
6.0	586.4	12.0	886.7	6.0	535.8	6.0	403.3	6.0	381.1	9.95	575.2	9.85	548.2	9.8	524.5
7.0	654.5	14.5	980.4	7.0	586.0	7.0	459.0	7.0	429.8	11.0	619.5	10.85	590.0	10.8	570.5
8.0	714.4			8.0	653.8	8.0	532.5	8.0	489.8	13.95	758.0	11.85	638.0	11.8	614.5
9.0	770.0			9.0	698.7	9.0	599.6	9.0	536.8			12.85	677.3	12.8	655.0
10.0	826.0			10.5	768.8	10.0	653.0	10.0	592.0			13.85	719.3	13.8	693.0
10.5	849.3			11.0	797.1	11.5	703.0	11.0	635.4						

TABLE 26.—*Temperature profiles (°C) measured in drill holes 2–24, 68–1*—Continued

Drill hole No. 20—Continued

Depth (ft)	8/17/65 (12.28)	Depth (ft)	9/27/65 (13.85)	Depth (ft)	11/4/65 (15.16)	Depth (ft)	12/13/65 (16.38)	Depth (ft)	2/3/66 (17.91)	Depth (ft)	2/25/66 (18.51)	Depth (ft)	4/11/66 (19.70)	Depth (ft)	6/2/66 (20.97)
11.5	904.0			12.5	858.0	12.1	768.0	12.0	692.0						
12.5	948.0			13.0	886.0	13.5	814.0	13.0	719.5						
13.5	983.5			14.5	937.5	14.1	861.3	14.0	777.0						
14.5	1,022.0														

Drill hole No. 21

Depth (ft)	10/25/65 (14.82)	Depth (ft)	11/27/65 (15.90)	Depth (ft)	12/20/65 (16.61)	Depth (ft)	2/1/66 (17.85)	Depth (ft)	2/25/66 (18.51)	Depth (ft)	3/28/66 (19.34)	Depth (ft)	4/11/66 (19.70)	Depth (ft)	7/8/66 (21.81)	Depth (ft)	8/15/66 (22.67)	Depth (ft)	9/13/66 (23.28)	Depth (ft)	10/13/66 (23.93)
1.0	97.0	1.85	99.6	1.0	98.0	1.0	91.5	6.65	353.8	7.8	427.0	6.6	375.8	10.8	556.0	8.6	412.0	10.65	520.0	10.5	498.0
2.0	165.3	2.85	101.0	2.0	98.0	2.0	98.7	7.65	420.3	9.8	538.5	7.6	430.8	12.8	640.4	9 6	460.0	12.65	607.0	12.5	588.0
3.0	275.8	3.85	166.3	3.0	98.0	3.0	114.8	8.65	489.3	11.8	641.0	8.6	484.9	14.8	715.3	10.6	532.5	14.65	682.0	14.5	661.0
4.0	373.3	4.85	288.5	4.0	104.0	4.0	200.8	9.65	547.8	13.8	727.0	9.6	536.0	16.8	784.5	11.6	573.0	16.65	745.5	16.5	726.0
5.0	459.8	5.85	375.3	5.0	255.0	5.0	274.0	10.65	605.7	15.8	805.0	10.6	586.4	18.8	848.0	12.6	620.0	18.65	812.0	18.5	789.0
6.0	527.1	6.85	469.3	6.0	349.5	6.0	354.2	11.65	659.0			11.6	634.5			13.6	653.0				
7.0	597.3	7.85	548.7	6.85	433.1	7.0	408.3	12.65	706.5			12.6	675.1			14.6	695.0				
8.0	650.0	8.85	618.5	7.0	432.0	7.8	455.6	13.65	751.8			13.6	718.3			15.6	724.0				
9.0	711.8	9.85	684.7	7.85	509.3	8.0	476.9	14.65	796.0			14.6	756.0			16.6	763.0				
10.0	758.3	10.85	743.8	8.0	509.5	9.0	524.5	15.65	834.0			15.6	794.8			17.6	790.0				
11.0	814.8	11.85	799.8	8.85	583.8	9.8	573.0									18.6	826.0				
12.0	856.0	12.85	844.5	9.0	573.0	10.0	588.7														
13.0	901.3	13.85	888.5	9.85	641.3	11.0	635.0														
14.0	936.3	14.85	929.8	10.0	637.4	11.8	680.0														
15.0	975.8	15.85	964.0	10.85	701.0	13.0	731.0														
16.0	1,000.3			11.85	754.0	13.8	771.1														
				12.85	803.0	15.0	816.0														
				13.85	846.1	15.8	849.3														
				14.85	890.5																
				15.85	922.8																

Drill hole No. 22

Depth (ft)	12/13/65 (16.38)	1/5/66 (17.08)	2/1/66 (17.85)	2/25/66 (18.51)	Depth (ft)	4/11/66 (19.70)	6/1/66 (20.95)	Depth (ft)	7/8/66 (21.81)
1.0	144.8	157.0	167.0						
2.0	173.0	145.0	172.0						
3.0	214.5	221.0	260.8						
4.0	301.3	295.4	308.0						
5.0	371.6	353.0	361.1						
6.0	439.0	415.5	414.0						
7.0	496.3	464.5	462.2	413.0	6.9	426.0	384.5	7.0	383.5
8.0	557.3	520.8	510.2	466.7	7.9	471.3	438.0	8.0	438.0
9.0	614.0	582.0	564.8	527.3	8.9	523.0	491.0	9.0	492.3
10.0	672.8	634 5	610.0	579.8	9.9	568.4	540.0	10.0	537.8
11.0	726.5	692.3	662.2	633.8	10.9	617.1	586.0	11.0	582.2
12.0	780.3	741.5	708.8	682.0	11.9	660.7	628.0	12.0	620.4
13.0	822.8	788.0	758.7	725.1	12.9	700.3	670.0	13.0	658.8
14.0	868.8	829.8	798.0	771.3	13.9	740.4	708.0	14.0	694.2
15.0	907.0	873.0	840.2	809.0	14.9	777.8	746.0	15.0	730.4
16.0	945.3	906.5	872.5	847.0	15.9	813.0	781.0	16.0	763.0

Drill hole No. 23

Depth (ft)	1/5/66 (17.08)	Depth (ft)	1/19/66 (17.48)	Depth (ft)	2/9/66 (18.08)	Depth (ft)	2/11/66 (18.13)	Depth (ft)	2/14/66 (18.21)	Depth (ft)	2/18/66 (18.32)	Depth (ft)	2/18/66 (18.32)	Depth (ft)	2/18/66 (18.32)	Depth (ft)	2/23/66 (18.46)	Depth (ft)	2/23/66 (18.46)
	Pt-PtRh10				Pt-PtRh10						Pt-PtRh10		Pt-PtRh10		Cr-Al		Pt-PtRh10		Pt-PtRh10
2.05	135.7	10.4	624.0	36.7	1,149.8	24.65	1,099	24.65	1,099	20.65	1,000	31.65	1,109	11.5	642.3	20.65	982	32.65	1,110
10.0	604.1	12.4	729.5			25.65	1,106	25.65	1,106	21.65	1,025	30.65	1,104	10.6	597.3	21.65	1,016	31.65	1,111
12.0	720.3	13.4	770.2			26.65	1,111	26.65	1,111	22.65	1,047	29.65	1,102			22.65	1,038		Cr-Al
14.0	817.4	14.4	825.5			27.65	1,118	27.65	1,118	23.65	1,064	28.65	1,098			23.65	1,058	19.5	970.2
15.0	861.2	15.4	859.8			28.65	1,119	28.65	1,119	24.65	1,075	27.65	1,092			24.65	1,071	18.5	937.3
16.0	903.5	16.4	903.5			29.65	1,120	29.65	1,120	25.65	1,083	26.65	1,086			25.65	1,079	17.5	901
16.5	923.4	17.4	932.8					20.6	1,004	26.65	1,089	25.65	1,079			26.65	1,085	16.5	865
17.0	941.7	18.4	973.3					21.6	1,037	27.65	1,094	24.65	1,071			27.65	1,092	15.5	825.8
17.5	959.8	19.4	998.3					22.6	1,056	28.65	1,101	23.65	1,062			28.65	1,101	14.5	786
18.0	978.3							23.6	1,075	29.65	1,109	22.65	1,043			29.65	1,108	13.5	737.3
18.5	996.4									30.65	1,110	21.65	1,022			30.65	1,112	12.5	693
19.0	1,011.0							24.6	1,081,	31.65	1,108?	20.65	996			31.65	1,115	11.5	637.3
19.4	1,017.0							26.6	1,086	33.65	1,113	19.65	963			32.65	1,118	10.5	585.7
								29.6	1,098	34.65	1,117	18.65	932			33.65	1,121		
								32.6	1,109	35.65	1,117		Cr-Al			34.65	1,124		
								35.6	1,112–	37.65	1,122–	19.5	976.7			35.65	1,125		
								38.2	1,118		1,126	18.6	947.5			36.65	1,126		
								34.6	1124	37.65	1,129	17.5	904.3			37.65	1,130		
								28.6	1,127	38.0	1,130	16.6	871.8			38.3	1,130		
								27.6	1,122	36.65	1,125	15.5	828.7			37.65	1,128		
								25.6	1,106	35.65	1,122	14.6	792.8			36.65	1,128		
									1,100	34.65	1,120	13.5	704.4			35.65	1,122		
									1,087	33.65	1,115	12.6	701.0			34.65	1,119		
										32.65	1,115					33.65	1,114		

TABLE 26.—*Temperature profiles (°C) measured in drill holes 2–24, 68–1*—Continued

Drill hole No. 23—Continued

Depth (ft)	2/28/66 (18.59)	Depth (ft)	3/1/66 (18.62)	Depth (ft)	3/3/66 (18.67)	Depth (ft)	3/8/66 (18.81)	Depth (ft)	3/8/66 (18.81)	Depth (ft)	3/15/66 (18.99)	Depth (ft)	3/22/66 (19.18)	Depth (ft)	3/22/66 (19.18)	Depth (ft)	3/28/66 (19.34)
	Pt-PtRh$_{10}$		Pt-PtRh$_{10}$		Pt-PtRh$_{10}$		Pt-PtRh$_{10}$		Cr-Al		Cr-Al						
21.65	1,004	19.65	938	20.65	967	21.65	988	19.0	945.3		890↑	30.0	1,087	35.65	1,123		1,036↑
22.65	1,034	20.65	972	21.65	997		1,016↑	18.0	909.8	17.65	890	29.0	1,083	37.65	1,128	23.6	1,028
23.65	1,057	21.65	999	22.65	1,020	22.65	1,016	17.0	876.5	18.65	929	28.0	1,079	37.75	1,127		1,056↑
24.65	1,074	22.65	1,022	23.65	1,040	23.65	1,036	16.0	838.5	19.65	959↑	27.0	1,076	36.65	1,125	24.6	1,050
25.65	1,082	23.65	1,040	24.65	[1]1,055↑		1,050↑	15.0	800.8		962	26.0	1,062	34.65	1,120	25.6	1,062
28.65	1,099	24.65	1,054		1,055	24.65	1,049	14.0	758.2	20.65	998	25.0	1,053	30.65	1,110		1,098.5↑
		25.65	1,060	25.65	1,064	25.65	1,060	13.0	709.8	21.65	1,018↑	24.0	1,043	28.65	1,098	26.6	1,073
		26.65	1,065	26.65	1,075↑		1,071↑	12.0	662.5		1,022	23.0	1,025	26.65	1,081	27.6	1,082
		27.65	1,075		1,074	26.65	1,068	11.0	609.1	22.65	1,046	22.0	1,010	24.65	1,047		1,095.5↑
		28.65	1,084	27.65	1,085	27.65	1,079	10.0	556.7	23.65	1,061↑	21.0	986	24.15	1,049	28.6	1,091
		29.65	1,090	28.65	1,092↑		1,088↑				1,068	20.0	960	24.35	1,051	29.6	1,098
		30.65	1,094		1,092	28.65	1,086			24.65	1,084	19.0	930	24.55	1,054		1,112↑
		31.65	1,099	29.65	1,099	29.65	1,093			26.65	1,102	18.0	903	24.75	1,058	31.6	1,109.4
		32.65	1,099	30.65	1,102↑		1,101↑			28.65	1,115	17.0	867	24.95	1,062		1,118↑
		33.65	1,102		1,103	30.65	1,101			30.65	1,124	16.0	829	25.15	1,064	33.6	1,114.5
		34.65	1,101	31.65	1,108		1,106↑			32.65	1,127	15.0	788	25.35	1,066		1,122↑
		35.65	1,109	32.65	1,109↑	31.65	1,102			34.65	1,131	14.0	747	25.55	1,070	35.6	1,118.5
		36.65	1,118		1,110		1,117↑			36.65	1,137	13.0	700			37.4	1,126
				33.65	1,114	32.65	1,109			37.80	1,141	12.0	650			36.6	1,123.5
				34.65	1,118↑		1,114↑			35.65	1,135	11.0	599			34.6	1,120
					1,118	33.65	1,109			33.65	1,131	25.65	1,067			32.6	1,114
				35.65	1,119↑		1,118↑			31.65	1,124	27.65	1,088			30.6	1,107
					1,120	34.65	1,116			29.65	1,116	28.65	1,102			25.1	1,062
				36.65	1,122↑		1,120↑			27.65	1,104	31.65	1,111			24.1	1,047.5
					1,121	35.65	1,118			25.65	1,088	33.65	1,115			24.35	1,051.3
				37.65	1,124↑		1,121↑									22.6	1,012
					1,112	36.65	1,119									21.6	988
				37.9	1,123?	37.65	1,123									19.6	929.5
						37.95	1,124									18.6	896
						20.65	964										
						18.65	902										

Drill hole No. 23—Continued

Depth (ft)	4/19/66 (19.90)	Depth (ft)	4/19/66 (19.90)	Depth (ft)	4/25/66 (20.05)	Depth (ft)	5/6/66 (20.32)	Depth (ft)	3/28/65 (19.34)	Depth (ft)	4/4/66 (19.52)	Depth (ft)	4/4/66 (19.52)	Depth (ft)	4/11/66 (19.70)	Depth (ft)	4/11/66 (19.70)
19.6	921	33.2	1,129	19.95	910	19.65	906.8	17.6	861.5	15.65	796	37.55	1,139	31.65	1,124↑	14.9	777.8
20.6	955	34.2	1,134	20.65	942	20.65	937.8	15.6	784	17.65	871.8	18.65	907		1,119	13.9	740.4
21.6	985	35.2	1,136	21.65	972	21.65	968.3	19.4	943	19.65	940↑	16.65	837.8		1,132↑	12.9	700.3
22.6	1,011	36.6	1,139	22.65	1,000	22.65	996.5	18.4	909.5		940	14.65	762.8	33.65	1,129	11.9	660.7
23.6	1,037			23.65	1,025	23.65	1,022	17.4	876	21.65	1,003	12.65	677.8	34.65	1,141	10.9	617.1
24.6	1,056			24.65	1,045	24.65	1,043	16.4	840	22.65	1,024.3	10.65	581		1,148↑	9.9	568.4
25.6	1,071			25.65	1,059	25.65	1,058	15.4	805		1,049↑			35.65	1,140	8.9	546.4
26.6	1,081			26.65	1,074	26.65	1,075	14.4	764	23.65	1,049.5			19.65	932	7.9	471.3
27.6	1,094			27.65	1,085	27.65	1,085	13.4	719.5	24.15	1,062.3			20.65	963	6.9	426
28.6	1,105			28.65	1,097	28.65	1,095	12.4	675.5	24.65	1,069.5				993↑		
29.6	1,112			29.65	1,106	29.65	1,105	11.4	625	25.15	1,076.8			21.65	993		
30.6	1,119			30.65	1,113	30.65	1,115	10.4	576.5	25.65	1,081.5				1,020↑		
31.6	1,124			31.65	1,116	31.65	1,121			26.15	1,086.5			22.65	1,019		
32.6	1,129			32.65	1,125	32.65	1,124			26.65	1,091				1,143↑		
33.6	1,131			33.65	1,128	33.65	1,132			27.15	1,097.8↑			36.65	1,140		
34.6	1,134			34.65	1,132	34.65	1,131				1,096.3				1,138↑		
35.6	1,136			35.65	1,134	35.15	1,134			27.65	1,101			34.65	1,135		
35.6	1,137			36.3	1,136	36.15	1,135			28.65	1,110.5				1,138↑		
20.2	937									29.65	1,120.9			33.65	1,132		
22.2	997									30.65	1,128.9				1,132↑		
24.2	1,045										1,124.9↑			32.65	1,129		
26.2	1,070									31.65	1,135.5				1,123↑		
28.2	1,099									32.65	1,139.5			30.65	1,121		
30.2	1,115									33.65	1,140			29.65	1,114		
31.2	1,120									34.65	1,142.8			28.65	1,107		
32.2	1,126									35.65	1,133.1↑			27.65	1,097		
											1,143.3			26.65	1,088		
										36.65	1,140.3			25.65	1,075		
														24.65	1,062		
														23.65	1,043		
														15.9	813		

Drill hole No. 24

Depth (ft)	6/2/66 (20.97)	Depth (ft)	7/8/66 (21.81)	Depth (ft)	9/13/66 (23.30)	Depth (ft)	10/13/66 (23.93)	Depth (ft)	11/29/66 (24.89)	Depth (ft)	11/29/66 (24.89)	Depth (ft)	2/2/67 (26.17)	Depth (ft)	2/2/67 (26.17)	Depth (ft)	4/7/67 (27.36)	Depth (ft)	6/22/67 (28.72)
24.25	1,021	22.0	946	40.5	1,137	40.5	1,134+	30.2	1,056	12.0	527	26.0	937	23.0	851		Cr-Al	26.4	842
23.3	996	21.0	918	39.0	1,135−	39.0	1,133	29.0	1,036	11.0	473	25.0	910.5	22.0	822.5	26.0	892.5	25.5	816
22.25	972.5	20.0	890	38.0	1,131+	38.0	1,130+	28.0	1,016	10.0	416	24.0	884	21.0	793.5	24.0	832	24.4	776.5
21.3	943	19.0	858.5	37.0	1,131+	37.0	1,129	27.0	993.5	9.0	346	23.0	837	20.0	762.5	22.0	775	23.5	749
20.25	916.5	18.0	828	35.0	1,126−	36.0	1,121?	26.0	971	8.0	265	22.0	829.5			20.0	707	22.4	709
19.3	882.5	17.0	794	34.5	1,123.5	35.0	1,129	25.0	949	7.0	98	21.0	798.5			18.0	625	21.5	681
18.25	844−	16.0	761.5	33.0	1,117	34.5	1,119.5	24.2	931			20.0	768			16.0	546.5	20.4	637.5
17.3	807.5	15.0	725.5	32.0	1,109+	33.0	1,110+	23.0	902			19.0	733			14.0	460	19.5	607
16.25	765	14.0	687.5	31.0	1,101	32.0	1,101	22.0	875.5			18.0	695			12.0	344	18.5	560
15.3	724.5	13.0	648.5	30.0	1,086+	31.0	1,090−	21.0	846			17.0	656			10.0	100+	17.5	517
14.3	683.5	12.0	605	29.0	1,075+	30.0	1,077	20.0	817			16.0	613.5					16.5	476

[1]Where two temperatures are given opposite one depth, the one without an arrow is taken moving downward in the hole and the one with the arrow (↑) is taken moving up the hole.

TABLE 26.—*Temperature profiles (°C) measured in drill holes 2–24, 68–1*—Continued

Drill hole No. 24—Continued

Depth (ft)	6/2/66 (20.97)	Depth (ft)	7/8/66 (21.81)	Depth (ft)	9/13/66 (23.30)	Depth (ft)	10/13/66 (23.93)	Depth (ft)	11/29/66 (24.89)	Depth (ft)	11/29/66 (24.89)	Depth (ft)	2/2/67 (26.17)	Depth (ft)	2/2/67 (26.17)	Depth (ft)	4/7/67 (27.36)	Depth (ft)	6/22/67 (28.72)
13.3	640.5	11.0	563.6	28.0	1,054	29.0	1,057	19.0	786.5			15.0	570.5				Pt-PtRh$_{10}$	15.5	431
12.3	596	10.0	520	26.0	1,013	28.0	1,037	26 12	974			14.0	532					15.0	405
11.3	554	9.0	474.5	24.0	970+	26.0	996	25.0	950			13.0	482			30.0	980	14.5	389
10.3	509	8.0	428	22.0	917+	24.0	949	24.0	925.5			12.0	437			29.25	970	14.0	355
9.3	465+	7.0	378.5	20 0	858.5	22.0	900	23.0	900			11.0	380			28.5	950	13.5	341
8.3	418.5	6.0	328	18 0	793	20.0	845	22.0	872			10.0	327			27.5	917.5	13.0	314
7.3	374	5.0	271.5	16.0	727	18.0	784+	21.0	845.5			9.0	265			26.5	902.5	12.5	297
6.3	327−	4.0	216.5	12.0	583	16.0	719	20.0	816			8.0	205			25.5	870	12.0	260
5.3	277	3.0	156.5	10.0	496			19.0	788			7.0	97			24.5	840.5	11.5	245
								18.0	755			30.0	1,019					11.0	212
								17.0	722.5			29.0	998					10.0	158
								16.0	685			28.0	974.5					9.0	106
								15.0	650			27.0	953					8.0	100+
								14.0	612			26.0	931						
								13.0	565			24.0	880						

Drill hole No. 68–1

Depth (ft)	12/11/68 (36.90)	Depth (ft)	1/22/69 (37.47)	Depth (ft)	1/22/69 (37.47)
53.6	1,085	53.4	1,079	27.4	305
53.3	1,080	52.4	1,067	26.4	266
53.0	1,073	51.4	1,053	25.4	231
52.0	1,067	50.4	1,035	24.4	199
51.0	1,057	49.4	1,015	23.4	165
50.0	1,042	48.4	991	22.4	134
47.0	961	47.4	963	21.4	107.5
45.0	900	46.4	935	20.4	100
43.0	829	45.4	908	19.4	96
41.3	764	44.4	879		
41.0	749.5	43.4	854		
40.0	720.0	42.4	826		
39.0	684.5	41.4	798		
38 0	653	40.4	765		
35.0	550.5	39.4	734		
33.0	490.5	38.4	705		
31.0	433	37.4	667		
29.3	370	36.4	635		
29.0	352	35.4	600		
28.0	328	34.4	567		
27.0	287.5	33.4	532		
26.0	262	32 4	494		
23.0	172	31.4	460		
21.0	108	30.4	423		
19.0	100+	29.4	382		
		28.4	342		

TABLE 27.—*Oxygen fugacity profiles, Makaopuhi lava lake*

[Measurements were made in drill holes using a solid Ni-NiO reference except for the last three profiles which were made using an O_2 gas reference. Figure 9B shows the solid-reference oxygen probe in use. Additional information is given in the text and by Sato and Wright (1966) and Sato and Moore (1973). N.E. = not equilibrated, as evidenced by fluctuating emf at the indicated depth.]

Date	Drill hole No.	Depth (ft)	Temperature (°C)	emf (volts)	log fO_2 (atm)
6/23/65	11	12.85	1,002	+0.023	−10.6
		11.85	955	+.018	−11.2
		9.85	840	−.0064	−12.9
		8.85	776	−.0430	−13.6
		7.85	701	−.658	− 2.6
		6.85	630	−.578	− 5.3
		5.85	555	N.E.	----
6/28/65	6	8.9	884	−.0007	−12.2
		7.9	829	−.017	−13.0
		6.9	769	−.033	−13.9
		5.9	700	−.052	−15.2
		4.9	626	−.068	−16.8
		3.9	548	−.090	−18.8
6/30/65	9	10.2	945	+.0120	−11.3
		9.2	895	+.0077	−12.1
		8.2	845	+.0013	−13.0
		7.2	776	−.0099	−14.2
		6.2	707	−.0175	−15.7
		5.2	635	−.0270	−17.5
		4.2	555	−.035	−19.9
		3.2	495	N.E.	----
		10.2	950	+.0135	−11.2
	11	12.85	989	+.0220	−10.7
		10.85	890	+.0091	−12.2
		9.0	775	−.036	−13.7
		8.0	710	−.520	− 5.3
		8.2	727	−.520	− 5.1
		8.4	740	−.500	− 5.3
		8.6	754	−.160	−11.8
		8.8	765	−.067	−13.4
		8.5	747	−.29	− 9.4
		6.0	575	−.580	− 6.2
		5.0	505	−.098	−20.1
7/3/65	8	9.7	937	+.0285	−11.7
		8.0	848	+.0210	−13.3
	10	10.4	963	+.005	−10.9
		9.0	895	+.0015	−12.0
		8.0	835	−.0033	−13.1
		7.0	767	−.0063	−14.5
		6.0	695	−.0177	−16.0
		5.0	612	−.0365	−18.0
		4.0	538	−.0455	−20.2
		10.0	945	+.0025	−11.1
	14	11.0	990	−.0029	−10.3
		10.0	940	−.0109	−11.0
		9.0	880	−.0144	−12.0
		8.0	825	−.0207	−13.0
		7.0	760	N.E.	----
		6.0	685	−.065	−15.3
7/16/65 (1 day after drilling)	16	12.85	1,030	−.011 (approx.)	− 9.6
7/22/65 (6 days after drilling)	17	14.5	1,068	−.0239	− 8.9
		14.0	1,052	−.0305	− 9.0
		13.0	1,024	−.036	− 9.3
		12.0	988	−.042	− 9.7
		10.0	883	−.0538	−11.3
		8.0	784	−.0620	−13.0
	11	12.9	909	+.017	−12.0
8/13/65		12.0	867	+.0128	−12.7
		11.0	819	+.0025	−13.5
		10.0	767	−.0030	−14.6
		9.0	713	−.152	−12.8
		9.2	725	−.068	−14.2
		9.3	731	−.0115	−15.2
		9.4	737	+.0172	−15.7
		9.6	749	+.0002	−15.0
		9.8	757	+.0017	−14.9
		10.0	767	+.0022	−14.7
		9.0	713	−.150	−12.9
	11	8.0	654	−.064	−16.1
		6.0	525	−.0012	−21.9
	10	10.3	866	+.040	−13.2
8/17/65		9.0	805	+.018	−14.1
		7.0	693	+.0018	−16.5
		6.0	638	−.0014	−18.0
		5.0	570	N.E.	----
	8	9.6	824	+.010	−13.5
		8.0	745	+.0033	−15.2
		7.0	690	−.0078	−16.4
		6.0	635	−.0217	−17.6
		5.0	572	−.035	−19.3
	20	14.5	1,020	+.065	−10.9
		13.0	967	+.0615	−11.7
		11.0	882	+.0405	−12.9
		9.0	770	+.0154	−15.0
		7.0	655	−.0105	−17.3
		6.0	585	−.0405	−18.7
		9.0	770	+.0226	−15.0
8/17/65	16	13.7	965	+.065	−11.8
		12.0	905	+.0465	−12.6
		10.0	813	+.0250	−14.1
		8.0	705	+.0086	−16.3
	16	6.0	590	−.0224	−19.0
		10.0	813	+.0074	−13.7
		13.7	965	+.068	−11.9
		12.0	905	+.017	−12.1
		8.9	771	−.013	−14.3
		7.0	668	−.269	−11.4
		8.0	722	−.167	−12.3
		8.3	740	−.035	−14.6
8/25/65–Con.		8.6	759	−.0246	−14.3
		7.2	680	−.252	−11.5
		7.4	690	−.284	−10.6
		7.6	700	−.305	− 9.9
		7.8	710	−.320	− 9.4
		8.8	767	−.044	−13.8
9/23/65	6	8.9	737	−.415	− 7.0
		8.0	689	−.420	− 7.8
		7.0	633	−.460	− 7.91
		6.0	570	−.355	−11.7
		5.0	503	−.330	−14.2
		4.0	435	−.166	−21.1
	9	10.2	810	−.0145	−13.4
		9.0	750	−.620	− 2.8
		8.0	700	−.685	− 2.1
		7.0	648	−.725	− 1.8
		6.0	581	−.755	− 2.0
		5.0	510	−.750	− 3.2
		4.0	430	−.570	− 9.8
	10	10.0	800	+.014	−14.1
		9.0	750	−.006	−14.9
		8.0	700	−.470	− 6.5
		7.0	648	−.540	− 5.9
		6.0	581	−.310	−12.5
		5.0	510	−.100	−19.9
		10.0	800	+.024	−14.3
9/27/65	11	12.9	850	+.0350	−13.5
		11.0	765	+.0135	−14.9
		10.0	720	−.001	−15.7
		9.0	665	−.310	−10.6
		8.0	610	−.410	− 9.5
		7.0	550	−.0800	−19.0
		6.0	490	N.E.	----
		12.0	810	+.02	−14.0
	8	9.7	785	+.0850	−15.8
		8.0	690	−.0130	−16.3
		6.0	565	−.0225	−19.8
		7.0	630	−.225	−13.2
		9.0	750	+.004	−15.1
10/25/65	20	6.0	530	−.01	−21.4
		8.0	655	−.068	−16.0
		10.0	760	−.044	−13.9
		14.5	955	+.003	−11.0
		13.0	890	+.001	−12.1
	16	6.0	535	−.022	−20.9
		8.0	650	−.0097	−17.4
		10.0	750	−.0025	−15.0
		12.0	840	+.005	−13.1
		13.7	902	+.0105	−12.0
		11.0	795	+.0044	−14.1
		9.0	710	−.0045	−15.9
		7.0	595	−.0166	−19.0
10/27/65	8	6.0	540	−.0440	−20.2
		8.0	650	−.0470	−16.6
		9.5	735	−.0775	−13.8
		9.0	710	−.0460	−15.1
		7.0	600	−.0415	−18.2
		8.0	650	−.0425	−16.7
	9	6.0	540	−.035	−20.4
		8.0	650	−.032	−17.0
		10.0	760	+.004	−14.9
11/4/65	10	7.0	605	−.0540	−17.8
		9.0	709	−.16	−12.7
		10.0	741	−.31	− 9.1
		8.0	659	−.013	−17.1
		6.0	550	−.021	−20.4
	11 (all temperatures extrapolated)	8.0	450	−.245	−18.3
		10.0	580	−.041	−18.9
		12.0	720	−.026	−15.2
		12.8	790	−.014	−13.8
		11.0	650	−.020	−17.2
	20	7.0	586	+.005	−19.8
		9.0	699	+.027	−16.8
		11.0	797	+.065	−15.2
		13.0	886	+.032	−12.7
		14.5	938	+.041	−11.9
		12.0	838	+.037	−13.8
		10.0	735	N.E.	----
		8.0	654	N.E.	----
		9.0	699	N.E.	----
11/27/65	6	7.0	485	+.008	−23.7
		8.7	605	−.028	−18.4
		8.0	560	−.026	−19.9
		6.0		N.E.	
	8	7.0	485	−.032	−22.7
		9.0	630	−.0225	−17.7
		8.0	560	−.017	−20.2
		6.0		N.E.	
	16	7.0	485	−.02	−23.0
		9.0	630	0	−18.2
		11.0	750	+.006	−15.1
		13.5	875	+.001	−12.4
12/20/65	20	8.0	510	−.020	−22.0
		10.0	637	−.005	−17.9
		12.0	761	+.001	−14.8
		13.9	846	+.003	−13.0
		13.0	809	−.0015	−13.7
		11.0	709	−.0025	−16.0
1/5/66	20	8.0	~560	−.003	−20.5
		10.0	604	+.0225	−19.6
		12.0	720	+.0140	−16.0
		14.0	817	+.0091	−13.7
		13.0	770	+.0039	−14.6
		12.0	720	−.0032	−15.7
		10.0		N.E.	
	21	8.0	~560	−.006	−20.4

Table 27.—*Oxygen fugacity profiles, Makaopuhi lava lake*—Continued

Date	Drill hole No.	Depth (ft)	Temperature (°C)	emf (volts)	log fO_2 (atm)
		10.0	604	−.005	−19.0
		12.0	720	−.025	−15.2
		14.0	817	+.022	−13.9
		16.0	904	+.031	−12.4
		13.0	770	+.0226	−15.0
2/21/66	20	10.0	585	−.100	−17.3
		12.0	677	−.060	−15.6
6/10/66	20	10.0	530	−.670	− 4.9
		11.0	575	−.600	− 5.8
		12.0	620	−.425	− 9.0
		13.85	690	−.159	−13.2
		13.0	660	−.121	−14.7
12/1/66	21	17.0	720	+.685	−13.94
		18.35	765	+.695	−13.55
		16.0	685	+.170	− 3.62
		15.0	650	+.115	− 2.56
		14.0	610	+.114	− 2.60
		13.0	565	+.100	−2.45
		12.0	525	+.100	− 2.57
		11.0	470	+.265	− 7.25
		10.0	416	+.410	−12.05
		9.0	340	+.505	N E.
		8.0	100	+ 460	N.E.
		9.5	385	+.490	−15.05
2/2/67	24	18.0	695	N.E.	
		16.0	613	+.277	− 6.31
		14.0	532	+.390	− 9.77
		12.0	437	+.525	−14.92
		13.0	482	+.460	−12.29
		15.0	570	+.380	− 9.09
		17.0	656	+.230	− 4.99
		18.0	695	+.150	− 3.12
		14.0	532	+.385	− 9.65

Table 28.—*Altitudes obtained by leveling the surface of Makaopuhi lava lake*

[Level stations are shown in figure 6; The level and rods in use are shown in figure 9. Dates of leveling are given with the square root of time in days corresponding to the time elapsed since March 24, 1965, when the level net was first installed and leveled. Columns labeled altitude (feet) give the elevation of each station relative to a point on the drainback (station 44) whose altitude is set arbirarily at 2,265.00 feet. Δ (feet) is the difference in altitude found in successive leveling runs]

Date / $\sqrt{t}$ / Station	3/24/65 "0" Altitude (ft)	Δ (ft)	4/8/65 3.87 Altitude (ft)	Δ (ft)	4/22/65 5.39 Altitude (ft)	Δ (ft)
45						
44	2,265.000		2,265.0		2,265.0	
1	2,209.692	+0.790	10.482	−0.011	10.471	+0.009
2	2,208.719	−4.908	03.811	−0.033	03.778	−0.028
3	2,207.503	−4.362	3.141	−0.612	2.529	−0.207
4	6.229	−1.381	4.848	−0.708	4.140	−0.623
5	7.669	−4.183	3.486	−0.054	3.432	−0.018
28	8.308	−4.061	4.061	−0.003	4.058	+0.010
29	6.939	−4.145	2.794	−0.093	2.701	+0.042
30	6.002	−4.230	2.772	−0.012	2.760	+0.044
31	9.099	−4.601	4.498	−0.010	4.488	+0.026
7	8.053	−4.247	3.806	−0.005	3.801	+0.043
8	9.529	−3.720	5.809	−0.367	5.442	−0.189
9	6.634	−1.724	4.910	−0.348	4.562	−0.044
10	6.771	−3.612	3.159	−0.507	2.652	−0.097
11	4.974	−1.445	3.529	−0.715	2.814	−0.434
12	2,210.539	−2.387	8.152	−0.689	7.463	−0.825
52						
13	06.727	−4.031	2.696	−0.112	2.584	+0.025
41	9.596	−3.427	6.169	−0.866	5.303	−0.800
42	2,210.194	−2.736	7.458	−0.744	6.714	−0.721
14	08.193	−4.550	3.643	−0.021	3.622	−0.001
15	7.877	−4.494	3.383	−0.131	3.252	−0.086
16	6.014	−1.283	4.731	−0.565	4.166	−0.547
17	7.008	−3.017	3.991	−0.551	3.440	−0.354
18	7.652	−3.946	3.706	+0.023	3.729	−0.004
19	8.564	−2.425	6.139	−0.155	5.984	−0.021
20	7.881	−4.140	3.741	+0.046	3.787	−0.036
21	6.950	−4.352	2.598	−0.028	2.570	−0.050
46						
47						
48						
22	8.051	−4.199	3.852	−0.373	3.479	−0.264
49						
50						
51						
23	8.807	−4.153	4.654	−0.266	4.388	−0.180
24	8.288	−4.809	3.479	−0.012	3.467	−0.113

Table 28.—*Altitudes obtained by leveling the surface of Makaopuhi lava lake*—Continued

Date / $\sqrt{t}$ / Station	3/24/65 "0" Altitude (ft)	Δ (ft)	4/8/65 3.87 Altitude (ft)	Δ (ft)	4/22/65 5.39 Altitude (ft)	Δ (ft)
25	8.948	−3.484	5.464	−0.255	5.209	−0.030
26	6.329	−0.917	5.412	−0.004	5.408	−0.024
53						
54						
55						
56						
57						
58						
59						
60						
61						
62						
63						
64						
65						
32	2,212.083	−3.543	8.540	−0.551	7.989	−0.369
33	12.415	−2.738	9.677	−0.594	9.083	−0.453
34	12.631	−3.853	8.778	−0.506	8.272	−0.311
35	05.086	−1.854	3.232	−0.646	2.586	−0.504
36	7.296	−3.054	4.242	−0.656	3.586	−0.338
37	8.475	−3.622	4.853	−0.817	4.036	−0.346
38	2.875	−2.463	0.412	−0.621	2,199.791	−0.443
39	8.365	−1.471	6.894	−0.676	2,206.218	−0.572
40	9.063	−2.123	6.940	−0.565	6.375	−0.512

Date / $\sqrt{t}$ / Station	5/19/65 7.48 Altitude (ft)	Δ (ft)	6/23/65 9.54 Altitude (ft)	Δ (ft)	7/26/65 11.14 Altitude (ft)	Δ (ft)
45			2,217.233		2,217.233	
44	2,265.0					
1	10.479	−0.008	10.471	−0.001	10.470	−0.001
2	03.750	+0.014	3.764	+0.003	3.767	−0.030
3	2.322	−0.130	2.192	−0.031	2.161	−0.081
4	3.517	−0.446	3.071	−0.098	2.973	−0.147
5	3.414	−0.081	3.333	−0.030	3.303	−0.106
28	4.068					
29	2.743					
30	2.804					
31	4.518					
7	3.839	−0.032	3.807	−0.052	3.755	−0.129
8	5.253	−0.114	5.139	−0.045	5.094	−0.096
9	4.518	−0.136	4.382	−0.029	4.353	−0.086
10	2.555	−0.050	2.505	−0.049	2.456	−0.088
11	2.380	−0.206	2.174	−0.089	2.085	−0.103
12	6.638	−0.339	6.299	−0.122	6.177	−0.130
52					8.541	−0.048
13	2.609	−0.085	2.524	−0.042	2.482	−0.101
41	4.503	−0.541	3.962	−0.239	3.723	−0.204
42	5.993	−0.453	5.540	−0.199	5.341	−0.175
14	3.621	−0.053	3.568	−0.026	3.542	−0.076
15	3.166	−0.028	3.138	+0.017	3.155	−0.038
16	3.619	−0.207	3.412	−0.045	3.367	−0.067
17	3.086	−0.105	2.981	−0.036	2.945	−0.047
18	3.725	+0.008	3.733	−0.011	3.722	−0.022
19	5.963	+0.006	5.969	−0.008	5.961	−0.016
20	3.751	−0.021	3.730	−0.026	3.704	−0.108
21	2.520	−0.093	2.427	−0.066	2.351	−0.124
46					2.651	−0.138
47					0.818	−0.135
48					2.310	−0.131
22	3.215	−0.148	3.067	−0.081	2.986	−0.128
49					2.766	−0.119
50					2.504	−0.106
51					2.609	−0.102
23	4.208	−0.110	4.098	−0.055	4.043	−0.105
24	3.354	−0.028	3.326	−0.051	3.275	−0.098
25	5.179	−0.001	5.178	−0.008	5.170	−0.052
26	5.384	−0.030	5.354	−0.001	5.353	−0.046
53					5.972	−0.103
54					3.520	−0.097
55					2.749	−0.097
56					4.266	−0.085
57					4.503	−0.053
58					5.877	−0.014
59					4.722	−0.112
60					5.064	−0.082
61					4.155	−0.082
62					3.422	−0.090
63					2.972	−0.101
64					5.671	−0.043
65					9.757	−0.040
32	7.620	−0.284	7.366	−0.084	7.252	−0.136
33	8.630	−0.351	8.279	−0.122	8.157	−0.154
34	7.961	−0.268	7.693	−0.076	7.617	−0.123
35	2.082	−0.353	1.729			−0.167
36	3.248	−0.240	3.008			−0.112
37	3.690	−0.192	3.498			−0.111
38	2,199.348	−0.232	2,199.116			−0.159
39	2,205.646	−0.471	2,205.175			−0.368
40	5.863	−0.488	5.375			−0.438

Table 28.—*Altitudes obtained by leveling the surface of Makaopuhi lava lake*—Continued

Date \ √t Station	9/8/65 (12.96) Altitude (ft)	Δ (ft)	10/20/65 (14.49) Altitude (ft)	Δ (ft)	12/22/65 (16.52) Altitude (ft)	Δ (ft)
45	2,217.233	"0"	2,217.233	"0"	2,217.233	"0"
44						
1	2,210.469	+.001	10.470	+.006	10.476	assumed unchanged
2	03.737	−.034	3.703	−.060	3.643	−.029
3	02.080	−.076	2.004	−.082	1.922	−.162
4	02.826	−.084	2.742	−.088	2.654	−.044
5	03.197	−.079	3.118	−.093	3.025	−.001
28						
29						
30						
31						
7	03.626	−.102	3.524	−.151	3.373	−.190
8	04.998	−.075	4.923	−.118	4.805	−.334
9	04.267	−.054	4.213	−.140	4.073	−.063
10	02.368	−.092	2.276	−.151	2.125	+.017
11	01.982	−.100	1.882	−.151	1.731	−.007
12	06.047	−.101	5.946	−.110	5.836	+.002
52	08.493	−.036	8.457	−.031	8.426	+.017
13	02.381	−.065	2.316	−.075	2.241	−.020
41	03.519	−.098	3.421	−.106	3.315	−.049
42	05.166	−.073	5.093	−.097	4.996	−.069
14	03.466	−.046	3.420	−.068	3.352	−.084
15	03.117	−.018	3.099	−.037	3.062	+.037
16	03.300	−.021	3.279	−.065	3.214	+.076
17	02.898	−.024	2.874	−.053	2.821	−.019
18	03.700	−.031	3.669	−.073	3.596	−.163
19	05.945	−.006	5.939	−.029	5.910	−.111
20	03.596	−.085	3.511	−.098	3.413	−.018
21	02.227	−.092	2.135	−.081	2.054	−.009
46						
47	00.683	−.087	0.596	−.062	0.534	+.010
48						
22	02.858	−.085	2.773	−.063	2.710	+.006
49						
50	02.398	−.082	2.316	−.046	2.270	+.011
51						
23	03.938	−.093	3.845	−.091	3.754	−.012
24	03.177	−.099	3.078	−.128	2.950	+.022
25	05.118	−.041	5.077	−.034	5.043	+.069
26	05.307	−.041	5 266	−.014	5.252	+.096
53	05.869	−.080	5.789	−.142	5.647	−.156
54	03.423	−.065	3.358	−.122	3.236	−.249
55	02.652	−.065	2.587	−.130	2.457	−.382
56	04.181	−.076	4.105	−.159	3.946	−.208
57	04.450	−.034	4.416	−.107	4.309	−.148
58	05.863		Bust	−.016	5.847	−.102
59	04.610	−.075	4.535	−.093	4.442	−.129
60	04.982	−.066	4.916	−.048	4.868	−.169
61	04.073	−.086	3.987	−.068	3.919	−.216
62	03.352	−.097	3.255	−.070	3.185	−.214
63	02.871	−.128	2.743	−.080	2.663	−.101
64	05.628	−.070	5.558	+.004	5.562	+.088
65	09.717	−.049	9.668	+.022	9.690	
32	07.116	−.078	7.038	−.048	6.990	−.005
33	08.003	−.090	7.913	−.063	7.850	−.012
34	07.494	−.076	7.418	−.030	7.388	−.003
35	01.552			−.130	1.422	−.067
36	02.896			−.094	2.802	−.078
37	03.387			−.096	3.291	−.076
38	2,198.957			−.116	2,198.841	−.036
39	2,204.807			−.201	2,204.606	−.035
40	04.937			−.215	4.722	−.039
66			2,206.406	−.107	6.299	−.458
67			01.725	−.112	1.613	−.013
68			06.085	−.059	5.926	−.071
69			06.285	−.158	6.127	−.065
70					02.206	−.109
71					05.133	−.102
72					04.497	+.042
73					06.018	+.078

Date \ √t Station	3/7/66[1] (18.65) Altitude (ft)	Δ (ft)	5/18/66 (20.49) Altitude (ft)	Δ (ft)	8/9/66 (22.43) Altitude (ft)	Δ (ft)
45						
44						
1	2,210.476	"0"	2,210.476	"0"	2,210.476	"0"
2	3.599	−.045	3.554	−.039	3.515	−.039
3	1.769	reset	1.610	−.004	1.614	−.096
4	2.610	−.062	2.548	−.096	2.452	−.106
5	3.024	−.028	2.996	−.058	2.938	−.079
28						
29						
30						
31						
7	3.183	−.089	3.094	−.046	3.048	−.022
8	4.471	−.126	4.345	−.052	4.293	−.014
9	4.010	−.041	3.969	−.070	3.899	−.074
10	2.142	−.097	2.045	−.118	1.927	−.121
11	1.724	− 098	1.626	−.092	1.534	−.096

Table 28.—*Altitudes obtained by leveling the surface of Makaopuhi lava lake*—Continued

Date \ √t Station	3/7/66[1] (18.65) Altitude (ft)	Δ (ft)	5/18/66 (20.49) Altitude (ft)	Δ (ft)	8/9/66 (22.43) Altitude (ft)	Δ (ft)
12	5.838	−.043	5.795	−.030	5.765	−.044
52	8.443	−.010	8.433	0	8.433	−.015
13	2.221	−.048	2.173	−.063	2.110	−.078
41	3.266	−.074	3.192	−.078	3.114	−.087
42	4.927	−.082	4.845	−.086	4.759	−.083
14	3.268	−.098	3.170	−.096	3.074	−.092
15	3.099	−.049	3.050	−.079	2.971	−.105
16	3.290	+.022	3.312	−.057	3.255	−.123
17	2.802	+.004	2.806	−.052	2.754	−.095
18	3.433	−.045	3.388	−.041	3.347	−.052
19	5.799	−.002	5.797	−.025	5.772	−.011
20	3.395	−.064	3.331	−.073	3.258	−.101
21	2.045	−.063	1.982	−.091	1.891	−.105
46						
47	0.544	−.040	0.504	−.083	0.421	−.094
48						
22	2.716	−.032	2.684	−.066	2.618	−.093
49						
50	2.281	−.028	2.253	−.056	2.197	−.087
51						
23	3.742	−.041	3.701	−.053	3.648	−.088
24	2.972	−.043	2.929	−.031	2.898	−.050
25	5.112	−.027	5.085	−.008	5.077	−.033
26	5.348	−.008	5.340	−.002	5.338	−.012
53	5.491	−.073	5.418	−.072	5.346	−.030
54	2.987	−.119	2.868	−.077	2.791	−.015
55	2.075	−.187	1.888	−.128	1.760	−.050
56	3.738	−.113	3.625	−.095	3.530	−.081
57	4.161	−.046	4.115	−.053	4.062	−.055
58	5.745	−.001	5.744	−.014	5.730	−.030
59	4.313	−.062	4.251	−.056	4.195	−.043
60	4.699	−.095	4.604	−.067	4.537	−.047
61	3.703	−.127	3.576	−.073	3.503	−.058
62	2.971	−.123	2.848	−.069	2.779	−.052
63	2.562	−.095	2.467	−.059	2.408	−.064
64	5.650	−.023	5.627	0	5.627	−.034
65						
32	6.985	−.029	6.956	−.072	6.884	−.078
33	7.803	−.035	7.803	−.073	7.730	−.086
34	7.385	−.024	7.361	−.060	7.301	−.087
35	1.355	−.080	1.275	−.110	1.165	−.120
36	2.724	−.094	2.630	−.112	2.518	−.118
37	3.215	−.096	3.119	−.110	3.009	−.130
38	2,198.805	−.069	2,198.736	−.103	2,198.633	−.106
39	2,204.571	−.054	2,204.517	−.084	2,204.433	−.093
40	4.683	−.044	4.639	−.082	4.557	−.092
66	5.841	−.086	5.755	−.034	5.721	−.033
67	1.600	−.068	1.532	−.074	1.458	−.075
68	5.855	−.086	5.769	−.092	5.677	−.079
69	6.062	−.057	6.005	−.068	5.937	−.125
70	2.097	−.008	2.089	−.029	2.060	−.032
71	5.031	+.002	5.033	−.014	5.019	−.018
72	4.539	−.001	4.538	−.013	4.525	−.037
73	6.096	−.031	6.065	−.010	6.055	−.029

Date \ √t Station	10/31/66 (24.21) Altitude (ft)	Δ (ft)	1/31/67 (26.04) Altitude (ft)	Δ (ft)	5/31/67 (28.25) Altitude (ft)	Δ (ft)
45						
44						
1	2,210.476	0	2,210.476	"0"	2,210.476	"0"
2	3.476	−.018	03.458	−.027	03.458	−.027
3	1.518	−.032	01.486	−.031	01.455	+.019
4	2.346	−.031	02.315	− 025	02.290	+.036
28						
29						
30						
31						
5	2.859	−.043	02.816	−.057	02.759	+.021
7	3.026	−.023	03.003	−.025	02.978	+.045
8	4.279	−.015	04.264	−.017	04.287	+.068
9	3.825	−.071	03.754	−.046	03.708	+.047
10	1.806	−.084	01.722	−.080	01.642	−.005
11	1.438	−.073	01.365	−.060	01.305	+.002
12	5.721	−.042	05.679	−.033	05.646	−.003
52	8.418	−.025	08.393	−.011	08.382	+.025
13	2.032	−.030	02.002	−.050	01.952	+.019
41	3.027	−.033	02.994	−.020	02.974	+.051
42	4.676	−.035	04.641	−.033	04.608	+.054
14	2.982	−.033	02.949	−.057	02.892	+.018
15	2.866	−.064	02.802	−.065	02.737	0
16	3.132	−.077	03.055	−.073	02.982	−.012
17	2.659	−.064	02.595	−.086	02.509	−.033
18	3.295	−.035	03.260	−.055	03.205	−.016
19	5.761	−.011	05.750	−.020	05.730	+.016
20	3.157	−.033	03.124	−.052	03.072	+.014
21	1.786	−.034	01.752	−.034	01.718	−.002
46						
47	0.327	−.040	00.287	−.037	00.250	−.008
48						
22	2.525	−.041	02.484	−.044	02.440	−.019

TABLE 28.—*Altitudes obtained by leveling the surface of Makaopuhi lava lake*—Continued

Date $\sqrt{t}$ / Station	10/31/66 (24.21) Altitude (ft)	Δ (ft)	1/31/67 (26.04) Altitude (ft)	Δ (ft)	5/31/67 (28.25) Altitude (ft)	Δ (ft)
49						
50	2.110	−.044	02.066	−.053	02.013	−.031
23	3.560	−.043	03.517	−.058	03.459	−.040
24	2.848	−.024	02.824	−.033	02.791	−.017
25	5.044	+.003	05.047	0	05.407	+.013
26	5.326	+.015	05.341	+.007	05.348	+.025
53	5.316	−.053	05.263	−.028	05.235	+.035
54	2.776	−.048	02.728	−.033	02.695	+.016
55	1.710	−.028	01.682	−.034	01.648	+.021
56	3.449	−.052	03.397	−.064	03.333	−.011
57	4.007	−.033	03.974	−.056	03.918	−.014
58	5.700	−.011	05.689	−.025	05.664	+.007
59	4.152	−.023	04.129	−.014	04.115	+.062
60	4.490	−.028	04.462	−.029	04.433	+.045
61	3.445	−.028	03.417	−.044	03.373	+.009
62	2.727	−.035	02.692	−.047	02.645	−.008
63	2.344	−.045	02.299	−.043	02.256	−.017
64	5.593	−.012	05.581	+.001	05.582	+.023
65						
32	6.806	−.020	06.786	−.033	6.753	+.035
33	7.644	−.023	07.621	−.028	07.593	+.041
34	7.214	−.017	07.197	−.043	07.154	+.036
35	1.045	−.042	01.003	−.036	00.967	+.025
36	2.400	−.050	02.350	−.040	02.310	+.023
37	2.879	−.038	02.841	−.040	02.801	+.019
38	2,198.527	−.064	2,198.463	−.039	2,198.424	+.016
39	2,204.340	−.023	2,204.317	−.020	2,204.297	+.048
40	4.465	−.021	04.444	−.019	04.425	+.055
66	5.688					
67	1.383	−.059	01.324	−.043	01.281	+.020
68	5.598	−.074	05.524	−.059	05.465	+.010
69	5.812	−.004	05.808	−.065	05.743	+.002
70	2.028	−.020	02.008	−.032	01.976	+.003
71	5.001	−.005	04.996	−.027	04.969	+.005
72	4.488	−.012	04.476	−.012	04.464	+.008
73	6.026	−.006	06.020	−.007	06.013	+.015
74		−.032	02.496	−.023	02.473	+.045
75		−.023	03.541	−.016	03.525	+.050
76		−.039	04.496	−.027	04.469	+.029
77		−.048	02.138	−.060	02.078	−.009
78		−.040	03.067	−.059	03.008	−.008
79		+.002	03.977	−.017	03.960	+.010
80		−.044	01.906	−.046	01.860	−.002
81		−.041	02.738	−.047	02.691	−.017
82		−.027	02.501	−.029	02.472	−.013
83		−.008	04.008	−.014	03.994	+.005
84		−.062	04.158	−.067	04.091	−.022
85		−.065	05.729	−.067	05.662	−.027
86		−.042	05.516	−.058	05.458	−.024
87		−.020	03.351	−.032	03.319	−.005
88						
89		−.060	02.761	−.064	02.697	−.018
90		−.023	02.281	−.045	02.236	−.026

Date $\sqrt{t}$ / Station	10/2/67 (30.36) Altitude (ft)	Δ (ft)	1/29/68 (32.26) Altitude (ft)	Δ (ft)	7/10/68 (34.70) Altitude (ft)	Δ (ft)
45						
44						
1	2,210.476	"0"	2,210.476	"0"	2,210.476	"0"
2	03.425	+.016	03.441	−.025	03.416	−.055
3	01.474	+.034	01.508	+.007	01.515	−.090
4	02.326	+.063	02.389	+.068	02.457	−.100
28						
29						
30						
31						
5	02.780	+.057	02.837	+.101	02.938	+.013
7	03.023	+.061	03.084	+.117	03.201	+.051
8	04.315	+.039	04.354	+.115	04.469	−.006
9	03.755	+.009	03.764	+.074	03.838	−.066
10	01.637	−.003	01.634	+.015	01.646	−.056
11	01.307	−.009	01.298	−.026	01.272	−.136
12	05.643	−.017	05.626	−.047	05.579	−.195
52	08.407	+.020	08.427	−.019	08.408	−.181
13	01.971	+.044	02.015	+.102	02.117	+.024
41	03.025	+.055	03.080	+.068	03.148	−.046
42	03.025	+.055	03.080	+.068	03.148	−.046
14	02.910	+.048	02.958	+.095	03.053	+.036
15	02.737	+.040	02.777	+.075	02.852	+.038
16	02.970	+.024	02.994	+.042	03.036	+.021
17	02.476	+.001	02.477	−.009	02.468	−.011
18	03.189	−.011	03.178	−.039	03.139	−.019
19	05.746	+.020	05.766	−.006	05.760	+.019
20	03.086	+.068	03.154	+.109	03.263	−.019
21	01.716	+.068	01.784	+.098	01.882	−.040
46						
47	00.242	+.066	00.308	+.092	00.400	−.051
48						
22	02.421	+.058	02.479	+.060	02.539	−.060
49						
50	01.982	+.048	02.030	+.029	02.059	−.087
51						

TABLE 28.—*Altitudes obtained by leveling the surface of Makaopuhi lava lake*—Continued

Date $\sqrt{t}$ / Station	10/2/67 (30.36) Altitude (ft)	Δ (ft)	1/29/68 (32.26) Altitude (ft)	Δ (ft)	7/10/68 (34.70) Altitude (ft)	Δ (ft)
23	03.419	+.031	03.450	+.002	03.452	−.115
24	02.774	+.014	02.788	−.032	02.756	−.134
25	05.060	+.030	05.090	+.006	05.096	−.123
26	05.373	+.017	05.390	+.017	05.407	−.122
53	05.270	+.035	05.305	+.069	05.374	−.047
54	02.711	+.032	02.743	+.046	02.789	−.045
55	01.669	+.041	01.710	+.037	01.747	−.050
56	03.322	+.021	03.343	−.021	03.322	−.063
57	03.904	−.005	03.899	−.060	03.839	−.080
58	05.671	+.004	05.675	−.027	05.648	−.053
59	04.177	+.033	04.210	+.087	04.297	−.086
60	04.478	+.035	04.513	+.077	04.590	−.104
61	03.382	+.035	03.417	+.045	03.462	−.142
62	02.637	+.037	02.674	+.009	02.683	−.176
63	02.239	+.018	02.257	−.038	02.219	−.191
64	05.605	+.026	05.631	−.011	05.620	−.162
65						
32	06.788	+.049	06.837	+.080	06.917	−.045
33	07.634	+.047	07.681	+.075	07.756	−.066
34	07.190	+.041	07.231	+.077	07.308	−.041
35	00.992	+.057	01.049	+.071	01.120	−.095
36	02.333	+.061	02.394	+.073	02.467	−.084
37	02.820	+.057	02.877	+.070	02.947	−.080
38	2,198.440	+.048	2,198.488	+.051	2,198.539	−.080
39	2,204.345	+.051	2,204.396	+.068	2,204.464	−.096
40	04.480	+.052	04.532	+.067	04.599	−.072
66						
67	01.301	+.011	01.312	−.016	01.296	−.161
68	05.475	+.019	05.494	−.029	05.465	−.150
69	05.745	−.001	05.744	−.058	05.686	−.139
70	01.979	+.015	01.994	−.029	01.965	−.024
71	04.974	+.003	04.977	−.030	04.944	−.020
72	04.472	+.031	04.503	−.004	04.499	−.136
73	06.028	+.032	06.060	−.002	06.058	−.124
74	02.518	+.037	02.555	+.007	02.562	−.108
75	03.575	+.036	03.611	+.026	03.637	−.091
76	04.498	+.042	04.540	+.039	04.579	−.055
77	02.069	+.016	02.085	+.020	02.105	−.037
78	03.000	+.002	03.002	−.028	02.974	−.015
79	03.970	+.016	03.954	−.041	03.913	+.015
80	01.858	+.024	01.882	−.007	01.875	−.088
81	02.674	+.016	02.690	−.020	02.670	−.084
82	02.459	+.022	02.481	−.028	02.453	−.096
83	03.999	+.025	04.024	−.016	04.008	−.095
84	04.069	−.019	04.050	−.031	04.019	−.172
85	05.635	−.009	05.626	−.048	05.578	−.200
86	05.434	−.003	05.431	−.050	05.381	−.207
87	03.314	+.004	03.318	−.032	03.286	−.209
88						
89	02.679	−.015	02.664	−.051	02.613	−.110
90	02.210	−.012	02.198	−.051	02.147	−.092

Date $\sqrt{t}$ / Station	12/11/68[1] (36.85) Altitude (ft)
45	
44	
1	2,210.476
2	03.361
3	01.425
4	02.357
28	
29	
30	
31	
5	02.951
7	03.252
8	04.463
9	03.772
10	01.593
11	01.136
12	05.384
52	08.277
13	02.141
41	03.102
42	04.733
14	03.089
15	02.890
16	03.057
17	02.457
18	03.120
19	05.779
20	03.244
21	01.842
46	
47	00.349
48	
22	02.479
49	
50	01.972
51	
23	03.337
24	02.622
25	04.973

TABLE 28.—*Altitudes obtained by leveling the surface of Makaopuhi lava lake*—Continued

Date $\sqrt{t}$ Station	12/11/68[1] (36.85) Altitude (ft)
26	05.285
53	05.327
54	02.744
55	01.697
56	03.259
57	03.759
58	05.595
59	04.211
60	04.486
61	03.320
62	02.507
63	02.028
64	05.458
65	
32	06.872
33	07.690
34	07.267
35	01.025
36	02.383
37	02.867
38	2,198.459
39	2,204.368
40	03.102
66	
67	01.135
68	05.315
69	05.547
70	01.941
71	04.924
72	04.363
73	05.934
74	02.454
75	03.546
76	04.524
77	02.068
78	02.959
79	03.928
80	01.787
81	02.586
82	02.357
83	03.913
84	03.847
85	05.378
86	05.174
87	03.077
88	
89	02.503
90	02.055

[1]The measured altitudes are affected by tilt of the lava surface. Corrected altitudes are given in table 29.

TABLE 29.—*Altitudes and differences corrected for ground tilt associated with the December 25, 1965, and October 1968 East rift eruptions*

[Derivation of ground tilt is shown in figure 13. Figure 12 is contoured using the corrected data in place of the data given in table 28.]

Station No.	Corrected altitude (ft) 3/7/66	Corrected altitude change (ft) 12/22/65 to 3/7/66
1	No correction	
2	Do.	
3	Do.	
4	Do.	
5	Do.	
7	Do.	
8	Do.	
9	Do.	
10	Do.	
11	Do.	
12	Do.	
52	Do.	
13	2,202.237	−.004
41	03.294	−.021
42	04.960	−.036
14	03.301	−.051
15	03.147	+.085
16	03.354	+.140
18	02.881	+.060
18	03.528	+.068
19	05.905	+.005
20	03.380	−.033

TABLE 29.—*Altitudes and differences corrected for ground tilt associated with the December 25, 1965, and October 1968 East rift eruptions*—Continued

Station No.	Corrected altitude (ft) 3/7/66	Corrected altitude change (ft) 12/22/65 to 3/7/66
21	02.014	−.040
47	00.506	−.028
22	02.671	−.039
50	02.228	−.042
23	03.681	−.073
24	02.895	−.055
25	05.022	−.021
26	05.254	−.002
53	05.506	−.141
54	03.018	−.218
55	02.122	−.334
56	03.799	−.147
57	04.239	−.070
58	05.836	−.011
59	04.300	−.142
60	04.670	−.198
61	03.659	−.260
62	02.911	−.274
63	02.485	−.178
64	05.557	−.005
32	06.990	.000
33	07.809	−.041
34	07.392	+.004
35	01.347	−.075
36	02.709	−.093
37	03.194	−.097
38	2,198.775	−.066
39	2,204.579	−.027
40	04.701	−.201
67	01.615	+.002
68	05.884	−.042
69	06.106	−.021
70	02.195	−.011
71	05.134	+.001
72	04.445	−.052
73	06.005	−.013
74		
75		
76		
77		
78		
79		
80		
81		
82		
83		
84		
85		
86		
87		
89		
90		

Station No.	Corrected altitude (ft) 12/11/68	Corrected altitude change (ft) 7/10/68 to 12/11/68
1	No correction	
2	2,203.378	−.038
3	01.456	−.059
4	02.413	−.044
5	03.018	+.080
7	03.335	+.134
8	04.562	+.093
9	03.887	+.049
10	01.724	+.079
11	01.282	+.010
12	05.546	−.033
52	08.410	+.002
13	02.197	+.080

TABLE 29.—*Altitudes and differences corrected for ground tilt associated with the December 25, 1965, and October 1968 East rift eruptions*—Continued

Station No.	Corrected altitude (ft) 12/11/68	Corrected altitude change (ft) 7/10/68 to 12/11/68
41	03.132	−.016
42	04.763	+.030
14	03.135	+.082
15	02.926	+.074
16	03.083	+.047
17	02.473	+.005
18	03.126	−.013
19	05.781	+.021
20	03.320	+.057
21	01.928	+.046
47	00.440	+.040
22	02.574	+.035
50	02.073	+.014
23	03.443	−.009
24	02.738	−.018
25	05.097	+.001
26	05.411	+.004
53	05.424	+.050
54	02.831	+.052
55	01.773	+.026
56	03.326	+.004
57	03.815	−.024
58	05.643	−.005
59	04.326	+.029
60	04.611	+.021
61	03.455	−.007
62	02.652	−.031
63	02.185	−.034
64	05.624	+.004
32	06.925	+.008
33	07.739	−.017

TABLE 29.—*Altitudes and differences corrected for ground tilt associated with the December 25, 1965, and October 1968 East rift eruptions*—Continued

Station No.	Corrected altitude (ft) 12/11/68	Corrected altitude change (ft) 7/10/68 to 12/11/68
34	07.320	+.012
35	01.078	−.042
36	02.441	−.025
37	02.928	−.019
38	2,198.526	−.013
39	2,204.411	−.053
40	04.563	−.036
67	2,201.278	−.018
68	05.449	−.019
69	05.671	−.015
70	01.776	+.011
71	04.941	−.003
72	04.513	+.014
73	06.069	+.011
74	02.477	−.085
75	03.559	−.078
76	04.527	−.054
77	02.062	−.043
78	02.943	−.031
79	03.902	−.011
80	01.829	−.046
81	02.637	−.033
82	02.418	−.035
83	03.983	−.025
84	04.006	−.013
85	05.547	−.031
86	05.352	−.029
87	03.265	−.021
89	02.612	−.001
90	02.151	+.004